QUANTIFYING GROUND ELEVATION CHANGE IN THE MISSISSIPPI DELTA REGION THROUGH SENTINEL-1 InSAR TIME-SERIES ANALYSIS

A THESIS

SUBMITTED ON THE THIRTEENTH DAY OF OCTOBER 2023

TO THE DEPARTMENT OF EARTH AND ENVIROMENAL SCIENCES

IN PARTIAL FUFILMENT OF THE REQUIREMENTS

OF THE SCHOOL OF SCIENCE AND ENGINEERING

OF TULANE UNIVERSITY

FOR THE DEGREE

OF

MASTERS OF SCIENCE

BY

Rory Elizabeth Escobedo
Digitally Signed on October 13th , 2023.

RORY ELIZABETH ESCOBEDO

APPROVED:

Mead Allison

MEAD ALLISON, PH.D.

Cathleen E. Jones

CATHLEEN JONES, PH.D.

TORBJÖRN E. TÖRNQVIST, PH.D.

THIS PAGE IS LEFT BLANK

ACKNOWLEDGMENTS

We are greatful for the funding of this project by the Lowermost Mississippi River Management Project (LMRMP) through the Louisiana Coastal Protection and Restoration Agency. Additional support was provided by Louisiana Sea Grant through the Coastal Science Assistantship Program.

THIS PAGE IS LEFT BLANK

Table Of Contents

©Copyright by Rory Elizabeth Escobedo 2023,
All Rights Reserved

List of Figures

Jefferson Parish (Kenner) on the east bank of the river and distal from the river on the west bank.

Figure 7: Results from Jones et al. (2016) showing total vertical velocities of ground motion in the Greater New Orleans area differenced from airborne SAR overflight elevation measurements conducted in 2009 and 2012.

Figure 8: Map showing rate of subsidence for permanent InSAR scatterers in Greater New Orleans and vicinity during 2002–05 from Dixon et al. (2006).

Figure 9: The Sentinel-1 SAR image tracks over the Mississippi Delta area utilized in the present study. The images were acquired by the Sentinel-1 satellite in three separate tracks called swaths (IW1 to 3) that relate to successive orbits of the satellite. Each swath can be analyzed separately or can be combined during the processing chain. (Image from Fiaschi et al, in prep.).

Figure 10: Each track in the InSAR data is divided into several overlapping sub-areas (red boxes) for SqueeSAR processing in the present study. Each subarea utilizes a stable ground target persistent scatterer within the subarea characterized by good coherence and phase quality to serve as a processing reference point as described in the text. Yellow polygon shows the total bounding area (~10,000 km^2) of the present study.

Figure 11: Total bounding subarea image of the study area (red polygon) and the results of SqueeSAR processing for the 4.2 million points (light blue) analyzed for the present study that exceeded the coherence cutoff.

Figure 12: Flowchart of Present study Sentinel-1 processing utilized in the present study to yield relative and absolute vertical ground motion in the MRD.

Figure 13: Schematic of relative and absolute measurements made by the InSAR processing chain. The shallow-based differential vertical motion is relative to the subarea reference point that is assumed to have no motion. Time-series vertical motion measurements from GPS and geodetic benchmarks are utilized to create a surface across the delta plain of regional (deeper) vertical motion that impacts all points including the subarea reference points. This correction for deeper is then applied to all points to derive an absolute total vertical motion. The present study utilizes only GPS stations (see Figure 14) while earlier studies (Byrnes et al., 2019; ACRE et al., 2019) referenced herein also utilize selected geodetic benchmarks that are resurveyed every few years showing shallow and deep subsidence boundary zones.

Figure 14: GPS stations used for the regional (deeper) subsidence correction within the study area to derive an absolute vertical motion. Station abbreviations refer to their designation in the Nevada Geodetic Laboratory database.

the shallow contribution. Right panels (both are the same) are absolute vertical velocity rates of motion (elevation loss expressed as a positive to match the CPRA method of expressing subsidence) within each polygon in the InSAR study area. All plots are in units of mm/yr.

List of Tables

List of Abbreviations

ACRE… Applied Coastal Research and Enineering

ASF… Alaska Satellite Facility

ATS… Average time series

CPRA... Coastal Protection and Restoration Authority

CRMS…. Coastwide Reference Monitoring System

cRTS… Common Time Series of Residuals

EGMS… European Ground Motion Service

ESA … European Space Agency

GEC… Ground Elevation Change

GNO… Greater New Orleans

GPS… Global Position System

HSDRRS…Hurricane and Storm Damage Risk Reduction System

ICM… Integrated Compartment Model

InSAR... Interferometric Synthetic Aperture Radar

IW… Interferometric Wide Swath

IPE… InSAR Processing Entity

JPL… Jet Propulsion Laboratory

LMRMP… Lower Mississippi River Management Program

LMR… Loermost Mississippi River

LOS… Line of Sight

LTS… Linear Time Series

MRD…. Mississippi River Delta

NISAR…NASA-ISRO Synthetic Aperture Radar

PSC… Persistent Scatter Candidate

RM… River Mile

R-SETs… Rod-sediment elevation tables

RSLR… Relative Sea Level Rise

SBAS… Small Baseline Subset

SEC… Surface Elevation Change

SWP… Southwest Pass

UAVSAR… Uninhabited Aerial Vehicle Synthetic Aperture Radar

1. INTRODUCTION AND PROJECT SIGNIFICANCE

Among the greatest threats to Louisiana's low-elevation Mississippi River Delta (MRD) ecosystem is the compounding impact of ground subsidence to accelerating global rates of sea level rise (Allison et al., 2016). Thick, easily deformed recent sediment packages characteristic of deltas, and the potential subsidence caused by fluid withdrawal (Kolker et al., 2011), can create a spatially and temporally variable subsidence pattern across the deltaic plain. Quantifying and communicating subsidence differences in specific regions is key to the sustainability of the huge area of MRD wetland ecosystems and linked coastal communities. The present project, funded by the State of Louisiana's Coastal Protection and Restoration Authority (CPRA) through the Lower Mississippi River Management Program (LMRMP), was focused on deriving subsidence rates through an examination of satellite measurements of Interferometric Synthetic Aperture Radar (InSAR) across much of the southeastern Louisiana deltaic plain of the Mississippi River. This builds on an earlier phase for CPRA that derived to measure InSAR ground elevation change in the New Orleans metropolitan region. Both studies aimed to evaluate the use of satellite-based InSAR methods as a tool to assess subsidence rates in wetlands and adjacent low-elevation areas of the MRD. The LMRMP, which is funded by RESTORE using Gulf oil spill finds, aims to identify, and evaluate holistic management strategies for the Lowermost Mississippi River (LMR) corridor below New Orleans. Understanding management strategies that balance navigation, ecological, and flood risk reduction on the LMR can also benefit the future of the entire MRD. The main goal of the present project to better understand subsidence in the LMR corridor will directly benefit the overall mission of the LMRMP to examine the resilience of this section, and adjacent interdistributary basins of the MRD.

The present study uses 143 images taken at 12-day intervals from 2016 to 2021 by the Sentinel-1 satellite launched by the European Space Agency (ESA). Images were processed by a proprietary SqueeSAR® multitemporal technique by TRE Altimira, Inc., yielding 4.2-million-point measurements of vertical elevation change of the ground surface in the MRD. These measurements represent surface displacement in the line-of-sight direction on a 10 x 30 m cell footprint for all locations in the MRD where radar reflectance is above a coherence cutoff applied in data processing as described herein. Results are corrected for horizontal motion and deep (regional) subsidence in the study area utilizing fixed, continuously operating GPS stations, state wetland monitoring (CRMS) sites, previous InSAR results, and historical imagery from Google Earth Pro. Most of the MRD data points in the SqueeSAR® results are higher coherence, non-wetland targets including roads, buildings, offshore platforms, levees and floodwalls, and high-coherence natural sites such as barrier islands (i.e., sand with limited vegetation cover). An objective of the present research is to derive spatial InSAR-derived ground elevation change maps for each of these target subsets to aid in the interpretation of when InSAR-derived ground elevation change is a valid proxy for ground subsidence, and when it is complicated by natural or anthropogenic erosion/accretion.

The overall goal of this project is to evaluate the value of using this remote sensing method as a tool to inform rates of shallow and total subsidence in the southeastern part of Louisiana encompassing the Mississippi River downriver of New Orleans and adjacent areas of Barataria and Breton Sound interdistributary basins (MRD; Figure 1). This work aims to optimize methods to extract a subsidence signal from measured InSAR-derived ground elevation change (vertical velocity change) where complicating factors characteristic of deltas are present such as (1) seasonally variable canopy heights in vegetated areas, (2) periodic tidal and meteorological inundation, (3) sediment erosion/accumulation, and (4) human alterations of the ground surface associated with construction and other land use change. The study is designed to provide comparative data to other, site-specific recent attempts to measure subsidence in the MRD using rod-sediment elevation tables (R-SETs; Jankowski et al., 2017) and GPS stations and coastal benchmark resurveys (Byrnes et al., 2019; ACRE, 2019). While effects such as sediment erosion/accumulation can be excluded from these measurements, in addition to being limited to a small number of MRD sites (10's-100's), these methods typically only measure subsidence over a subset of the total sediment and basement column (e.g., the ground surface to the center of the Earth). Total subsidence remains the measurement of greatest value to the coastal protection and restoration community. These site-specific methods do, however, provide a validation tool for InSAR results produced for the present study and will be re-examined in that context.

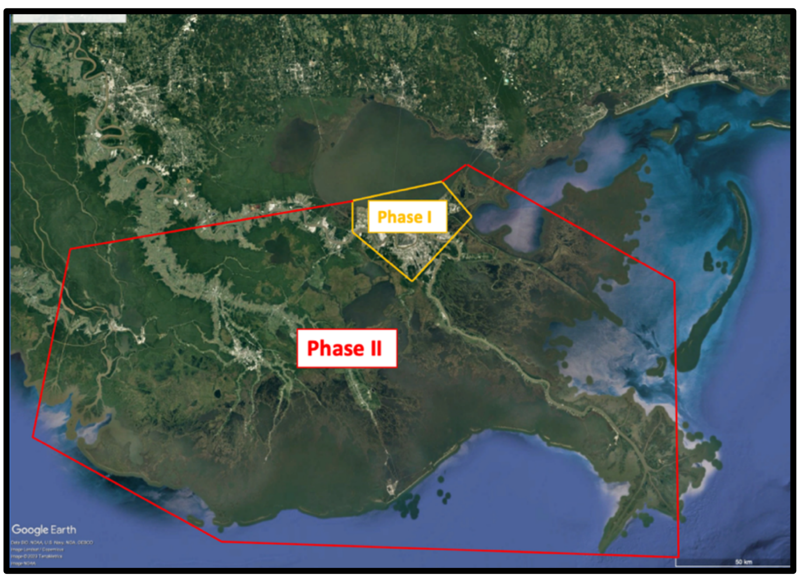

Figure 1: *InSAR study areas of the earlier CPRA-funded study of the New Orleans metropolitan area (Phase I) outlined in Fiaschi et. al. (in prep.) and the present (Phase II) study in Southeastern Louisiana. Previous results from Fiaschi et al. (in prep.) are briefly summarized in the present thesis.*

2. OBJECTIVES

The overall objective of the present study is to explore the utility of InSAR satellite remote sensing for measuring subsidence in the Mississippi River Delta (MRD) region of southeastern Louisiana (Figure 1 captioned above) Several issues that stem from the nature of the synthetic aperture radar signal are key to answering this overall objective. Firstly, it is a measurement of InSAR- derived ground elevation change, not a direct measure of subsidence in the MRD. Extracting a subsidence signal from this dataset is an interpretative exercise requiring understanding the geomorphic controls on InSAR-derived ground elevation change in natural settings and areas of human infrastructure (e.g., buildings, roads, etc.). Site-specific measurements of subsidence from R-SET and GPS/benchmark studies (referenced in Background) conducted in previous studies serve two roles in the present study: they can be a valuable means of comparing direct measurements of subsidence with the InSAR-derived ground elevation change, but, because they typically do not measure the total subsidence signal (e.g., Earth's surface to the center of the Earth), this comparison also provides a means of examining how much of the total subsidence signal is contained in various depth intervals.

A second sub-issue of the overall objective is to determine if the SqueeSAR® InSAR processing technique utilized in the present study can give meaningful information about subsidence in wetland areas. Wetland subsidence is a key need for planning for the preservation and restoration of the MRD coast (CPRA, 2023a) but the use of radar imagery in this ground type is complicated by time-variable factors such as seasonal variation in the canopy height and density (growth-senescence cycles) and periodic tidal inundation of the wetland surface in the MRD region. While InSAR has been used previously to examine subsidence in deltas to a limited extent (Minderhoud et al., 2020), an objective of the present study will be to determine how the wetland setting and processing methodology impact the utility of the MRD. This tool's utility in wetland settings also depends on the InSAR sensor—in this case, the European Space Agency's Sentinel-1 C-band (5.6 cm wavelength) radar. It should be noted that longer wavelength SARs likely will perform better in wetland settings. An example would be the NASA-ISRO Synthetic Aperture Radar (NISAR) satellite planned for launch in late 2023; NISAR is an L-band radar of 24 cm wavelength.

A final sub-objective of this thesis is to utilize the time-series information inherent in each spatial point (ground elevations are provided at each 12-day passage of the Sentinel-1 satellite over the MRD) to examine temporal changes in ground elevation velocities—both gradual and abrupt trend alterations. This can provide information about (1) subsidence mechanism(s) at play, (2) non-subsidence controls on ground-elevation change in natural settings such as erosion/deposition, and (3) non-subsidence controls on ground-elevation change around human infrastructure such as settling of a house or roadbed construction.

3. BACKGROUND

3.1 Study Area

Ground subsidence seriously impacts human infrastructure in coastal cities (Schmidt, 2015) and compounds the effects of accelerating global sea level rise (IPCC, 2022) in low-elevation areas marginal to the oceans such as coastal wetlands. Deltas, because of their thick Holocene sediment wedges generally deposited since the late Holocene stabilization of sea levels at about 6.5-8.5 ka (Stanley and Warne, 1993) are areas of particular concern for rapid subsidence that threatens their vast coastal wetlands and linked human infrastructure. The Mississippi River Delta (MRD) is a highly active and evolving area morphologically that is crucial to the transport of goods by water, possesses vast ecosystem services for Louisiana and the U.S., and serves as home to a culturally diverse mélange of coastal communities and a bulwark protecting communities further inland from the effects of sea level rise and storm surges.

The MRD is one of the largest delta plains in the world that was constructed in the late Holocene as a series of sequentially active aggregational and progradation distributary lobes (Figure 2). The MRD is comprised of two active major distributaries that receive freshwater and riverine sediment: the Mississippi River lobe (also known as the Plaquemine or Balize) and the Atchafalaya River lobe. These lobes cross the subaerial deltaic plain and emit sediment onto the continental shelf and are, for most of the deltaic reach, constrained within flood protection levees. In the later Holocene (~7,500 yBP to present), the Mississippi River has shifted its course periodically on 10^3-year timescales, with abandoned deltaic lobes undergoing degradation from the effects of relative sea level rise (global + subsidence) and reworking of the lobe front by marine processes (Hijma et al., 2017). Presently, the Mississippi River distributary, which carries 70% of the combined flow of the Mississippi and Red Rivers, is constrained by federal flood control levees to Venice, LA on the right descending bank (River Mile [RM11] above Head of Passes) and to Bohemia, LA (RM44) on the left descending bank. The right bank is bounded by Barataria Basin and the left by the Pontchartrain-Breton Sound Basin. This isolation from riverine sediment has been one of the multiple factors that have resulted in rapid wetland loss in these adjacent interdistributary basins (Edmonds et al., 2023). Wetland loss rates in the MRD averaged 27 km^2-y^{-1} between 1932 and 2010 but approached 100 km^2-y^{-1} at times in the 1960s and 1970s, cumulatively accounting for 90% of all coastal wetland lost in the coterminous US over this period (Gagliano and Meyer-Arendt, 1981; Couvillion et al., 2011;). With accelerating global sea level rise rates predicted for the remainder of the 21st century (CPRA, 2023) and episodic decadal-timescale regional accelerations apparent for the Gulf of Mexico (Dangendorf et al., 2023), understanding the additional elevation loss contribution by subsidence over this region is likely key to predicting the scale and pace of future land loss in the MRD, and ultimately the sustainability of these ecosystems and communities.

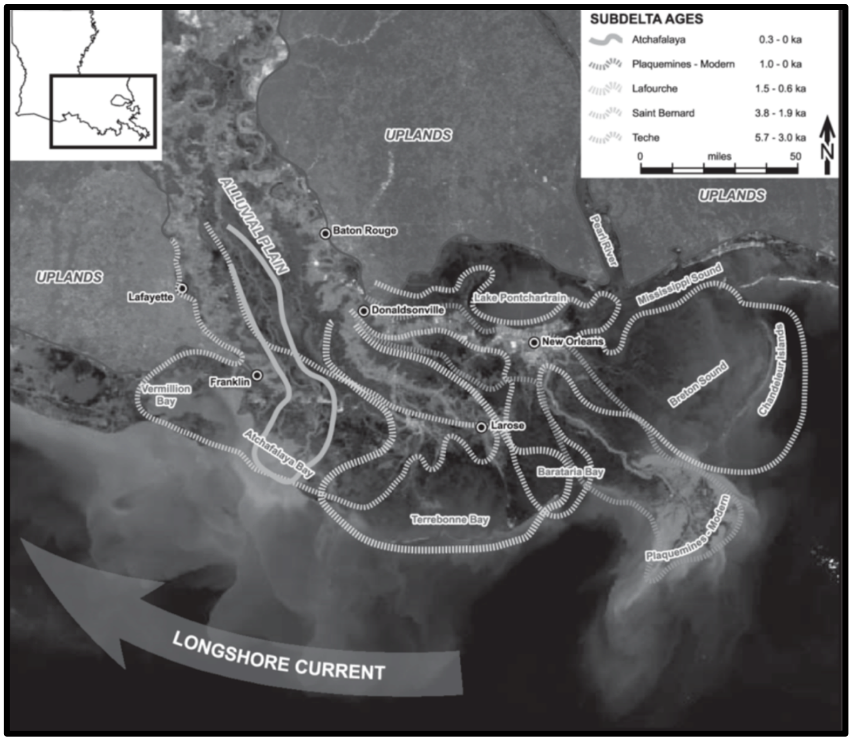

Figure 2: *Map of the Mississippi Deltaic plain showing late Holocene subdeltas and associated river and distributary courses. The two active lobes are referred to in this image as the Plaquemine-Modern (Mississippi River) and the Atchafalaya. Image from O'Leary et al (2020) and modified from Gould and McFarlan (1959) and (Hijma et al., 2017).*

3.2 Mechanisms of Subsidence in the Mississippi Delta

Efficiently measuring and mapping subsidence in the MRD is a complicated issue that many studies have tried to address. The MRD is a vast alluvial plain formed by the deposition of sediment carried by the Mississippi River and is a region of complex subsurface geology. While substantial progress has been made by scientists in the community, there are still many aspects that remain elusive, primarily due to the complexity imparted by (1) stratigraphic heterogeneity and (2) the multiple mechanisms of subsidence that are acting on distinct spatial and temporal scales under the MRD.

Natural subsidence in the MRD includes near-surface processes such as the self-compaction of sediments by depositional loading and consolidation of organic matter (Jankowski et al., 2017) and processes occurring at depth including tectonic subsidence, lithospheric sediment loading, and glacial isostatic adjustment (Wolstencroft et al. (2014). Deep rates from glacial isostatic adjustment and other mechanisms are estimated to be only ~1-3 mm/yr for much of the MRD (Jankowski et al., 2017). Marsh surface elevation change was the primary driver of land loss in the MRD, indicating the importance of dynamic processes occurring near in the organic-rich surficial layer. Wang et al. (2019) and Keogh et al. (2021) investigated the influence of organic matter decomposition on subsidence and emphasized the role of microbial activity in facilitating sediment compaction and subsequent land subsidence in wetlands. Investigations (conducted by Keogh et al., 2019) have delved into the usefulness of extensive tide gauge records spanning decades in swiftly sinking coastal zones with low elevation, like the MRD. The results highlighted that the compression of underlying Holocene layers might result in an understated measurement of the relative sea-level rise (RSLR), when contrasted with tide gauges connected to reference points established in Pleistocene layers. These findings highlight the significance of near-surface processes in shaping the natural subsidence patterns observed in wetland areas of the MRD.

Anthropogenic activities in coastal settings such as fluid withdrawal (oil/gas, groundwater) or sediment loading by sediment placement for marsh creation and barrier island restoration (CPRA,2017) can create a non-steady state temporal pattern of subsidence that declines through time after the disturbance. For example, Kolker et al. (2011) examined this issue in the MRD and showed that the timing of the highest rates of wetland loss coincided with a maximum period of oil/gas extraction in the 1960's and 1970's. River engineering, including the construction of levees and the regulation of river flow, can directly (e.g., levees) and indirectly impact subsidence by sediment loading. (Allison et al., 2016). The channelization and leveeing of the Mississippi-Atchafalaya River system crossing the MRD has resulted in a reduction and redistribution of mineral sediment to coastal wetlands (DeLaune et al., 2013). Indirectly, this may be impacting the distribution of loading subsidence induced by sediment depositing in the last century relative to late Holocene patterns (DeLaune et al., 2013).

The overall thickness of the late Holocene deltaic sediment package may play an overarching role in loading-induced subsidence. Folcks et al. (2015) found that the timing of deposition, the weight of the sediment layers, combined with the consolidation of fine-grained sediments, causes the underlying deposits to compact and settle, leading to subsidence. The spatial distribution of strata package thickness in the region, combined with its relatively young, and, hence, high porosity, are likely important factors in understanding subsidence patterns. Previous studies have classified the uppermost Quaternary stratigraphy of the Mississippi River delta region into two distinct lithofacies. The first lithofacies, known as "substratum," mainly comprised coarse-grained sediments that were deposited within lowstand-incised stream valleys and can be expected to have reached relative stability (i.e., are not readily deformable). The second lithofacies, referred to as "topstratum," consists of relatively finer-grained sediments of the late Holocene MRD lobe expansion. In the region's interfluves, the topstratum directly overlays weathered late Pleistocene sediments. (Kulp et al., 2002). It is anticipated that this package is more subject to ongoing deformation and more subject to acceleration of subsidence were loaded further by anthropogenic processes like marsh creation and barrier island restoration (CPRA, 2023b).

Several methods have been employed to measure subsidence within and below the top stratum in the MRD. Continuously recorded high-precision Global Positioning Systems (GPS) provides a means of monitoring ground elevation change with mm-scale vertical accuracy. Byrnes et al. (2019) utilized this method for examining subsidence rates in Barataria Basin (and ACRE, 2019 in Pontchartrain-Breton) and measured surface elevation loss interpreted as subsidence at rates up to 10 mm/y. Karegar et al. (2015) utilized GPS sites concentrated in Greater New Orleans and found shallow displacements over a range from 0.8 cm to 4.1 cm/yr and a deep rate of -0.8 to 0.1 cm/yr. These site measurements in both studies were taken from GPS fixed stations on buildings and other structures that have provided a decade or more of continuous data, supplemented by geodetic coastal benchmarks that are surveyed by high-precision GPS every few years (CPRA, 2023). This methodology only quantifies subsidence occurring below the foundation depth (e.g., building or benchmark rod) of the site: foundation depth differs from site to site. As such, it is referred to here as "deep subsidence" because it does not measure subsidence in the shallow, readily deformable (late Holocene upper topstratum) sediments in the MRD above the depth of the antenna foundation (pers. comm., C. Jones)

Another method for site-specific subsidence measurements applied previously in the MRD is the use of the State of Louisiana's Coastwide Reference Monitoring System (CRMS) network of 400+ wetland stations across the coast. These stations typically twice annually measure changes in elevation of the wetland surface using a rod surface elevation table (R-SET; Cahoon et al., 2002) and independently measure total sediment (organic+mineral) accumulation each time interval using feldspar marker horizons (CPRA, 2023). Jankowski et al. (2017) utilized this data from stations in operation for eight or more years to derive a "shallow" subsidence rate for the sediment column above the foundation of the R-SET rod (Figure 3). Nienhuis et al. (2017) took these results and combined them with deep subsidence estimates to derive a total subsidence map for coastal Louisiana (Figure 3). As foundation depths for the R-SETs differ from site-to-site since they were emplaced to the depth of refusal, they do not measure subsidence over the same depth interval. Hence, the Jankowski et al. (2017) method also does not measure total subsidence from the ground surface to the center of the Earth and is inherently spatially variable (Figure 4).

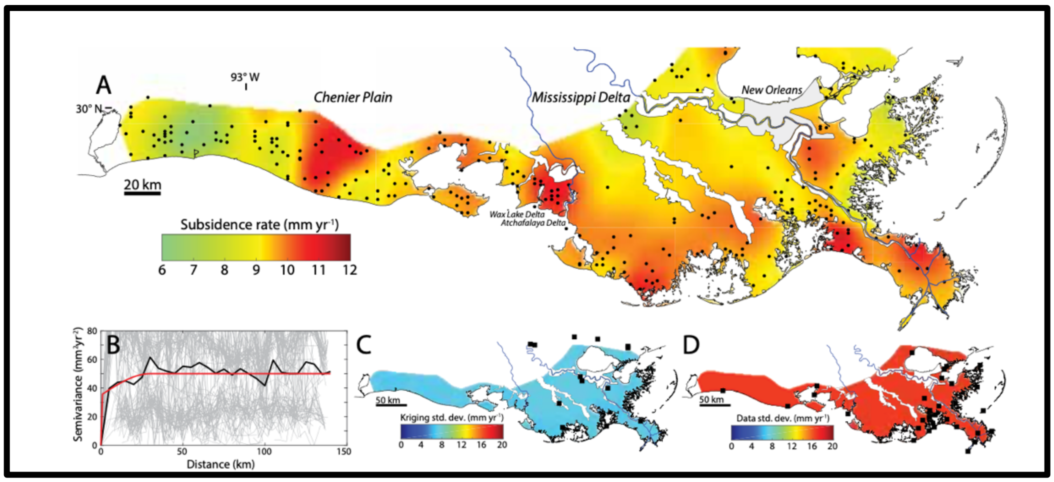

Figure 3: *Total subsidence map for coastal Louisiana wetland areas based on geostatistical interpolation (kriging) of 274 observations (black dots) from R-SET CRMS stations records over a 6–10-year period (Nienhuis et al., 2017)*

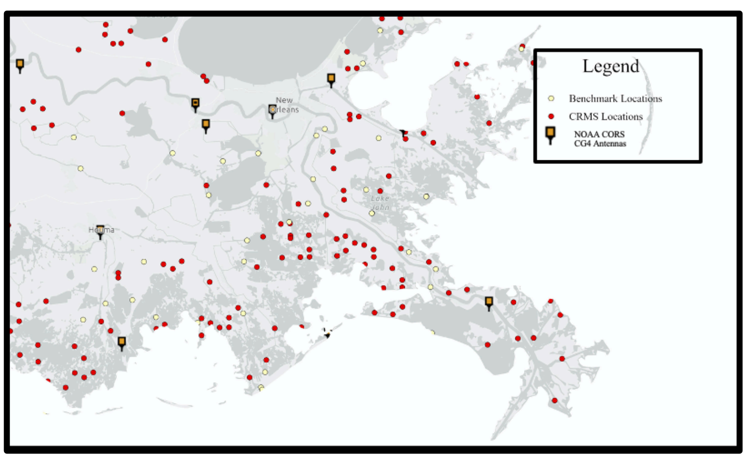

Figure 4: *Compilation of site measurements of subsidence previously conducted in the MRD study area by R-SET (Jankowski et al. 2017, GPS/benchmark (Brynes et al., 2019; ACRE, 2019), and from deconvolution of the subsidence signal from tide gage records (Keogh et al., 2019). The tide gauge sites*

shown are anchored (by benchmark reference) at an average depth of 21.5 m below the land surface. Because at least 60 % of subsidence occurs in the top 5 m of the sediment column in this area in wetland sites,, tide gauges in coastal Louisiana do not capture the primary contributor to RSLR. Similarly, global navigation satellite system (GNSS) stations (n=10) are anchored an average of > 14.3 m below the land surface and therefore also do not capture shallow subsidence. Conversely, R-SET has foundations that mean rod depths of 22.9 ± 6.3 m below the sediment surface in the MRD and provides information on shallow subsidence rates above these depths, but not information on deeper subsidence.

Other studies (Keogh and Törnqvist, 2019) have examined the utility of long-term (decades) tide gauge records in rapidly subsiding low-elevation coastal zones such as the MRD. They found that the compaction of deeper Holocene strata may lead to an underestimation of the measured rate of relative sea-level rise (RSLR) compared to tide gauges with benchmarks anchored in Pleistocene strata. In line with these findings, Cahoon (2015) highlighted the limitations of tide gauges with depth-anchored benchmarks in capturing this crucial aspect of RSLR. However, while Jankowski et al. (2017) and Nienhuis et al. (2017) recognized this issue, neither study provided an in-depth analysis of the problem.

In a related study conducted by Keogh et al. (2021), geotechnical modeling was employed to assess subsidence across 330 sediment cores in the Mississippi River Delta (MRD). The study focused on measuring density and organic matter content in the cores, particularly in the coastal regions of Louisiana. The objective was to determine the extent of thickness loss due to compaction and evaluate the sediment's ability to support wetland preservation against rising sea levels. The findings revealed that sediment compaction primarily depends on the organic content, as well as the thickness and density of the overlying layers, collectively influencing the effective stress. This study found that most compaction occurs within the top 1-3 meters and during the initial 100-500 years after deposition. In areas with significant organic-rich (peat) beds, sediment successions up to 14 meters thick have experienced compaction rates of approximately 50%.

3.3 Use of MRD Subsidence Rates in Coastal Protection and Restoration

The State of Louisiana's Coastal Protection and Restoration Authority (CPRA), tasked with creating a Coastal Master Plan, has attempted to merge the results of these site-specific studies in its most recent plans for 2017 and 2023 plans to derive a useful map for planning purposes of rates of subsidence across the MRD (Figure 5) despite the inadequacies in existing site-specific measurement studies. This subsidence map is a key parameter fed into the Integrated Compartment Model (ICM). The ICM is a hydrodynamic and sediment transport model specifically designed for the coastal Louisiana landscape. It simulates the complex interactions between water, sediment, and land within the coastal system (CPRA, 2023). Each polygon (compartment) along the coast is assigned a subsidence value based on the maps in Figure 5 for different subsidence (low vs high) scenarios.

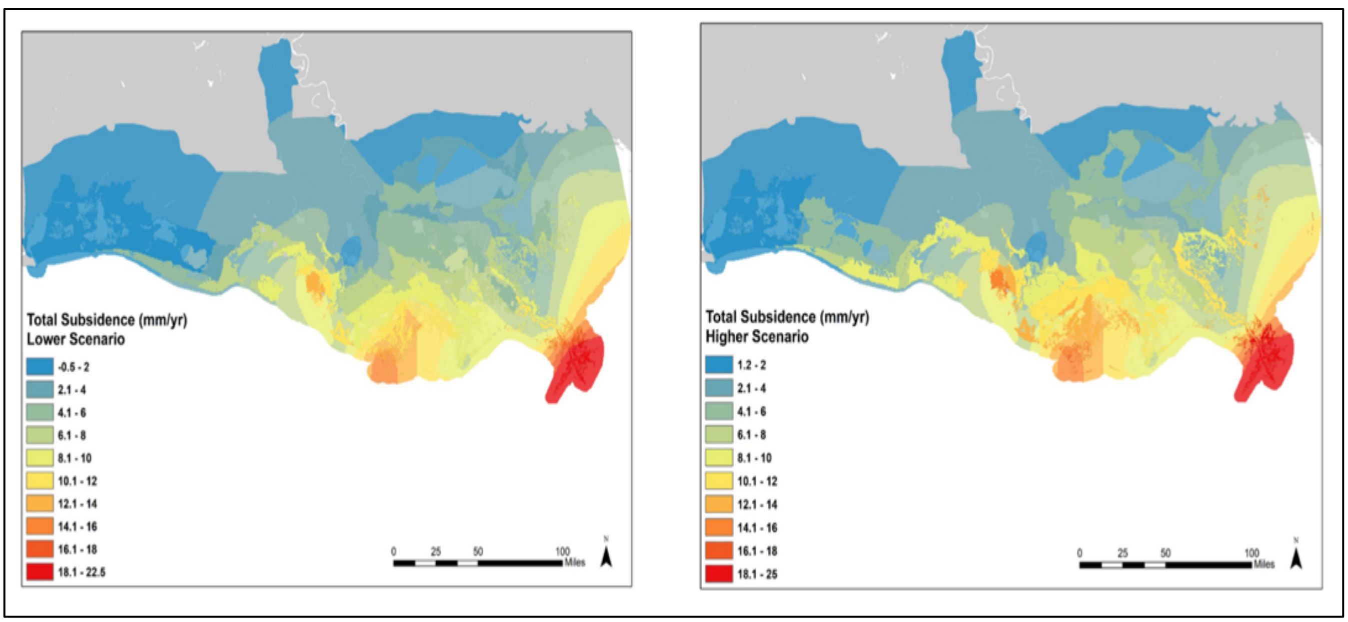

Figure 5: *Map of total subsidence rates in coastal Louisiana derived for the 2023 Coastal Master Plan (CPRA, 2023) using two different (low, high) scenarios for the contribution of the highly spatially variable shallow subsidence contribution to the total (shallow + deep) rate.*

3.4 Application of InSAR in the MRD

Understanding the complex interplay between geological, hydrological, and anthropogenic processes involved in subsidence as described above using site-specific studies is an ongoing challenge. InSAR provides an alternative means of measuring subsidence in the MRD that, by measuring ground elevation change at the surface encompasses the various mechanisms of operation over different depth intervals to derive a total subsidence for a site and allows for a denser spatial grid than the site-specific studies.

InSAR has been utilized in the MRD region previously only to examine surface elevation change (SEC) in the Greater New Orleans (GNO) area (Dixon et al., 2006; Jones et al., 2016; Fiaschi et al., in prep.). This focus in previous efforts is partly a function of difficulties in the MRD, which is largely wetlands, in solving the many factors that can affect the results of a smooth and cohesive InSAR-derived ground elevation change map (Jones et al., 2016). These include, but are not limited to periodic tidal inundation, and seasonal changes in the height or extent of vegetation cover (Fiaschi et al., in prep.; Figure 6).

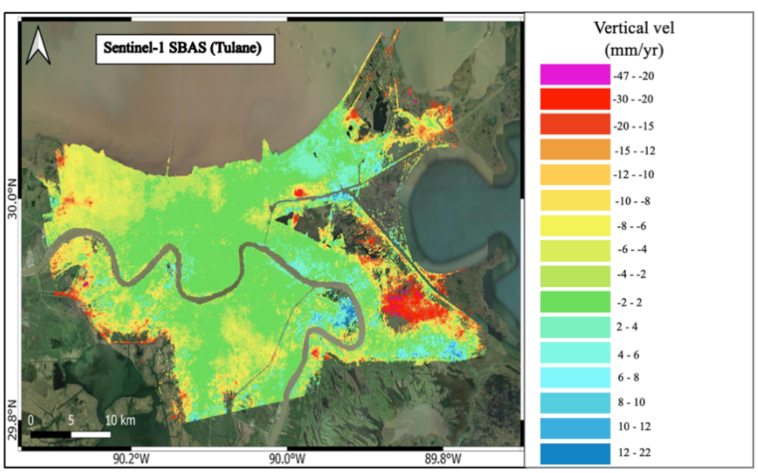

Figure 6: *InSAR vertical velocity map of Greater New Orleans produced in the Fiaschi et al.(in prep.) CPRA-funded study over a 2016-2020 period of record. Stable areas (vertical motion less than +2 to -2 mm/y) include eastern Jefferson Parish on the east bank of the river, the west bank of Jefferson in areas proximal to the river, and St. Bernard Parish near the river in the Chalmette-Arabi corridor. Significant apparent subsidence rates are found in western Jefferson Parish (Kenner) on the east bank of the river and distal from the river on the west bank.*

Dixon et al. (2006) conducted the first space-borne InSAR study of metropolitan New Orleans to estimate the yearly rate of deformation of both structures, and the concrete and grass-covered levee structures that ring the area. To achieve sub-wavelength accuracy of the radar signal, the study utilized a new InSAR technique referred to as *joint pixels InSAR* to acquire high-quality and high-resolution (up to 1 meter) SAR images (Figure 7). This is the most spatially comprehensive of the InSAR studies in this area and reported an average vertical ground motion (subsidence) rate of -5.6 +/- 2.5 mm/yr. The maximum rate observed was -29 mm/yr and the highest rates were found in areas more distant from the Mississippi River where coarser, more stable natural levees were settled earliest in metropolitan New Orleans (Dixon et al., 2006; Figure 7).

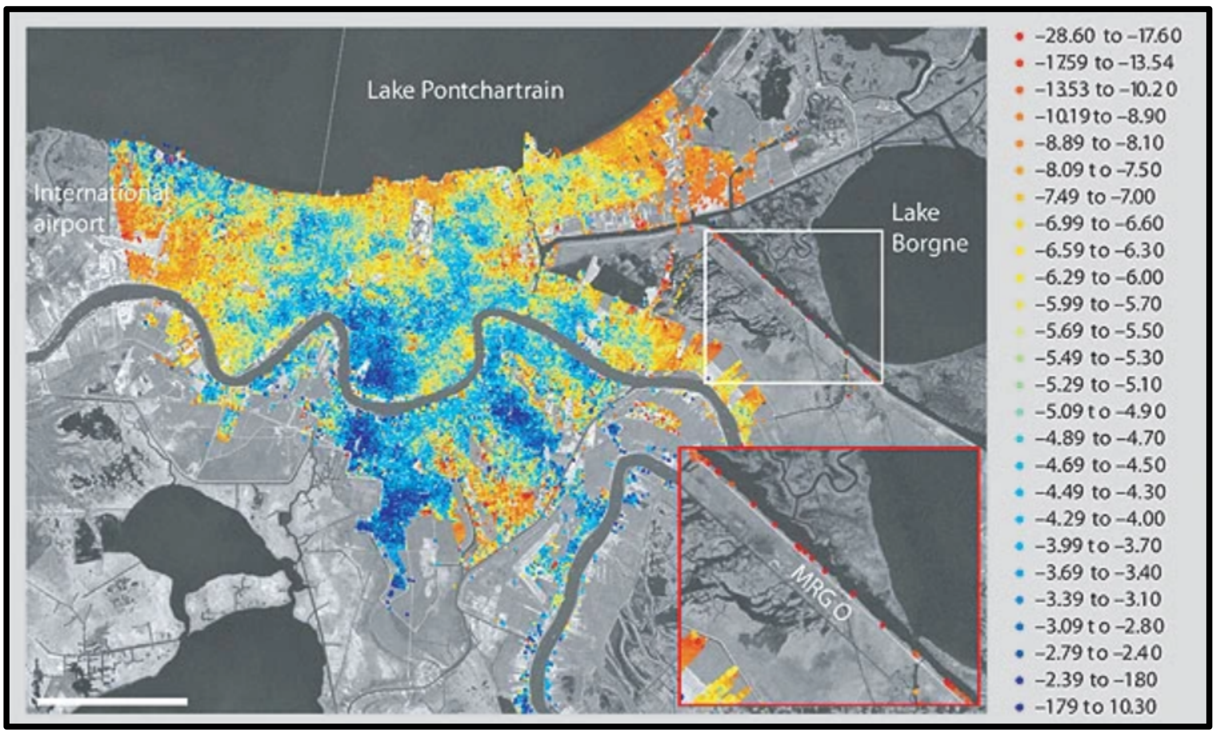

***Figure** 7: Map showing rate of subsidence for permanent InSAR scatterers in Greater New Orleans and vicinity during 2002–05 from Dixon et al. (2006).*

InSAR studies that have analyzed New Orleans have used different approaches to understand ground movement. Jones et al. (2016) used Uninhabited Aerial Vehicle Synthetic Aperture Radar (UAVSAR), an airborne instrument operated from 12.5 km altitude and elevation differences from surveys over the study area from June 16, 2009, to July 2, 2012. As an airborne instrument, UAVSAR has both a higher signal-to-noise ratio than spaceborne SARs and has different predominant systematic error sources. It also has a limited number of repeat measurements (flights) over the study period. To take into account ground movement, the results were calibrated with localized measurements from Global Positioning System (GPS) to give some information about the relative contribution of deep and shallow processes. Jones et al. (2016) results (Figure 8) support the conclusion that groundwater withdrawal is a primary subsidence driver in areas with major industries in Greater New Orleans, particularly in Norco and Michoud areas.

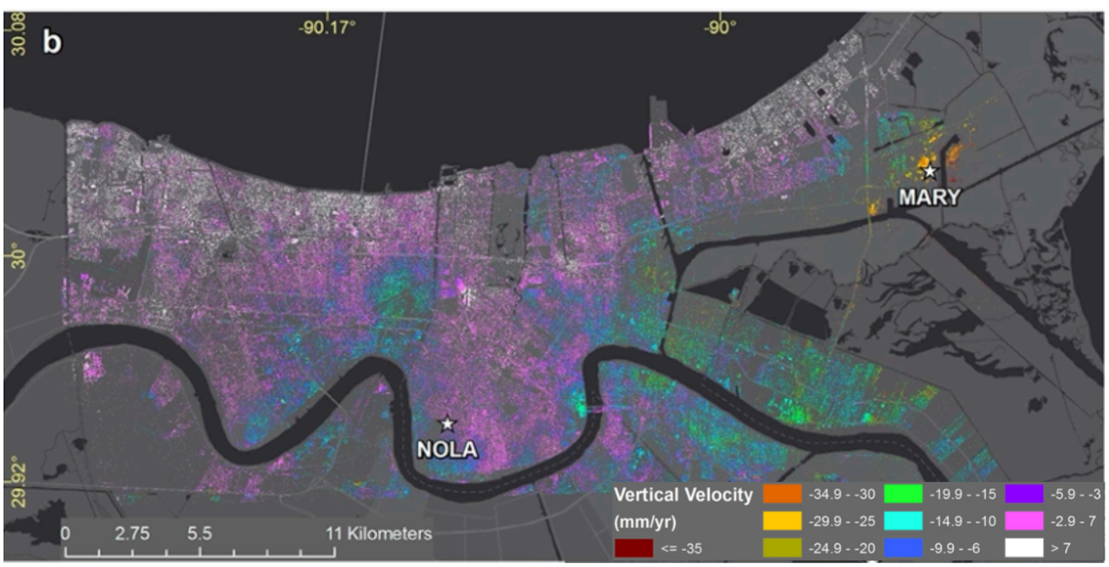

Figure 8: *Results from Jones et al. (2016) showing total vertical velocities of ground motion in the Greater New Orleans area differenced from airborne SAR overflight elevation measurements conducted in 2009 and 2012.*

The work of Fiaschi et al. (*in prep.*) is a precursor to the present study but also focused only on metropolitan New Orleans. This Fiaschi et al, in prep work (Figure 6) found that most urban areas such as eastern Jefferson Parish on the east of the riverbank, the west bank of Jefferson in areas proximal to the river, and St. Bernard Parish near the river in the Chalmette-Arabi corridor are relatively stable (vertical elevation loss at velocities < 2 mm/yr). Other urbanized areas, specifically near Kenner on the east bank of the MR and distal from the MR on the west bank, have higher vertical velocities and appear to be affected by subsidence (Figure 6). One key difference between the Fiaschi et al, in prep study and the present work is that the previous work was not calibrated using GPS to correct for regional (deep) subsidence occurring over the entire Greater New Orleans study area.

A key aspect limiting the utility of InSAR in the MRD, and similar settings is that it is used to determine cumulative ground deformation between successive observations by measuring phase changes in the line-of-sight distance to the target, a method sensitive to changes of a small fraction of the radar wavelength (Jones et al., 2016). The rate of InSAR- derived ground elevation change that can be accepted must pass a certain level of coherence. Coherence is a measure of the correlation between corresponding pixels in an interferometric pair of images. The rate ranges from 0, where there is no useful information, to 1, where there is no noise in the interferogram (the two images are locally identical but with a constant phase shift). In InSAR, coherence serves as a measure of quality and is adversely affected, for example, by excessive variations in the acquisition geometry or changing/moving elementary scattering centers within each resolution cell (EGMS, 2021). High levels of coherence are typical of man-made structures, such as buildings, roads, and other human infrastructure characteristic of the earlier studies of Greater New Orleans, while low levels are generally typical of surfaces covered by vegetation, which are extremely variable in reflectivity with time. Water bodies have low coherence because wind and currents cause ripples on the surface that change rapidly. Water is also radar-dark because the relatively flat surface reflects the energy in the forward direction, not back toward the instrument. From a practical point of view, this parameter affects the distribution of the measured points since the areas presenting very low coherence (close to or below the level of ambient noise) cannot be used to extract reliable displacement information. Thus, towns in the MRD (e.g., Houma, Morgan City, Grand Isle, etc.) can be anticipated to have a high coherence rate while immediately adjacent wetlands or even highly vegetated portions barrier islands may have low coherence rates.

In Fiaschi et al, in prep of this project (Fiaschi et al., in prep.), it has been shown that the InSAR post-processing methods can be designed to partly compensate for issues that cause low coherence. The final Fiaschi et al, in prep map of velocity was processed using Small Baseline Subset (SBAS) multi-temporal InSAR technique (Yunjun et al., 2019). In SBAS, Sentinel-1 images are connected multiple times to generate a highly redundant connection network. From each connection, an interferogram is generated and stacked to perform the time-series analysis. The original pixel size of the image is multi-looked (increased) to better preserve coherence in vegetated areas and to obtain smoother results over such areas. The final result (Fiaschi et al., in prep.) uses only pixels above a 0.25 coherence threshold (Figure 6). This threshold, which is just above the background noise of ~ 0.20, was selected to retrieve only values of focus (Fiaschi et al, in prep). This processing routine yielding reliable information at such low coherence thresholds was possible due to the relatively small area but also resulted in a degraded spatial resolution (60 x 60m) of the Sentinel-1 data. The Fiaschi et al. (in prep.) Greater New Orleans (GNO) effort also followed a strategy of utilizing independent methods of measuring subsidence to aid in interpreting vertical velocities.

4. METHODS

As mentioned previously, the present project to utilize Sentinel-1 InSAR data in the Mississippi Delta was carried out in two phases. Fiaschi et al. (in prep.) of the project was completed by Dr. Simone Fiaschi in 2020 for the Greater New Orleans (GNO) region. This analysis was conducted first because it is an area of major human infrastructure (i.e., high coherence to radar), and is a location where previous InSAR efforts had been conducted (Dixon et al., 2006; Jones et al., 2016) to allow for comparison of developed Sentinel-1 processing methods in league with previous results. The processing method for the earlier study (Fiaschi et al., in prep.) utilized the Small Baseline Subset (SBAS) multi-temporal InSAR technique (Berardino et al., 2002). SBAS is a low-resolution (large ground pixel size) approach that is capable of extracting information not only from objects with good SAR signal reflectively (hard structures) but also from areas characterized by high temporal variability and lower quality of the reflected signal (soft structures including wetlands). This method connects each image multiple times to generate a highly redundant connection network. The connected interferogram is stacked before performing a time-series analysis. The original pixel size of the image is multilocked (increased) to better preserve coherence in vegetated areas, and to obtain smoother results over such areas (Fiaschi et al., in prep). This process is designed to minimize difficulties caused by periodic tidal inundation, and seasonally variable vegetation canopies and soil moisture.

In the present study, the methodology used is different from that in Fiaschi et al. (in prep.). The study described here utilized a SqueeSAR® technique mainly due to the much larger area being analyzed (~10,000 km^2) and the fact that the earlier study had established that, despite the attempt to maximize processing to preserve signal in wetlands, limited success was achieved (Fiaschi et al., in prep.). Hence, the present study focused on developing a methodology appropriate for higher coherence (e.g., non-wetland) areas that provided the highest spatial resolution and maintained high quality results. The SqueeSAR® technique utilized in the present study is a proprietary methodology developed by TRE Altimira, Inc. to analyze ground motion in large areas by dividing each Sentinel image swath into several sub-areas and processing them separately at full satellite radar resolution (~15 x 5 m pixel size). In each subarea, a stable ground target with good coherence and phase quality is identified and utilized as a reference (multi-reference approach) to all other points in the sub-area. All the subareas are then merged to a seamless surface using proprietary methods to minimize differences in vertical velocity rates across subarea boundaries. SqueeSAR® processing utilized in the present study was done by Dr. Simone Fiaschi, who is now employed by TRE Altamira.

4.1 InSAR Processing to Derive Relative Rates of Ground Motion

The Sentinel-1 mission was launched by the European Space Agency (ESA) in April 2014 and began acquiring images over southeastern Louisiana in April 2016. The satellite is equipped with a C-band sensor radar (56 mm λ) that has an acquisition frequency (re-visit time) of every 12 days. The images were obtained in (Figure 9) Interferometric Wide Swath (IW) mode at a 2.3 x 14.1 m resolution in Range (across-track) and Azimuth (along-track), respectively. The SAR signal contains both vertical and horizontal components when analyzing ground elevation change between acquired images (Table 1). This is due to orbiting SAR acquisitions being taken at an inclined angle from the zenith, referred to as the line of sight

(LOS). Only the line of sight derived from a vertical disposition is used during the post-processing.

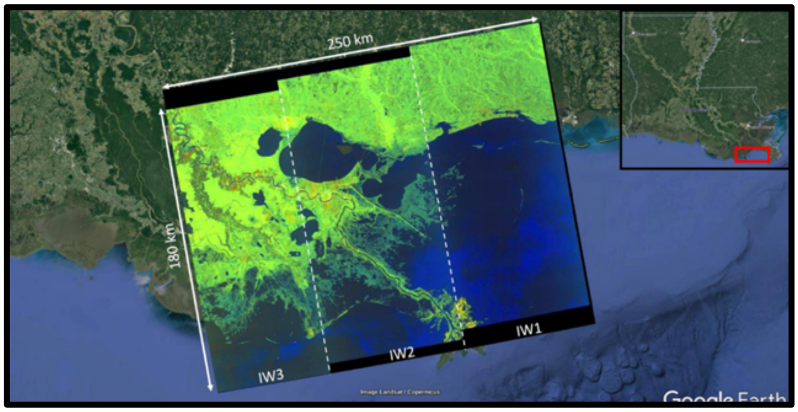

Figure 9: *The Sentinel-1 SAR image tracks over the Mississippi Delta area utilized in the present study. The images were acquired by the Sentinel-1 satellite in three separate tracks called swaths (IW1 to 3) that relate to successive orbits of the satellite. Each swath can be analyzed separately or can be combined during the processing chain. (Image from Fiaschi et al, in prep.).*

Table 1. *Characteristics of InSAR Sentinel-1 dataset utilized in the present MRD study.*

Sensing Period	Max prep baseline	Max temp baseline	Revisit time	Average incidence angle	Imgs	Ifgs
28 Jan 2016 to 31 March 2020	224 m	168 days	12 days	38°	107	585

The Sentinel-1 images utilized in the present study are publicly available from two main providers, ESA's Copernicus Open Access Hub (https://scihub.copernicus.eu/) and the Alaska Satellite Facility (ASF) Distributed Active Archive Center (https://asf.alaska.edu/). The present study uses a total of 276 (133 of track 165 and 143 of track 63) Sentinel-1 ascending orbit images (Figure 9) acquired from 2016 to 2021 (e.g., one year longer than the Fiaschi et al, in prep that extended only to 2020) and covering much of the MRD (~10,000 km^2 in total; Figure 10).

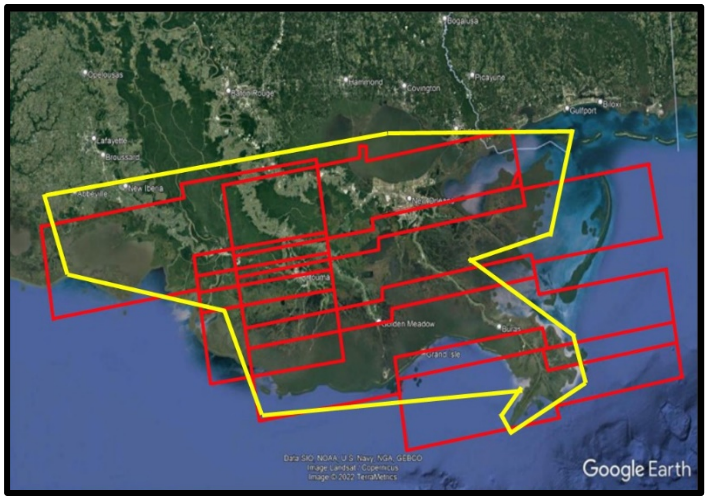

Figure 10: *Each track in the InSAR data is divided into several overlapping sub-areas (red boxes) for SqueeSAR processing in the present study. Each subarea utilizes a stable ground target persistent scatterer within the subarea characterized by good coherence and phase quality to serve as a processing reference point as described in the text. Yellow polygon shows the total bounding area (~10,000 km^2) of the present study.*

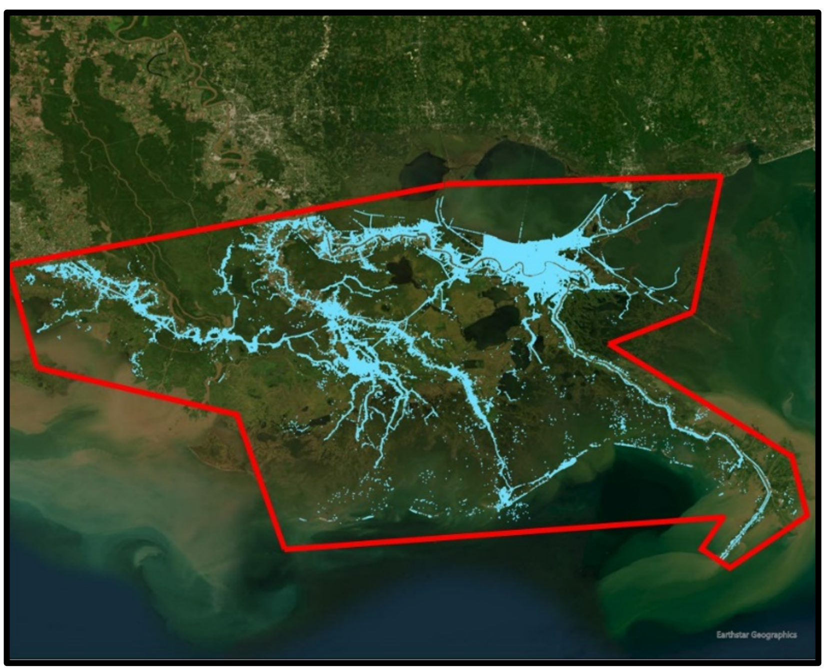

Figure 11*: Total bounding subarea image of the study area (red polygon) and the results of SqueeSAR processing for the 4.2 million points (light blue) analyzed for the present study that exceeded the coherence cutoff.*

The adopted processing approach for the present study is similar to the one used for the European Ground Motion Service (EGMS) project (EGMS, 2021), which follows a strategic InSAR Processing Entity (IPE). In this approach (Figure 10), each track is divided into several sub-areas and processed separately at full resolution (~15 x 5 m pixel size) by selecting a stable ground target in each subarea with good coherence and phase quality as a reference (multi-reference approach). The processing strategy is broken into two strategies. First, all interferograms are unwrapped on a sparse grid of Persistent Scatterer Candidate (PSC). This is for pixels whose amplitude dispersion index is within the specified threshold selected (Devanthéry et al. 2014). Second, after processing estimation and removal of the atmospheric components, all points providing useful information are identified and output. Due to the high spatial correlation of atmospheric phase components, even a sparse grid of measurements may allow proper sampling of the atmospheric effects. This is when the important parameter of coherence must be taken into effect. All areas are then merged by minimizing differences in velocity rates between each area as described in the Figure 12 processing flowchart.

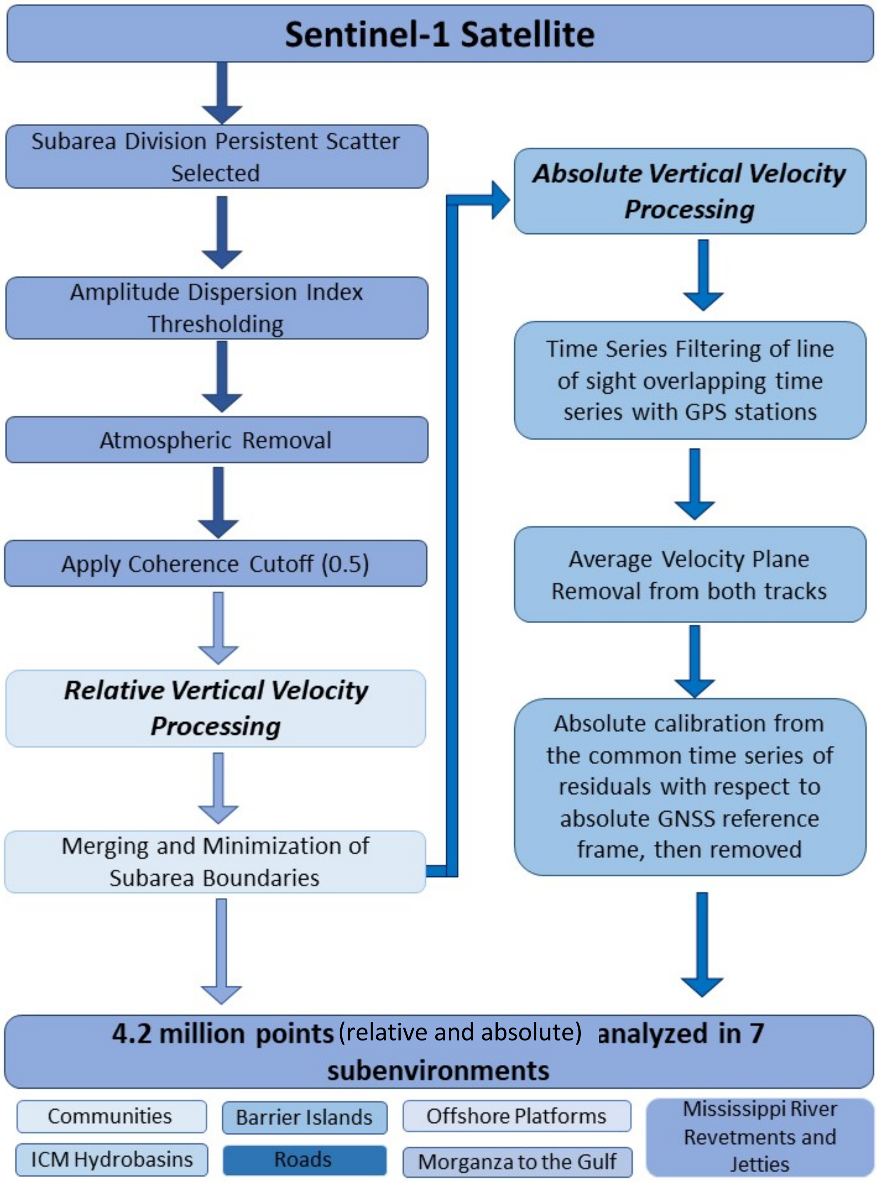

Figure 12: *Flowchart of the present study Sentinel-1 processing utilized in the present study to yield relative and absolute vertical ground motion in the MRD.*

The results yielded a total of 4.2 million measurement points within the Mississippi Delta study area (Figure 11) utilizing a coherence cutoff of 0.5. The resultant rates of vertical motion are referred to hereafter as "relative" vertical motion and reflect any local spatial motion relative to the PS reference points in each subarea. Any regional motion that occurs across the entire study area including the reference points, which presumably is from deeper regional subsidence, is not taken into account in these measurement points. The deeper motion is addressed by referencing the PS and measurement points to continuously operating GPS stations in the survey area as described below to derive a total, or "absolute" vertical motion.

The final output of the InSAR relative processing is either a raster or shapefile with the SEC rated in velocity (mm/yr). Each of these points gives an individual time series of velocity (movement of the surface) at the 12-day orbit interval over the imagery catalog period (2016-2021). Further information on the processing strategy can be found in the EGMS documentation (https://www.eea.europa.eu/about-us/tenders/eea-dis-r0-20-011).

4.2 GPS Calibration to Derive Absolute Rates of Ground Motion

To derive a meaningful vertical ground motion (absolute ground motion velocity) that takes into account both the shallow (Holocene) and deeper subsidence as well as surface elevation changes due to other mechanisms (e.g., erosion/accretion), InSAR measurements derived from the sub-area method required further processing in the MRD (Figure 13). As mentioned previously, the ~10,000 km^2 study area is divided into six different sub-areas that are processed separately at full resolution (~15 x 5 m pixel size) by selecting a stable ground target (persistent scatterer or PS) with good coherence and phase quality as a reference (multi-reference approach) (Figure 10). If all the points in the subarea, including the PS reference point, are subsiding at a background rate, as could be expected from the action of deep processes such as glacial isostatic adjustment or crustal loading Hijma et al. (2017), this component is not included in the "relative: processing strategy outlined above (Figure 12). Jankowski et al. (2017) noted that a significant part of shallow subsidence in coastal Louisiana occurs in the top 5-10 m (then reduced to top 1-3 m in Keogh et al. (2021)), hence the GPS stations, which tend to be anchored (either attached to wells or building foundations) below this depth, are recording deeper motion from subsidence. This was recognized by Byrnes et al. (2019) and ACRE (2019) who utilized

GPS stations and re-surveyed benchmarks in coastal Louisiana to derive a deeper subsidence rate (Figure 5).

To derive the absolute vertical motion of the SAR points on the ground surface, it is necessary to add back in the deeper subsidence taking place at the PS reference location of each subarea. First, nearby GPS stations within the study area (8 for swath T165 and 5 for swath T63; Figure 14) were chosen based quality of the signal, e.g., only those in operation over the 2016 to 2021 InSAR period of record and without any significant time series gaps. GPS station data (Table 2) was obtained from the Nevada Geodetic Laboratory GPS Network site (website listing here).

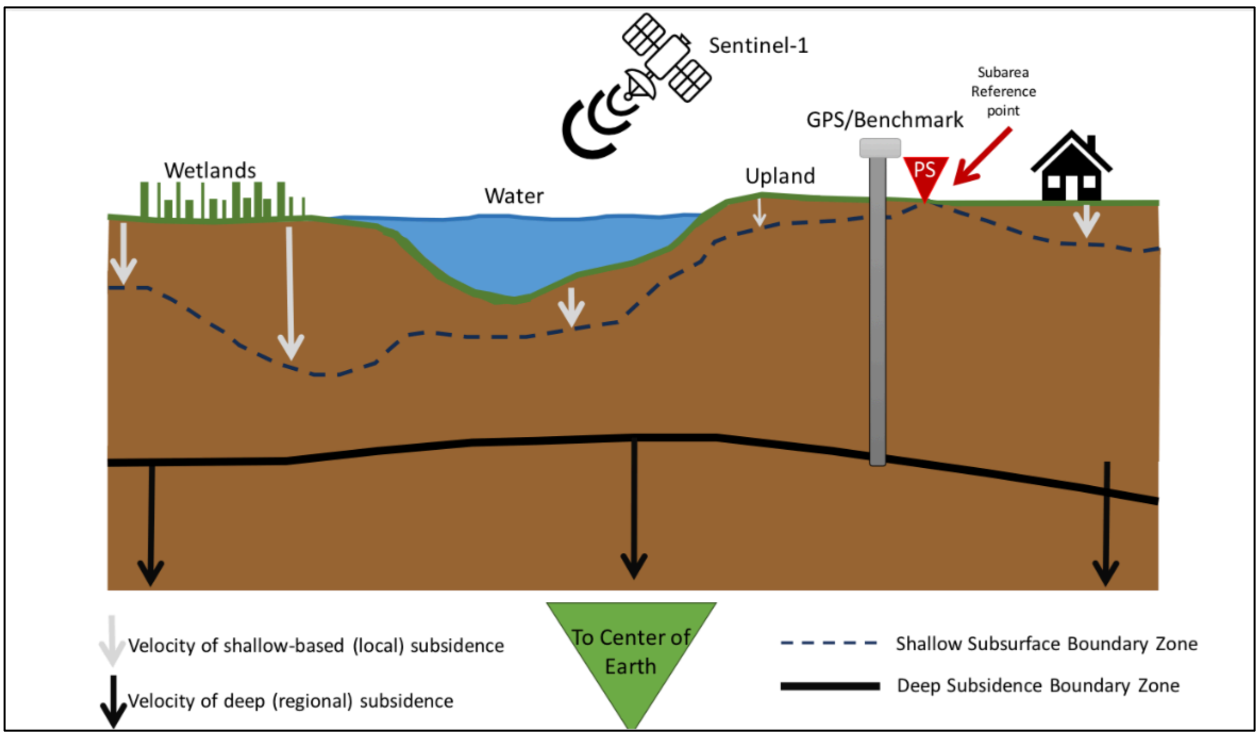

Figure 13: *Schematic of relative and absolute measurements made by the InSAR processing chain. The shallow-based differential vertical motion is relative to the subarea reference point that is assumed to have no motion. Time-series vertical motion measurements from GPS and geodetic benchmarks are utilized to create a surface across the delta plain of regional (deeper) vertical motion that impacts all points including the subarea reference points. This correction for deeper is then applied to all points to derive an absolute total vertical motion. The present study utilizes only GPS stations (see Figure 14) while earlier studies (Byrnes et al., 2019; ACRE et al., 2019) referenced herein also utilize selected geodetic benchmarks that are resurveyed every few years.*

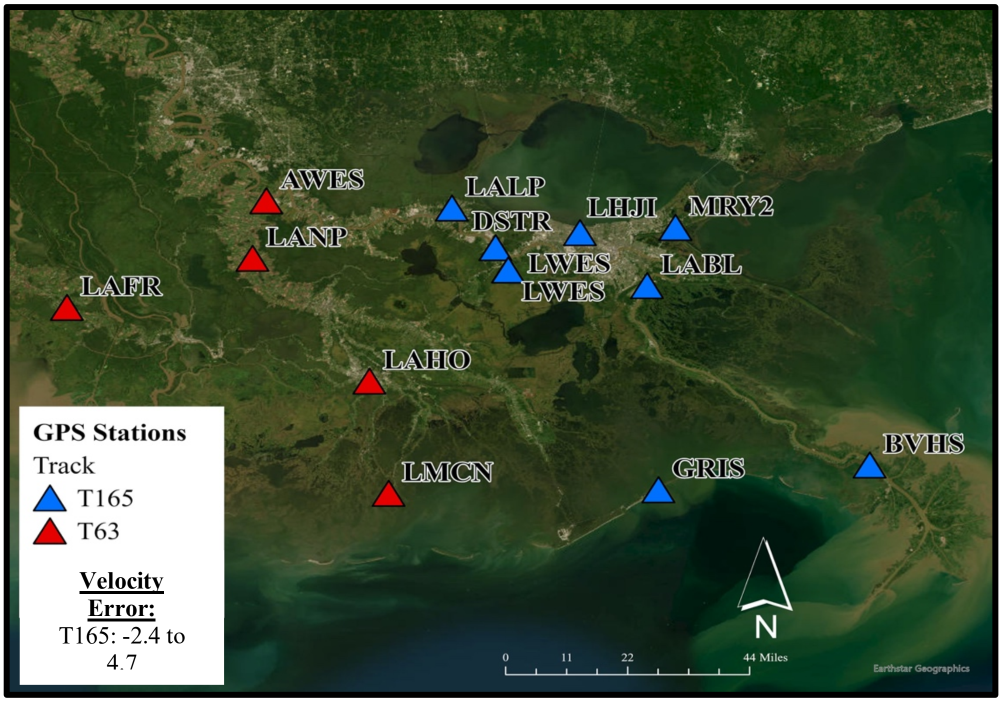

Figure 14: *GPS stations used for the regional (deeper) subsidence correction within the study area to derive an absolute vertical motion. Station abbreviations refer to their designation in the Nevada Geodetic Laboratory database.*

Table 2. *Characteristics of the GPS stations utilized for the deep subsidence correction of the InSAR results in the present study. Height is in reference to above the reference ellipsoid.*

SITE	Longitude	Latitude	Motion (mm/yr)	Height (m)	Swath
BVHS	-89.41	29.34	-2.3	-15.68	T165
DSTR	-90.38	29.96	-0.66	-19.98	T165
GRIS	-89.96	29.27	-4.08	-17.00	T165
LABL	-89.99	29.86	-0.57	-17.70	T165
LALP	-90.50	30.08	-0.69	-18.31	T165
LHJI	-90.16	30.01	0.21	-19.06	T165
LWES	-90.35	29.90	-0.71	-17.05	T165
MRY2	-89.91	30.02	1.85	-24.28	T165
AWES	-90.98	30.10	-1.51	-10.31	T63
LANP	-91.02	29.93	-0.86	-10.51	T63
LAFR	-91.50	29.79	-3.91	-10.71	T63
LAHO	-90.71	29.58	-1.50	-15.40	T63
LMCN	-90.66	29.26	-3.83	-16.07	T63

To reduce the noise of the Global Navigation Satellite System (GNSS) signal from each GPS antenna utilized, the daily time series were filtered using a 60-day moving time average.

The filtered GNSS measurements were then projected to the satellite line of sight (LOS) to create a GNSS LOS time series (LTS). From this, the best quality 100 Sentinel-1 InSAR LOS measurement points within a 100 m radius of each GPS station were selected and used to calculate an average time series (ATS) for the period overlapping with the GNSS time series. This calculation resulted in a plane removal to remove any inconsistencies. To achieve this, a difference in average velocity (linear trend) was calculated for each ATS and corresponding LTS. The differences calculated for each ATS and LTS pair were then used to estimate and remove a first-order surface (plane) from the InSAR data. This removes possible linear errors in the measurements. Since the plane is calculated and removed independently for each InSAR track using a different GNSS network, the removal of the plane introduced inconsistencies in terms of velocities between the two tracks. For this reason, a common plane using the full GPS network of stations in each swath (Table 2) was calculated and removed for both tracks. While this procedure eliminated differences between the results of the two tracks, it also introduced a greater error in the calculated vertical motion rates (e.g., on the order of 2 to 3 mm/y in the calibrated data).

Overall, this method gives a time series of residuals generated by comparing the ATS to the corresponding LTS for each GPS station. All the time-series of residuals are then averaged to define a common time series of residuals (cRTS). This cRTS represents the movement of the PS reference points in each subarea relative to the absolute GNSS reference frame. The cRTS is then removed from the time series of every InSAR measurement point in the subareas.

The TRE processing of the InSAR dataset utilizes only high-quality GPS station data with no time gaps within the study area, and a higher precision integration method is applied to the individual points. The results of the processing chain result in two values for each data point within a sub area: a value associated with vertical motion relative to the PS reference points, the "relative vertical velocity", and a value referenced to GPS stations to correct for deep subsidence referred to hereafter as the "absolute vertical velocity" as it also includes both the relative and deep components of motion. At points in the interpretation (see Discussion), this deep signal (vertical motion measured by the GPS station network) is analyzed separately by subtracting (absolute – relative) vertical motions.

4.3 Analysis of Geomorphic and Infrastructure Setting

The relative and absolute vertical velocity of 4.2 million data points of ground motion in the 2016 to 2021 Sentinel-1 InSAR imagery catalog was analyzed in an ArcGIS Pro geodatabase. Seven areas of relatively high coherence were identified as having distinct and potentially consistent controlling drivers of ground motion (subsidence plus natural or anthropogenic erosion/accretion) measured by the InSAR methods: (1) barrier islands, (2) Mississippi River revetments and jetties, (3) inshore oil and gas platforms, (4) key major roads, (5) the Morganza to the Gulf hurricane protection levee, (6) towns and cities. In addition to these subsets of the results, the entire point cloud was analyzed in a seventh category for polygons of the State of Louisiana Master Plan model grid. Wetland areas are generally not included in these results as they generally had insufficient coherence and were removed in the SqueeSAR processing as it was determined that reducing the coherence cutoff would result in unreliable results. Artificial levees, such as those along the Mississippi River and hurricane protection levees along the west bank of the Mississippi River and around Bayou Lafourche communities (e.g., Raceland to Leeville), also had low coherence and are not represented, perhaps due to seasonal variations in mowed (grass) vegetation.

Barrier islands are natural depositional environments that have relatively high coherence due to the limited vegetation cover and the sandy substrate and, hence, can be expected to experience natural erosion/accretion sediment processes that complicate the subsidence signal. In addition to wind and water-driven erosion/deposition, some of these islands have been renourished in the past several decades by the State of Louisiana, including in the 2016 to 2021 InSAR period of record, using material dredged from the Mississippi River and conveyed by long-distance pipeline or hopper dredged from offshore sand sources. Renourishment sites and timing were documented for those islands concerned. The barrier islands were treated individually and are divided into specific geomorphic sub-areas (overwash fan, beach face) with a separate category for nearby structures (jetties, platforms, sea walls).

Five focus areas for the present study are significant types of human infrastructure. Major roads (Area 1) were selected that (a) cross large parts of the MRD in onshore-offshore and E-W transects, and (b) have been in place for decades to reduce the impact of post-construction settling of the roadbed on ground motion. This does not exclude any alteration of the road surface by maintenance or repaving. This was done by selecting only points that intersected with the road surface itself or the lane median. Once these points were selected, they were assigned a category to define the rate for their particular location. Free-standing and platforms over open water (Area 2) are a unique way to examine ground motion and subsidence in submerged areas of the MRD. The present study is limited to platforms landward of the land-ocean interface (e.g., located in coastal bays and lakes). These are generally platforms utilized for hydrocarbon extraction, storage, or pipeline pumping or access stations. The depth of the foundation of platform piling and the time since their emplacement (e.g., settling history) are additional controls on their vertical motion. While foundation depths were unavailable for each platform, Google Earth imagery was utilized to approximately document their time of construction. Platforms were grouped into pre-and post-year 2000 to provide a general estimate of time since emplacement. All InSAR points relating to an individual platform complex (see Figure 15 for examples) were averaged to determine a mean vertical velocity (relative and absolute) for that platform.

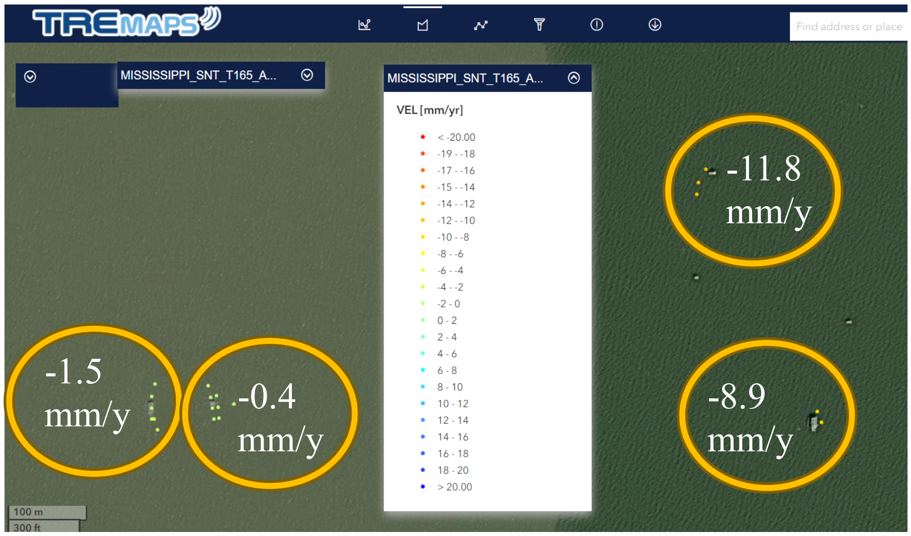

Figure 15: *An example of InSAR point cloud density and averaged relative rate of vertical motion over several platforms complexes in Barataria Bay superimposed on a Google Earth (2022) image of the platforms.*

Communities (towns and cities) (Area 3) are an amalgamation of a variety of human infrastructure including buildings and smaller road networks. This amalgamation includes features with a range of foundation depths. New Orleans and surrounding communities within the InSAR study areas were analyzed in Fiaschi et al, in prep of the study (Fiaschi et al., in prep.). For the present study, the largest community (Houma) and the only community located on a barrier island (Grand Isle) were selected, as were towns along the banks of the Mississippi River downriver of New Orleans and along major bayous that cross the MRD. The river and bayou communities were chosen because of their susceptibility to storm surges with rising relative sea levels. Communities (towns and cities) were defined by clipping points to those within their municipal boundaries as defined by the State, or, for smaller communities, by amalgamating all features within the flood-protection levees that surround these (bayou and river) communities.

The bank revetments and jetties along Southwest Pass (Area 4) are for the protection of this critical deep draft navigation channel of the Mississippi River. Jetties at the end of Southwest Pass are used as a way to funnel Mississippi River flow to reduce dredging need in this 45 ft (14 m) channel (USACE, 2011). Concrete revetments line the banks of the Mississippi River channel within and upriver of Southwest Pass to the upriver limit of the study area and are designed to stem bank erosion (USACE, 2011). As they generally extend above the high (flood) river stage, their (upper) apron provides a high coherence signal that is generally free of inundation issues.

Morganza to the Gulf (Area 5) is a hurricane and storm damage risk reduction project involving a 98-mile (158 km) alignment of earthen levees under construction in the MRD approximately 97 km southwest of New Orleans, including portions of Terrebonne and Lafourche Parish. This protection system, in addition to earthen levees, includes floodgates, environmental water control structures, road/railroad gates, and fronting protection for existing pump stations. This system is being designed to reduce the risk of damage related to flooding for the 1% Annual Exceedance Probability in these parishes where a historical deterioration of coastal marshes has led to an increased risk of inundation (USACE,2023). This system is designed to reduce the risk of damage related to flooding to approximately 52,000 structures and a population of 200,000 in an area of intense concentration of energy infrastructure near the confluence of two nationally significant navigation corridors in the Mississippi River and the Gulf Intracoastal WaterWay (USACE, 2023). Construction for Morganza to the Gulf (MTG) began in 2002 but has experienced construction delays and slowdowns due to difficulties in securing federal approval: in 2021 $4.19 billion in federal funding was allocated. Hence, in the InSAR project period (2016-2021), only certain reaches of the absolute protection system were complete or under construction. For analysis in the present study, the MTG was divided into sections (reaches), both those under construction and those not yet begun, and an average rate was defined for each reach based on all data points relating to the MTG with that reach.

The final analysis of the InSAR results utilized the entire 4.2 million data points and their subdivision into the polygons over the entire study area associated with a modeling effort by the State of Louisiana utilized for coastal restoration and protection planning. Starting with the 2017 Coastal Master Plan by the Louisiana Coastal and Protection and Restoration Authority, a numerical modeling effort was developed to provide a tool for testing and selection of proposed projects on the coastal landscape to rank benefits and any potential negative outcomes of their construction (CPRA, 2017).   This simplified representation of the Louisiana coast, referred to as the Integrated Compartment Model (ICM), subdivides the region into polygons. Each polygon is further subdivided in the model into wetland, water, and upland areas based on the modern landscape. Future predictive simulations measure the response of these components to anticipated environmental drivers (e.g., sea level rise, subsidence, etc.) and the performance of proposed protection or restoration projects tested on the coastal landscape. For the present study, the ICM polygons provide (a) a means of assessing the entire InSAR study area, and (b) results that may be able, in future Master Plan modeling efforts, to define a subsidence rate for each polygon upland area since the present InSAR results do not measure the elevation of wetland (low coherence) or open water areas. Polygon boundaries (Figure 16) are irregular and were created based on coastal hydrology, wetland, morphology, vegetation dynamics, and the suitability of habitat to support an array of fish and wildlife (CPRA,2017). All InSAR points within a polygon were assumed to relate to the upland area, which might include natural or human infrastructure), and were averaged to provide a mean value and time series of ground motion (relative and absolute) for that polygon.

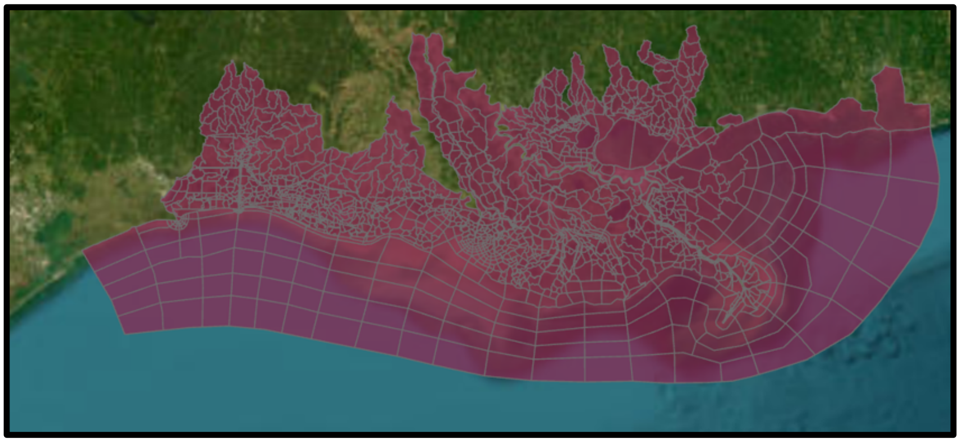

Figure 16: *2023 Coastal Master Plan Integrated Compartment Model (ICM) polygons in the MRD utilized for the InSAR analysis (CPRA,2023a).*

5. RESULTS

In the Phase 1 study, 1.1 million points were generated for the GNO study area utilizing the SqueeSAR® methodology. This utilized a coherence cutoff of 0.5 and yielded a point density of approximately 95 points/km^2. In the present study of the Phase 2 region the TRE processing yielded 4.2 million data points over the MRD study area reported as both relative and absolute rates (Figure 17). The mapped area included extensive vegetated areas (upland and wetland) as well as urbanized zones and utilized a more data that did not meet the coherence cutoff included permanently flooded areas, such as bayous, lakes, and coastal bays, as well as tidally or The coherence cutoff removing much of the coastal wetland area of the MRD from the dataset is likely due to interference from the dense and seasonally variable vegetation canopy, soil characteristics due to the intermittent (e.g., astronomical, and meteorological tide) presence of water, and other surface changes. Earthen levees that line the Mississippi River channel (MR&T levees) and hurricane protection levees were also not retained by the coherence cutoff using the TRE processing methodology, likely because of the variation in canopy height of the mowed (grass) vegetation. The areas of the MRD recorded by the Sentinel-1 processing tended to be upland areas, except for barrier island areas with relatively low vegetation cover. The results are divided below into focus areas with high temporal resolution and enough coherence to be analyzed. These include natural substrates (e.g., barrier islands), key roads and communities, protection structures (e.g., Morganza to the Gulf and Mississippi River revetments and jetties), and platforms located in coastal bays. The entire MRD study area is also analyzed for rates of vertical motion in a section below through the lens of the Louisiana Coastal Master Plan compartment model grid. All results are presented as both the relative component of vertical motion and the absolute (e.g., corrected by regional GPS station motion) as explained in the methods.

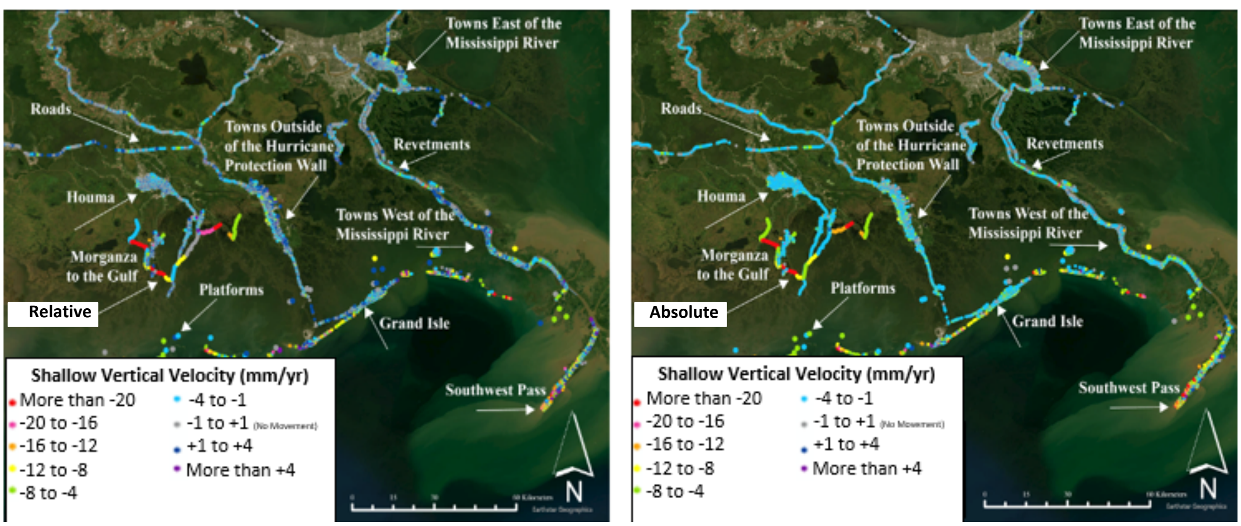

Figure 17: *Map of the MRD study area InSAR results point cloud showing an overview of the rates of relative (a) and absolute (b) vertical motion (expressed as velocities in mm/yr) and identifying locations of the focus area described in the text.*

5.1 Barrier Islands

Barrier islands line much of the coastline of Louisiana and are related to the erosive and subsidence-induced retreat of late Holocene deltaic headlands (CPRA, 2021). The barrier islands within the InSAR study area fronting Barataria and Terrebonne Bay relate to the multiple distributary accretionary phases of the Lafourche deltaic lobe (Kulp et al., 2017). Barrier islands are formed by the accumulation of sediment parallel to a coastline and are highly dynamic in location and elevation in response to the local wave and current regime and aeolian transport in non-wetted zones (Fruerggard et al., 2015). The evolution of these areas is a function of sediment transport, erosion, deposition, as well as any vertical motion induced by subsidence (Fruerggard et al., 2015). The InSAR point results were found in a subset of the main geomorphic provinces characteristic of barrier islands (Morales, 2022) that includes the (a) beachface closest to the ocean, (b) dune ridges (sand accumulation shaped by wind), (c) back-barrier platforms including maritime forest and wetlands (low-lying marshy areas behind the forest), (d) tidal inlet margins (openings connecting the ocean and back-barrier), and (e) ebb/flood tidal deltas (depositional features formed by tidal currents at the inlet). No inlet or tidal delta features were imaged directly in the TRE processing, however, hard structures (e.g., jetties, etc.) in their immediate vicinity provided vertical motion information.

Many of the deltaic-formed barrier islands of the Louisiana coast have experienced rapid retreat and degradation in the previous few decades (CPRA, 2021). As a result, the beach face, and back-barrier platforms of many islands, where the bulk of the InSAR information was imaged, have been artificially renourished using dredged sand, which can impact both substrate elevation immediately upon placement (e.g., increased elevation), and longer-term, through elevation loss through loading-induced subsidence (CPRA, 2021). To assess the impact of this on the InSAR results, the renourishment history of each island in the study area was documented before and during the imaging period from 2016 to 2021 (Table 3).

Table 3. Restoration activities conducted on Louisiana barrier islands before and during the InSAR study period (CPRA, 2021).

Island Name	Restoration from 2016-2021	Out of Time Frame (pre-2016 and post 2021)
Racoon Island	2016 (Headland beach and dune restoration, Increment 2 (BA-143)	1994, 1997, 2007, 2013
Whiskey Island	2016 (Headland beach and dune restoration, Increment 2 (BA-143)	1999, 2009, 2010
Trinity Island East	2017 (Barrier island Restoration BA-76)	1999
Timbalier Island	2017 (Restoration West NRDA BA-111)	1996, 2004
East Timbalier Island	None	2000
West Belle Pass	None	2012
Caminada Headland	None	2015, 2016
Grand Isle	None	2016, 2020
Grand Terre	None	None
East Grand Terre	None	None
Chenier Ronquille/ Chaland Headland/ Bay Joe Wise	None	2017
Shell Island	None	2013, 2017
Pelican Island	None	2007, 2010, 2012
Scofield Island	None	2013, 2010

The majority of InSAR points on the barrier islands fronting Barataria and Terrebonne Bay did not fully fit within the standard geomorphic province classification of barrier islands. Data imaged were present on three types of substrates: (1) hard structures (jetties, groins, seawalls) on or near the island and oil/gas infrastructure platforms within 1 km of the island, (2) sparsely vegetated overwash sand platforms immediately landward of the beach and primary dune ridge, and (3) the uppermost (rarely submerged) beach face (Figure 18).

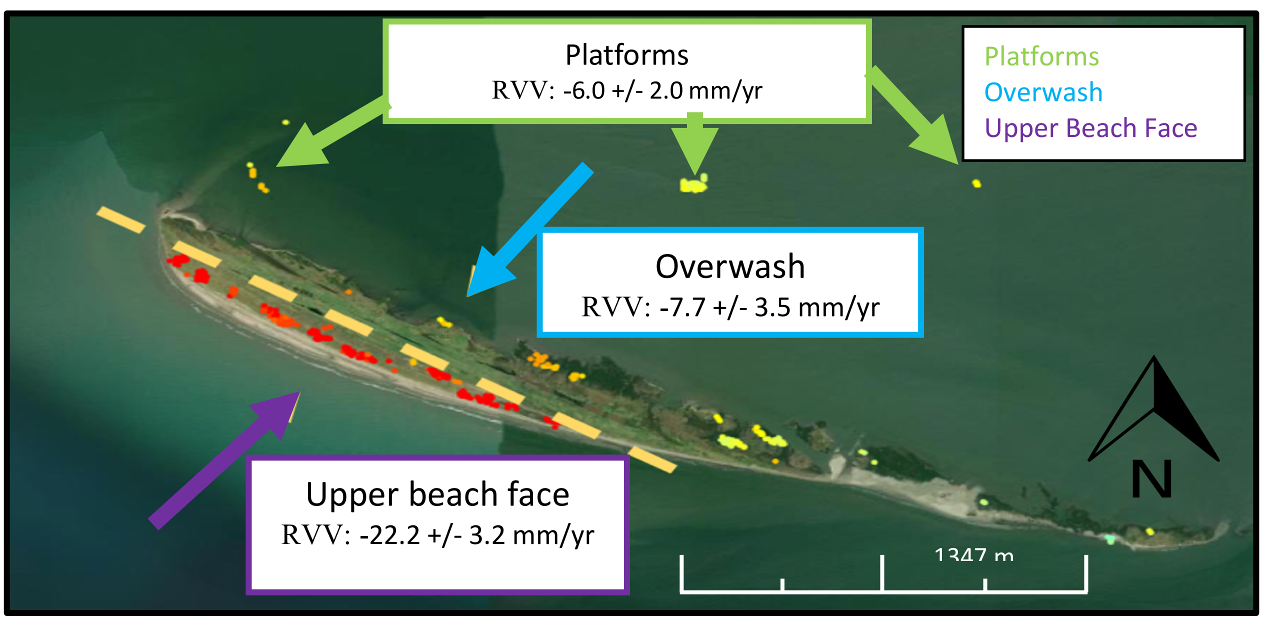

Figure 18: *Example of a barrier island setting (West Timbalier Island) and averaged relative vertical InSAR velocities where point data were available including platforms within 1 km of the island. The dotted line is an approximate dividing line between the overwash (back barrier) side) and the upper beach face (Gulf side).). RVV=Relative Vertical Velocity.*

Given that hard structures are not subject to erosional/depositional processes and their subsidence is impacted by their foundation depth and time since emplacement, vertical ground motion for these areas was treated as a separate, island-average category of results. Google Earth Pro historical imagery was utilized to determine the approximate timing of structure emplacement (pre- and post-2000). All InSAR data points for overwash and beach face areas were averaged together and presented separately for each island from the hard structures in Figures 19 and 20. Whole Island averages (combined sand and hard structures) are presented in Table 4. The beachface and overwash fans averages for each island are presented separately in Appendix 8A. Figures 19a (relative) and 19b (absolute) show InSAR- derived relative vertical velocity and absolute vertical velocity for the islands west of the Lafourche headland (Timbalier Islands) fronting eastern Terrebonne Bay. Figures 20a and 20b show the equivalent values for islands fronting Barataria Bay east of the Lafourche headland.

Table 4. *Average rates of relative and absolute vertical motion from InSAR measurements for barrier islands on the coast of Louisiana.*

Island Name	Latitude	Longitude	Total # of Points on Island	Relative VV (mm/yr)	Absolute VV (mm/yr)
Racoon Island	29.05	90.93	71	-1.5 +/- 2.2	4.4 +/- 1.9
Whiskey Island	29.05	90.79	150	-4.8 +/- 4.9	-7.0 +/- 4.2
Trinity Island East	29.05	90.71	4432	-9.2+/- 3.5	-10.7 +/-2.9
Timbalier Island	29.09	90.54	753	-11.8 +/- 6.5	-14.2 +/- 5.9
East Timbalier Island	29.07	90.33	257	-7.6 +/- 3.3	-9.1 +/- 3.3
West Belle Pass	29.10	90.26	53	1.2 +/- 7.2	-1.7 +/- 5.8
Caminada Headland	29.13	90.15	4259	-2.5 +/- 6.7	-4.7 +/- 5.6
Grand Isle	29.23	90.01	21344	-1.3 +/- 3.4	3.3 +/- 2.7
West Grand Terre	29.29	89.92	867	-0.1 +/- 2.8	-2.3 +/- 2.3
East Grand Terre	29.31	89.88	1031	-9.0 +/- 4.7	-9.5 +/- 4.2
Chenier Ronquille/ Chaland Headland/ Bay Joe Wise	29.31	89.78	2294	-6.1 +/- 6.7	-6.8 +/- 5.2
Shell Island	29.28	89.63	3	-5.3 +/- 1.34	-6.2 +/- 0.9
Pelican Island	29.25	89.58	240	-9.2 +/- 5.9	-10.5 +/- 5.5
Scofield Island	29.24	89.54	130	-17.5 +/- 2.6	-18.6 +/- 3.3
					Separated based on structures
					Analyzed island as whole

Both overwash and beachface have been treated as a combined category in results (Figure 19 and 20) for individual barrier islands in the study area (Figure 19 and 20). This was done to reflect either no significance to the results for different geomorphic settings and/or there were so few points that the error range became extreme if treated separately. However, there are significant differences between the two substrates in global averages: both the overwash and beach faces on the three islands have data that had measurably slightly higher absolute vertical velocities (-7.3 to -14 .5 mm/y). Absolute rates of vertical elevation loss (negative) were greater (more negative) on all islands studied except Grand Isle (Table 4): in all 13 of the cases, however, these differences fell within one standard deviation of error. The four islands with the greatest total elevation loss (>10 mm/yr) in 2016-2021 (Scofield, Timbalier, Trinity East and Pelican) were all either restored through sand placement within, or immediately prior to the study period (Table 3). Limited total elevation loss (< 3 mm/yr) was observed on three islands (Grand Isle, West Belle Pass, Grand Terre) (Table 4). Figures 19 and 20 show that for the six islands where both sand substrate and hard structure data are available (e.g., Whiskey, Trinity, Timbalier, Caminada Headland, West Grand Terre, Chenier Ronquille/ Chaland Headland/ Bay Joe Wise), on four of the islands sand substrates were losing elevation (total values) more rapidly than hard structures (not the case on West Grand Terre and Caminada headland). However, this difference falls within one standard deviation for all four cases (Table 4). Some islands were addressed differently if solid structures near the island presented different rates than the physical island.

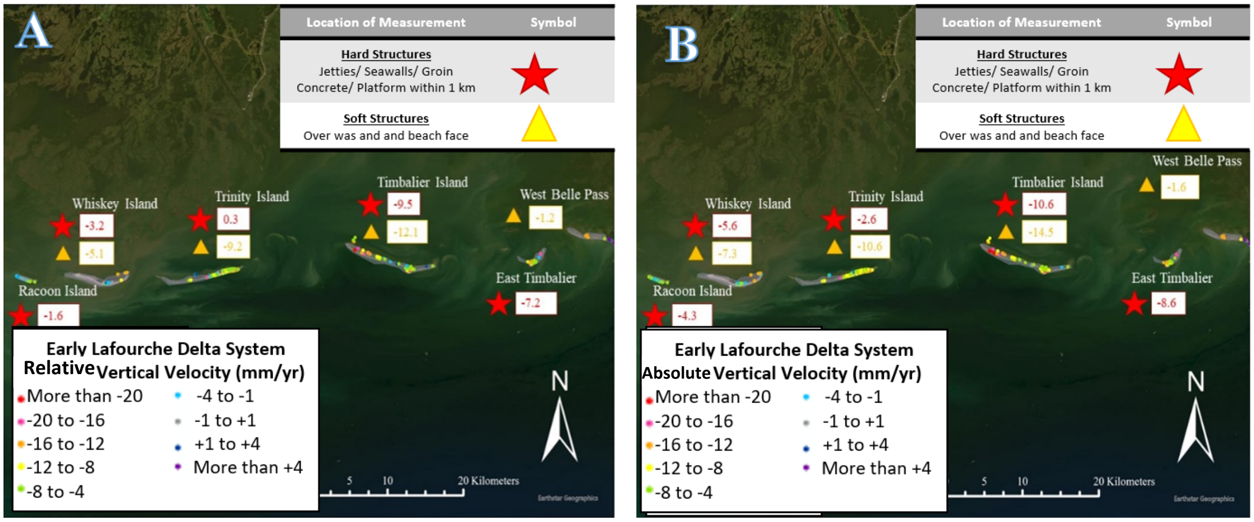

Figure 19: *Average relative (a) and absolute (b) vertical velocities (mm/yr) for the Terrebonne-fronting Western barrier islands from InSAR results.*

.

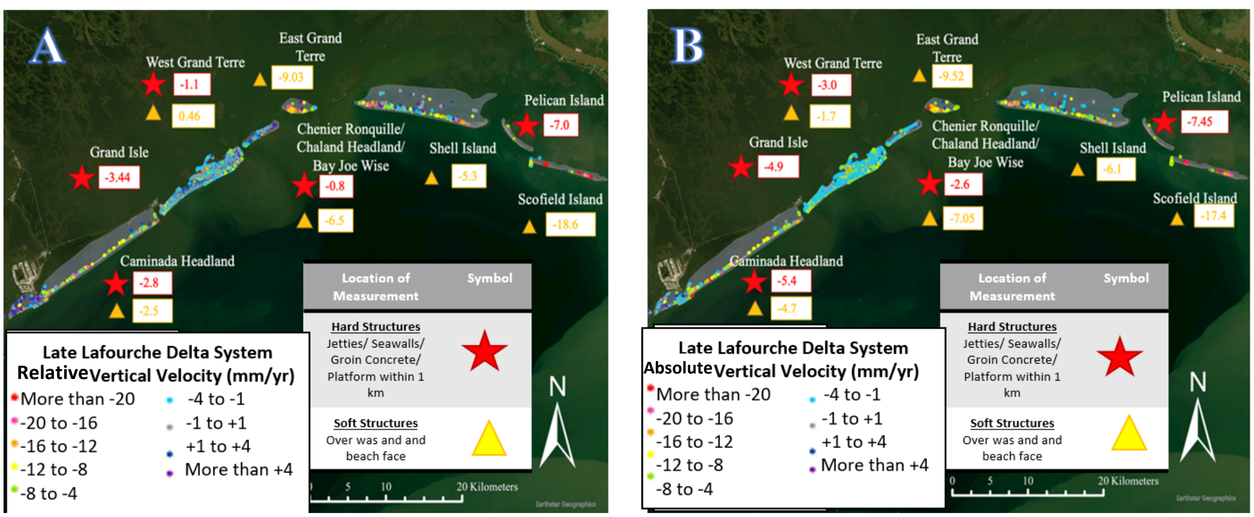

Figure 20: *Average relative (a) and absolute (b) vertical velocities (mm/yr) for the Terrebonne-fronting Eastern barrier islands from InSAR results.*

5.2 Submerged Platforms

A variety of oil and gas service and production platforms are present in the MRD study area in shallow interdistributary bays and coastal lakes (e.g., landward of the Gulf of Mexico shoreline) in addition to those in the immediate vicinity of the barrier islands (presented above in Section 5.1). Additional platforms were imaged near Venice, LA west of the Mississippi River and on the east bank of the river opposite Buras, LA (Figures 21 & 22). Relative and absolute vertical velocities were averaged for individual platforms (multiple points) or for platform complexes, where the individual platforms were separated by less than 200-300 m. Google Earth Pro historical imagery was used to subdivide results into those constructed before or after 2000 (Appendix B). This was done to assess whether the structure settling of more recently constructed platforms is a major component of the observed absolute elevation change of the platform superstructure.

Figure 21 shows relative and absolute InSAR-derived vertical velocity for the pre-2000 platforms and Figure 22 shows measurements for the post-2000 platforms. When averaged for all platforms in each of the five basins, the range of all pre-2000 five basins for relative rates is +1.9 +/- 6.4 (Mississippi Delta Basin) to -0.7 +/- 2.3 mm/yr (Brenton Sound Basin), and post-2000 range relative rates rise slightly to between -1.1 +/- 2.8 mm/yr (Terrebonne Basin) and -4.1 +/- 4.5 mm/yr (Mississippi Delta Basin) and The range for all post-2000 five basins in absolute rates is -0.7 +/- 4.9 mm/yr (Mississippi Delta Basin) to -4.3 +/- 3.6 mm/yr (Terrebonne Basin) , and post-2000 absolute rates range from -2.9 +/- 4.6 (Breton Sound) and -5.5 +/- 3.3 mm/yr (Mississippi Delta Basin).

Relative and absolute vertical velocities of motion (Table 5) in all five basins for post-2000 platforms show no significant difference (within one standard deviation of error) than those constructed pre-2000. Absolute elevation loss exceeds relative in all basins (pre- and post-2000 platforms) but again, none of these differences are statistically significant within one standard deviation. Grand averages (five basins combined) show pre 2000 relative rate of -0.4 +/- 1.4 mm/yr and absolute rate of -2.4 +/- 1.3 mm/yr. Post 2000 show a relative rate of -2.2 +/- 1.3 mm/yr and absolute rate of -3.7 +/- 1.1 This is showing an overall increase negatively between pre- and post-2000.

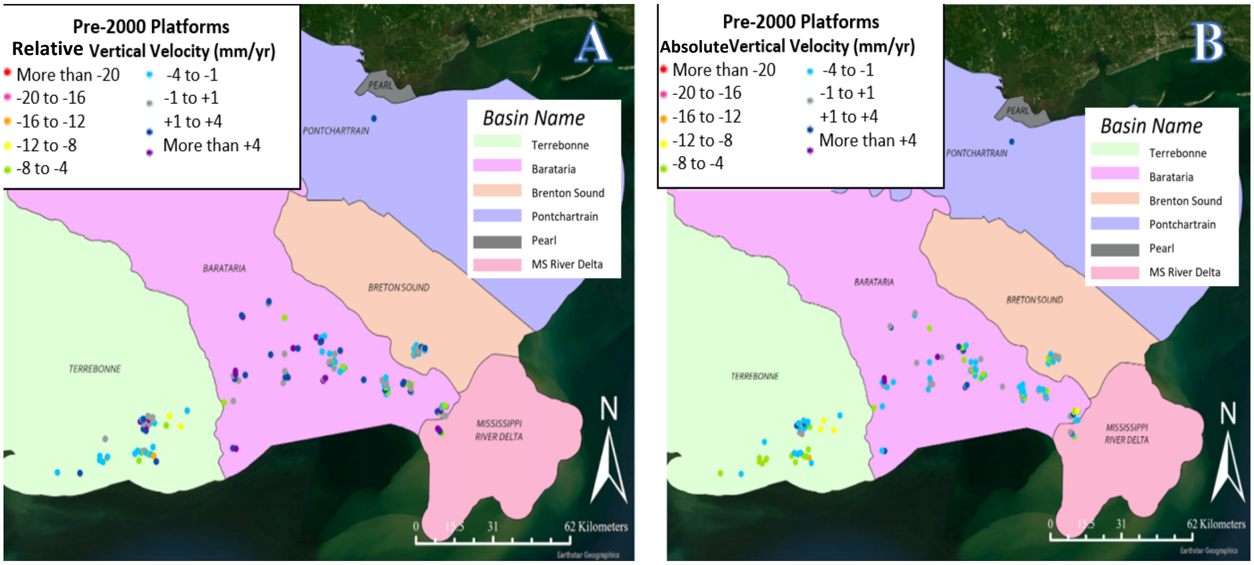

Figure 21: *Location of Pre-2000 platforms imaged by InSAR with corresponding relative (A) and absolute (B) vertical rates of motion. Locations of four basin subdivisions used to average results in Table 5 are shown.*

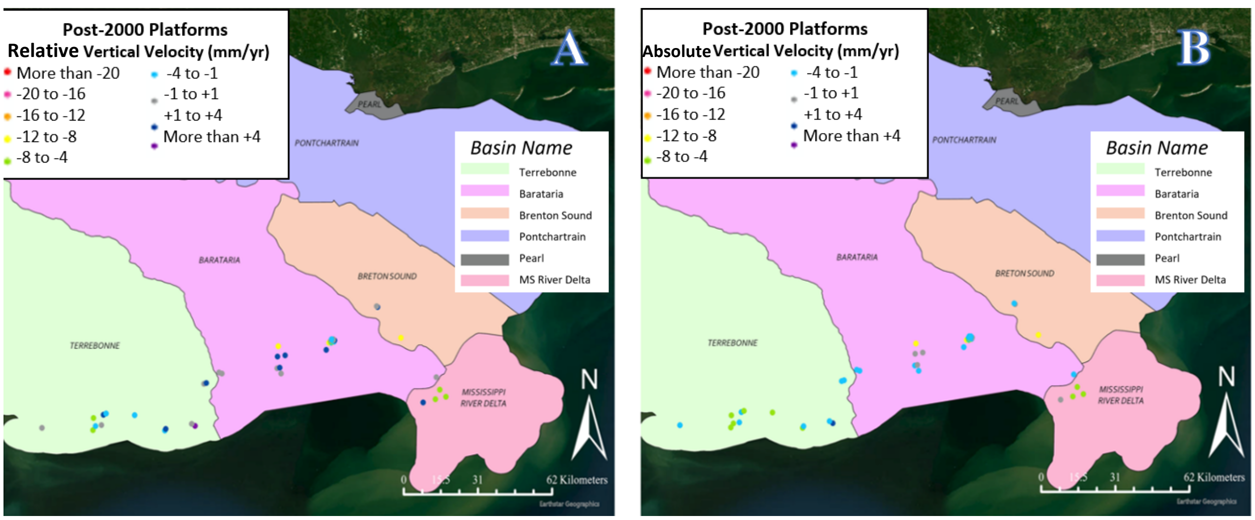

Figure 22: *Location of Post-2000 platforms imaged by in SAR with corresponding relative and absolute rates. Locations of four basin subdivisions used to average results in Table 5 are shown.*

Table 5. *Average vertical velocity rates (relative and absolute) derived from InSAR for each of the five basins analyzed and for all platforms.*

	Terrebonne Basin 41 Platforms	Barataria Basin 89 Platforms	Mississippi Delta Basin 4 Platforms	Brenton Sound Basin 23 Platforms	Ponchatrain Basin 1 platform
Pre 2000:Relative	-1. 9 +/- 4.4	-0.5 +/- 4.3	1.9 +/- 6.4	-0.7 +/- 2.3	-0.8 +/- 4.2
Pre 2000:Absolute	-4.3 +/- -3.6	-2.2 +/- 3.3	-0.7 +/- 4.9	-2.2 +/- 1.8	-2.7 +/- 3.4
Post 2000:Relative	-1.1 +/- 2.8	-1.8 +/- 3.4	-4.1 +/- 4.5	-1.7 +/- 5.9	N/a
Post 2000:Absolute	-3.4 +/- 2.2	-3.15 +/- 2.4	-5.3 +/- 3.3	-2.9 +/- 4.6	N/a

5.3 Roads

Major highways play a crucial role in facilitating hurricane evacuation efforts, ensuring the safety and well-being of coastal residents in Louisiana. With the state's vulnerability to hurricanes and tropical storms, a well-connected highway system is an essential lifeline during such emergencies. Louisiana's highways are also strategically designed and maintained to withstand severe weather conditions, ensuring their reliability during hurricane events. Thus, they provide a relatively stable substrate for InSAR analysis of ground motion, and their subsidence would progressively degrade their facility as emergency evacuation routes during high water (storm surge) events.

A selection of seven major roads--Highway 1, 23, 39, 56, 90, 300, and Interstate 10--were chosen for detailed analysis in the InSAR dataset due to their significance for emergency evacuations and their extensive spatial coverage of the MRD. Figure 22 illustrates the relative and absolute vertical motion derived from InSAR of these key roads in Louisiana. Overall, the road network exhibits relatively minimal vertical movement, with grand average values of -0.3 +/- 1.7 mm/year (relative) and -1.7 +/- 2.1 mm/year (absolute). However, when examining the four north-to-south roads that traverse the MRD (Highway 1, 23, 39, and 56). On average the four roads show an increase of approximately 0.1 mm/yr (relative) and 0.5 mm/yr (absolute) in their southern portion relative to the northern. The only noticeable increases in the major road network examined are site-specific (e.g., perturbations confined to a limited stretch of a road; Figure 23). Generally, east-west roads crossing the MRD (Highway 90, Highway 300, and Interstate 10) display relatively low rates of absolute vertical motion (< -0.6 mm/year). As with the north-to-south major roads, variations in absolute vertical motion along the path of the highway are generally relatively small (-0.1 to -0.7 mm/yr).

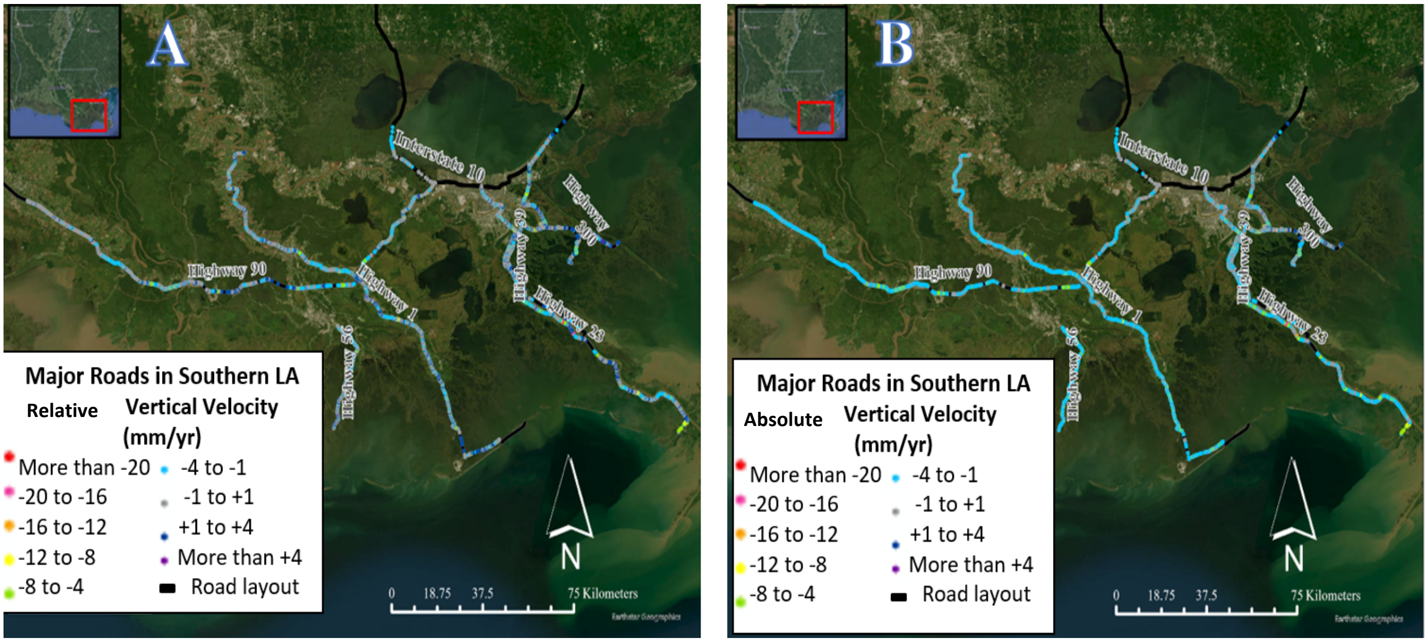

Figure 23: *InSAR (a) relative and (b) absolute vertical velocity rates measured in (mm/yr) for major roads that cross the MRD study area.*

5.4 Communities

Houma

The city of Houma, LA has a population of 31,979 (2020 US Census data) within the municipal boundary (LA DOTD) and is the largest community in the study area outside of metropolitan New Orleans, which was the focus of the Fiaschi et al, in prep study. An absolute of 131,653 InSAR data points were obtained within the boundaries of the City of Houma (LA DOTD). The layout of the city of Houma indicates that most of the urban areas of high coherence are associated with structures and roads along Highway 24 corridor (Figure 24 a and b). Non-urban areas within the city limits are clustered mainly within the Mandalay National Wildlife Refuge (Figure 24 a and b). InSAR results are recorded in the southern portion around Houma-Terrebonne Airport excepting those areas that are permanent water, including Bayou Petit Gallio.

Overall, the city of Houma has an average relative vertical velocity rate of 0.3 +/- 1.5 mm/yr (Figure 24a). The absolute average vertical velocity rate of motion is (Figure 24b) -2.3 +/- 1.4 mm/yr, ranging from a minimum elevation loss rate of -29.5 mm/yr to a maximum uplift of 9.1 mm/yr. Areas that experience the most significant absolute ground elevation loss (> -10 mm/y) include the banks of the Gulf Intercoastal Waterway (GIWW) Figure 23b), and the southwestern region of the city along the port facilities in the intercoastal waterway (red box in Figure 23). Other areas that experience absolute ground elevation loss above >-5 mm/yr are along major roads leading to multiple manufacturing businesses along the GIWW. Terrebonne Airport and neighborhoods extending off Highway 24 in the city center tend to have higher than average absolute elevation loss rates (-2 to -5 mm/yr) compared to other urbanized parts of the city. There is an area of apparently high absolute elevation loss (-5 to -10 mm/yr) along the eastern portion of the Mandalay National Wildlife Refuge in an area apparently covered in vegetation and is broken by areas of permanent water (Figure 24b).

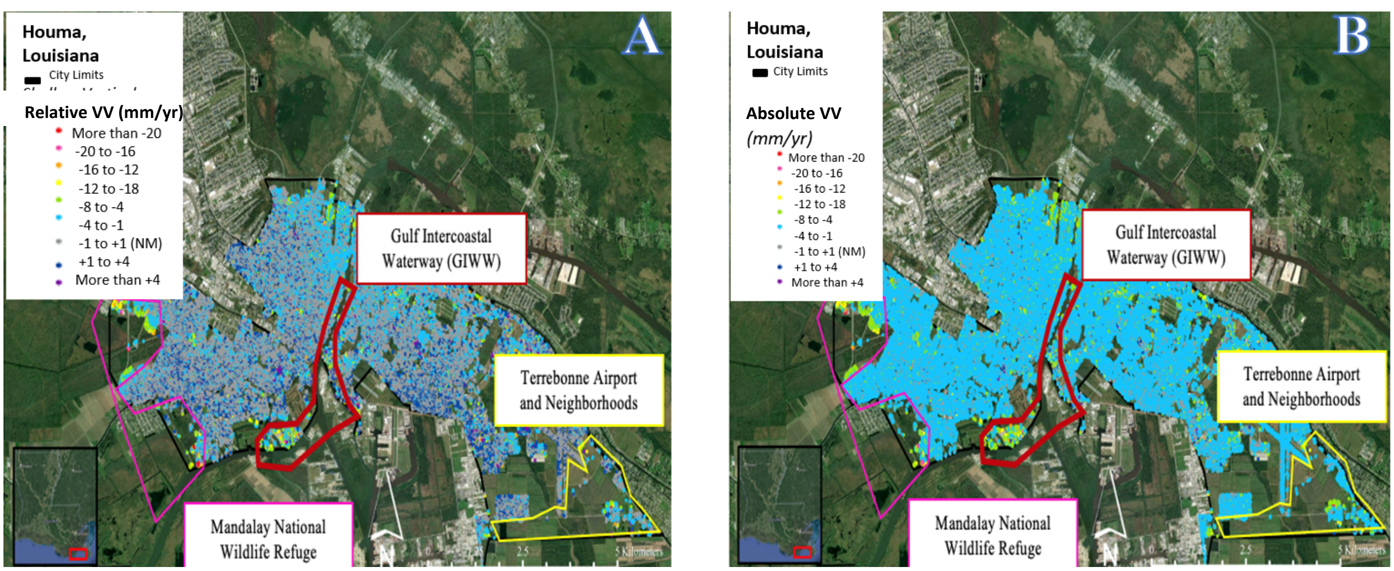

Figure 24*: Houma city boundaries with corresponding relative (a) and absolute (b) vertical velocity rates measured in mm/yr defined by the InSAR results.*

Grand Isle

The town of Grand Isle, Louisiana, holds significant importance in coastal resiliency efforts due to its vulnerability to the impacts of climate change and coastal erosion as the only permanently inhabited low-elevation barrier island in the study area. The structures on Grand Isle, each with a depth of foundation, and small paved roads form the main InSAR targets within the town's boundaries. Grand Isle is also categorized into the barrier island section above, but these elements (e.g., structures and roads) were not included in that analysis of InSAR results. The average relative vertical velocity for the town (LADOTD limits) is -0.8 +/- 2.8 mm/y, and the absolute vertical velocity is -2.9 +/- 2.2 mm/y. Areas with significant total vertical motion -5 mm/yr to >-20 mm/yr) are present near the eastern Gulf side of the island and on the back side of the central section of the island (Figures 25a and 25b). On the extreme western end of the island opposite Caminada Pass, rates are also high (relative -7.2 +/- 2.6 mm/y; absolute -7.6 +/- 2.2 mm/y).

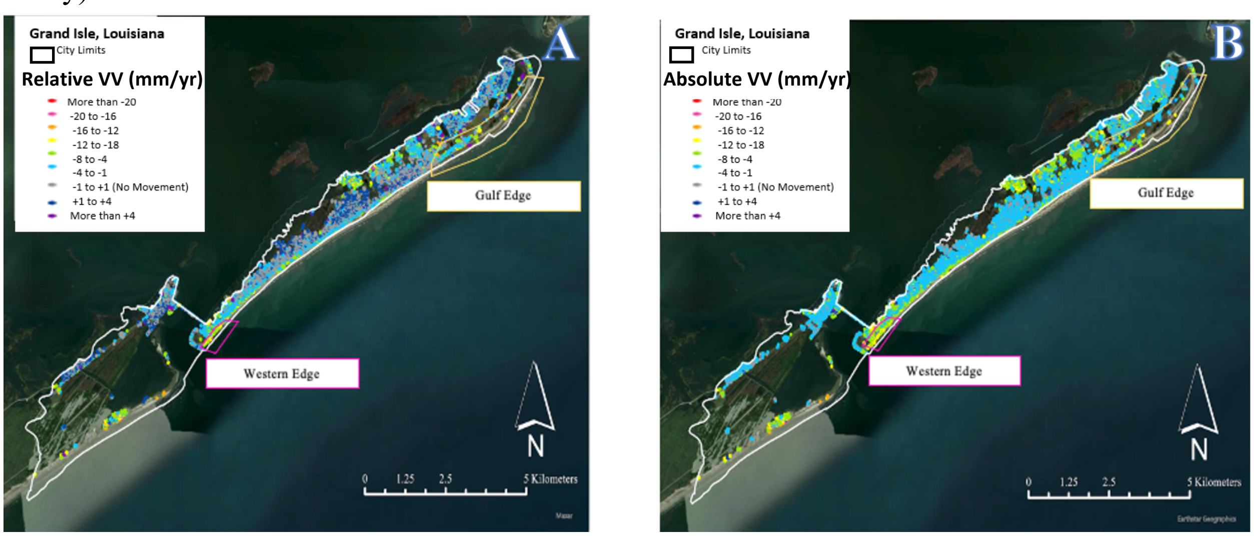

Figure 25: *Grand Isle city boundaries with corresponding (a) relative and (b) absolute vertical velocity rates measured in mm/yr from the InSAR results.*

Southern Bayou Communities

Communities along the southern section of the Highway 1 corridor formed by the Bayou Lafourche headlands (Larose to Golden Meadow, LA) are protected from storm surges by an earthen levee that contains much of the built infrastructure. Similar hurricane protection levees of differing elevations protect MRD communities along Bayou Grand Caillou (Dulac), Bayou Terrebonne (Montegut to Chauvin), and Bayou Barataria (Jean Lafitte to Lafitte) (Figure 25). While the levee itself did not provide InSAR results of these features using the TRE methodology, vertical velocities are recorded for the structures and roads within the protection levees. In general, rates in all InSAR imaged communities (Figure 26) are relatively low (less than an average of -3 mm/yr absolute vertical motion). The average relative vertical velocity for the leveed area of Bayou Grand Caillou is -0.2 +/- 0.7 mm/y, and the average absolute velocity is -2.6 +/- 1.8 mm/y. Bayou Terrebonne protected communities have an average relative velocity of -0.3 +/- 1.7 mm/yr and an absolute of -2.5 +/- 1.1 mm/yr. Bayou Lafourche communities have an average relative vertical velocity of -0.25 +/- mm/yr and an absolute average velocity of 0.2 +/- 3.3 mm/yr. Bayou Barataria communities have an average relative velocity of -0.1 +/- 3.3 mm/yr and an average absolute velocity of -0.5 +/- 1.7mm/yr.

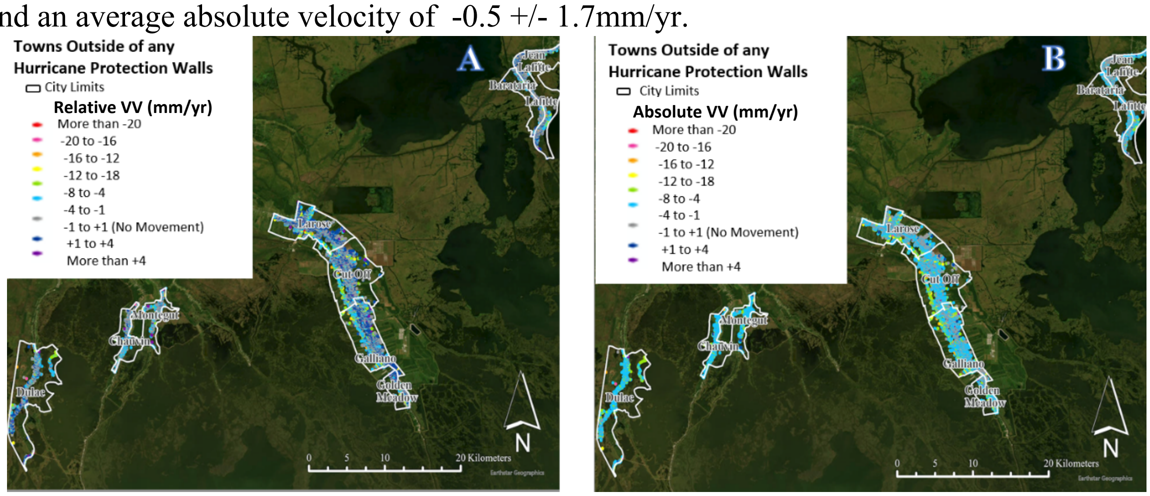

Figure 26*: Southern Bayou communities surrounded by protection levees within the MRD with corresponding (a) relative and (b) absolute vertical velocity rates measured in mm/yr by InSAR.*

Lowermost Mississippi River Communities

Communities along both banks of the Mississippi River extend downriver from Greater New Orleans to as far as Venice, LA along the right descending bank. The upstream section of this area of InSAR interest is bounded by the Hurricane and Storm Damage Risk Reduction System (HSDRRS) flood wall that encloses the city of New Orleans and the surrounding areas of Jefferson and St. Bernard Parish and was analyzed in the Fiaschi et al, in prepstudy (Fiaschi et al., in prep.). The present (Present study) effort focused on the river-side communities downstream of the HSDRRS with some exceptions along the left-descending bank. On the left-descending bank, the communities were analyzed from the Orleans-St. Bernard Parish line to the end of Highway 39 and the levee protection system near Bohemia, LA. This includes several communities within the HSDRRS (e.g., Arabi, Chalmette, Violet). These communities were also analyzed in Fiaschi et al, in prepof this study but are included for comparative purposes. Communities along the river (right and left descending banks) downriver of the HSDRRS are protected from river floods by the Mississippi River and Tributaries (MR&T) reinforced earthen levee, and on the bay/Gulf side are protected from hurricane storm surges by earthen "back levees". The MR&T and back levees were not imaged by InSAR so results reported herein are for the minor roads and structures within the bounding levees excluding the major roads (reported in Section 5.3) that traverse the left descending (Highway 39) and right descending (Highway 23) bank of the Mississippi River.

Towns on the East (left descending) bank of the Mississippi River have an average relative vertical velocity (Figure 27a) rate of -0.4 +/- 1.5 mm/yr and an absolute vertical velocity (Figure 27b) rate of -1.0 +/- 1.6 mm/yr as measured from InSAR data. Towns along the upriver section of this bank (Arabi, Chalmette, Meraux, Violet, and Poydras) have an average relative vertical velocity of -0.2 +/- 1.1 mm/yr and an average absolute vertical velocity of -0.5 +/- 1.5 mm/yr (Table 6). Towns on the West (right descending) bank of the Mississippi River have an average relative vertical velocity (Figure 28a) rate of -0.35 +/- 1.7 mm/yr and an absolute vertical velocity (Figure 28b) rate of 2.0 +/- 1.9 mm/yr. These rates are presented in Table 7.

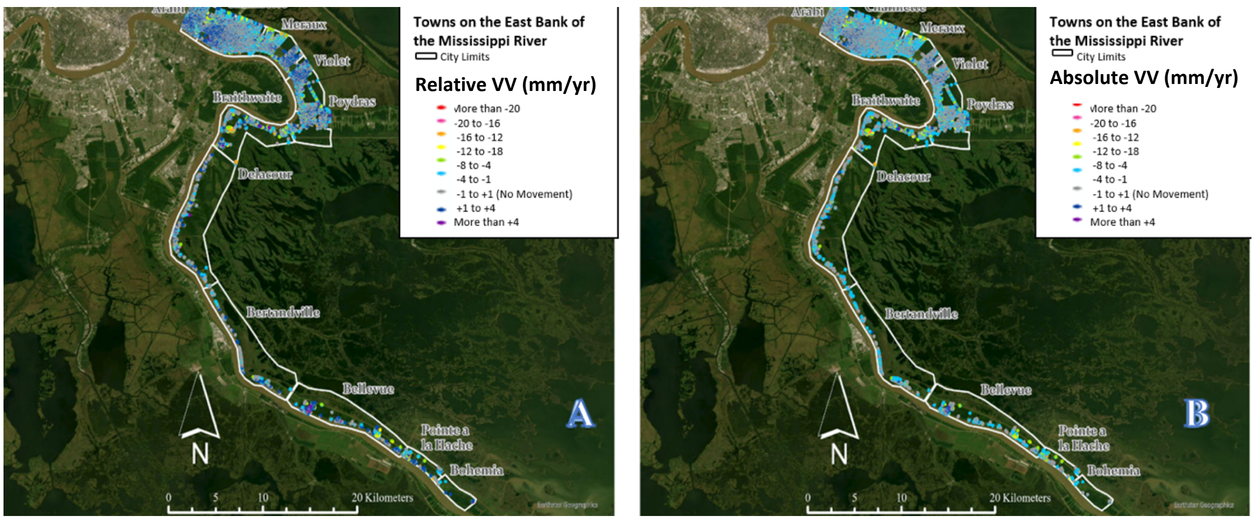

Figure 27*: East bank of the Mississippi River city boundaries with corresponding relative(a) and absolute (b) vertical velocity rates measured in (mm/yr).*

Table 6. *Average relative and absolute vertical velocity rates derived from InSAR for each of the East bank towns analyzed.*

Town Name (Moving Downstream)	Relative VV (mm/yr)	Absolute VV (mm/yr)
Arabi	0.3 +/- 1.1	-0.2 +/- 1.7
Chalmette	-0.1 +/- 0.7	-0.5 +/- 0.1
Meraux	-0.3 +/- 0.7	-0.8 +/- 2.1
Violet	0.1 +/- 1.1	-0.4 +/- 0.7
Poydras	-0.1 +/- 1.9	-0.6 +/- 3.1
Braithwaite	-1.4 +/- 2.2	-1.8 +/- 1.1
Delacour	-0.1 +/- 1.1	-1 +/- 2
Bertandville	-0.9 +/- 0.7	-1.9 +/- 0.9
Bellevue	-2.2 +/- 2.8	-3.0 +/- 3.1
Pointe a la Hache	-1.2 +/- 2.9	-2.3 +/- 2
Bohemia	1.3 +/- 1.1	-0.45 +/- 0.7

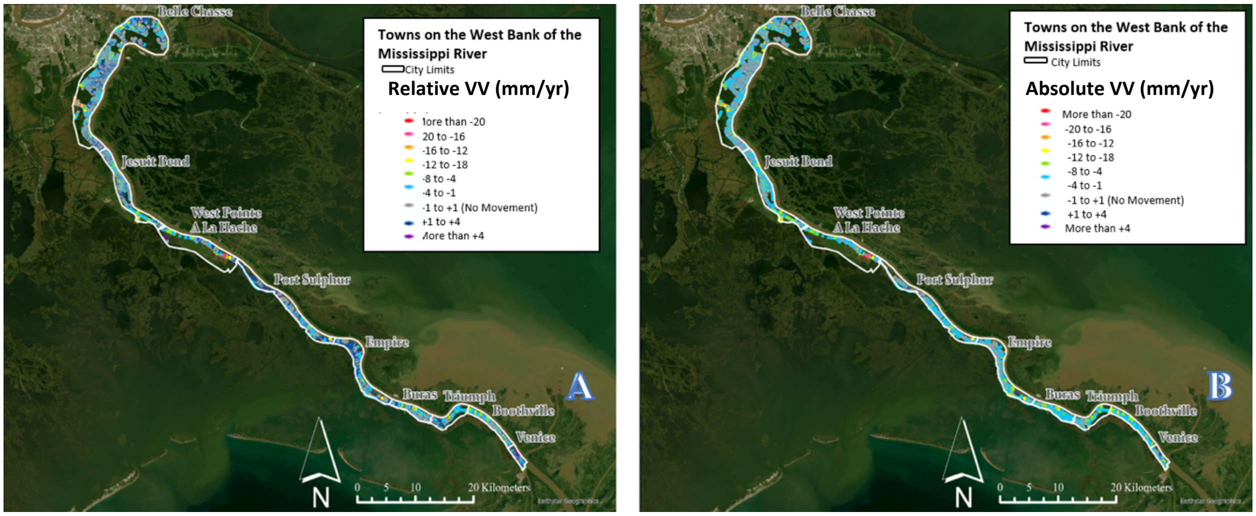

Figure 28: *West bank of the Mississippi River city boundaries with corresponding relative(a) and absolute (b) vertical velocity rates measured in mm/yr using InSAR.*

Table 7. *Average relative and absolute vertical velocity rates derived from InSAR for each of the West bank towns analyzed.*

Town Names (Moving Downstream)	Relative VV (mm/yr)	Absolute VV (mm/yr)	STDV Relative	STDV Absolute
Belle Chasse	-0.6 +/- 2.5	-1.3 +/- 2	2.5	2
Jesuit Bend	-1 +/- 2.8	-2 +/- 2.3	2.8	2.3
West Pointe A La Hache	-0.9 +/- 3.9	-2.2 +/- 3.4	3.9	3.4
Port Sulphur	-0.5 +/- 1.8	-1.9 +/- 2	1.8	2
Empire	-0.2 +/- 0.5	-1.9 +/- 1.4	0.5	1.4
Buras	-0.5 +/- 0.7	-2.2 +/- 0.6	0.7	0.6
Triumph	-0.4 +/- 0.9	-2.1 +/- 2.3	0.9	2.3
Boothville	-1.1 +/- 1.7	-2.6 +/- 2	1.7	2
Venice	0.6 +/- 0.7	-1.4 +/- 1.1	0.7	1.1

5.5 Morganza to the Gulf

Morganza to the Gulf is a critical flood protection and coastal restoration project in the central MRD aimed at reducing the risk of devastating flooding and mitigating the impact of coastal wetland erosion experienced by the region in the past ~80 y (USACE, 2023). This engineered system is composed of a series of levees, floodgates, and other infrastructure measures that stretches from the Morganza Floodway on the MR&T to the edge of Cut Off, Louisiana where Hwy 3235 and 3161 meet. Morganza to the Gulf is separated into reaches that have been constructed in stages staggered in time. These reaches are used to categorize the InSAR vertical motion: rates in each reach are shown in Table 8 and in map form with relative vertical velocity (Figure 29a) and absolute vertical velocity (Figure 29b). Areas that have most recently experienced construction activities (2016-2021) have relatively high rates of vertical motion (Reach E = -25.2 +/- 8.1 mm/y [absolute] and -20.4 +/- 9.1 mm/y [relative]; Reach G2 = 26.9 +/- 8.7 [absolute] and -21.7 +/- 9.7 [relative], J2a = -17.0 +/-13.1 [absolute] 14.1 +/- 8.1 [relative], and J3 = -27.6 +/- 11.1 [absolute] and -24.7 +/- 9.8 [relative]). Areas that have not been under construction within the InSAR period or were constructed before 2016 have lower rates of vertical motion (Reach F = -2.0 +/- 1.1 [absolute] and -4.1 +/- 3.3 [relative] Reach H2 = -2.3 +/- 1.7 [absolute] -4.4 +/- 1.7 [relative], Reach I = -0.9 +/- 0.1 [absolute] and -3.1 +/- 0.9 [relative]). In general, roads or bridges within the reach averages have lower rates of motion (~ -1.5 to +/- 2.5 mm/yr) than relatively unvegetated areas of the earthen levee itself (-5.5 to -7.5 mm/y).

Table 8. *Rates of relative and absolute vertical motion from InSAR for individual reaches of the Morganza to the Gulf protection system.*

Reach Name	Relative Vertical Velocity (mm/yr)	Absolute Vertical Velocity (mm/yr)
Reach J2a	-24.7 +/ 14.1	-27.6 +/- 17.1
Reach K	-5.27 +/ 9.1	-5.2 +/ 9.1
Reach E	-20.4 +/ 10.8	-25.2 +/ 11.2
Reach J3	-14.2 +/ 9.8	-14.7 +/10.5
Reach I	-0.1 +/1.8	-0.9 +/ 2.5
Reach J2	-14.1 +/ 13.9	-17.0 +/ 14.1
Reach F	-2.1 +/ 1.8	-2 +/ 2.1
Reach B	-2.1 +/ 2.8	-2.3 +/- 3.9
Reach H2	-2.4 +/ 2.2	-2.3 +/ 3.1
Reach G2	-21.7 +/ 14.8	-26.9 +/ 15.1
Reach G1	-6.1 +/ 6.7	-6.2 +/-5.1
Reach H3	-8.2 +/ 7.6	-8.1 +/ 6.4
Reach F1	-7.9 +/ 9.3	-8.2 +/ 8.1
Reach H1	-8.2 +/ 9.7	-8.6 +/ 9.1
Levee Barrier Plan	N/A	N/A
Reach A	N/A	N/A
Reach J1	N/A	N/A
Reach L	N/A	N/A

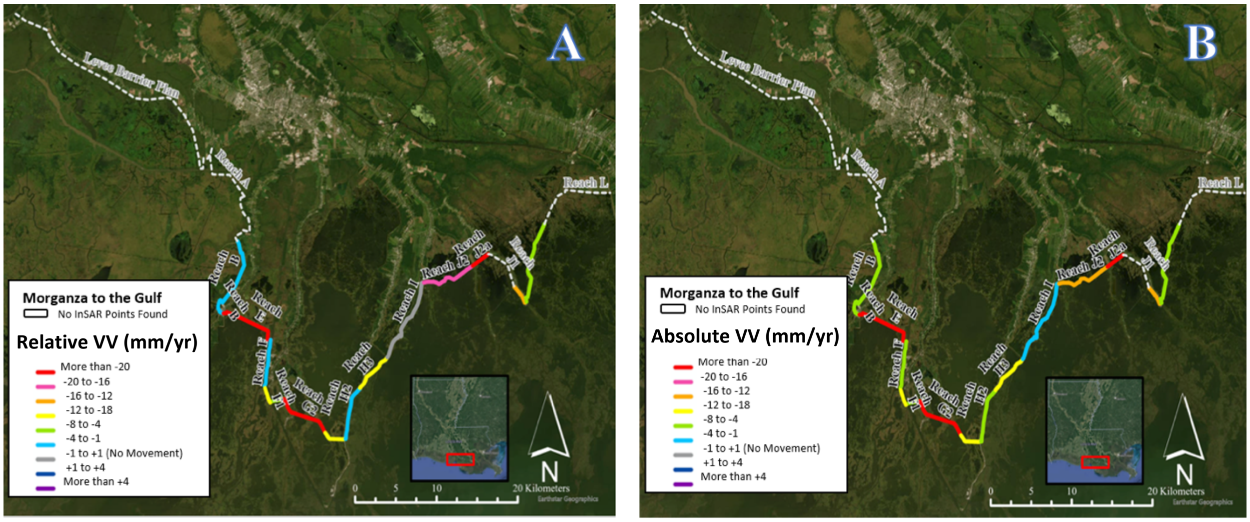

Figure 29: *Morganza to the Gulf rates of relative and absolute vertical velocity (mm/yr) averaged for each reach from the InSAR results.*

5.6 Lowermost Mississippi River Revetments and Jetties

The deepwater navigation channel in the Mississippi River is maintained at a 40 ft (12.2 m) depth from New Orleans to the mouth of Southwest Pass (SWP). Revetments have been constructed along the Mississippi River to protect the riverbanks from erosion and help maintain a consistent channel width, allowing for safe and efficient navigation. These revetments are engineered structures made of concrete mats, rocks (rip-rap), or other materials that armor the riverbanks, providing stability to resist the erosive forces of the flowing water. Below the Head of Passes trifurcation of the navigation channel of the Mississippi River, the navigation channel continues within the westernmost (Southwest Pass) channel. Rock revetments line this channel as well as stone and timber pile groins that narrow the flow path to reduce dredging needs. The revetment-groin system is extended offshore at the mouth of Southwest Pass using rock jetties. All of these features were imaged by the Sentinel-1 InSAR in 2016-2021 and were referred to Google Earth Pro to be placed in a construction/emplacement time frame.

The rock jetties (Figure 30) on the eastern side of Southwest Pass have a lower rate of vertical motion (relative -3.9 +/- 1.1 mm/yr and absolute -5.6 +/- 2.2 mm/yr) compared to west side jetties (Figure 31) (relative -7.2 +/- 3.3 mm/yr and absolute -8.1 +/- 2.2 mm/yr). The structures built along the Southwest Pass reach of the navigation channel have lower rates than the jetties (relative -1.2 +/- 0.8 mm/yr and absolute -3.4 +/- 1.1 mm/yr.): these rates (both relative and absolute) increase toward the mouth of the pass (e.g., offshore). Ground surface points along Southwest Pass, likely from recent dredge spoiling with low vegetation cover, have a much higher rate of vertical motion than the other types (relative -30.1+/- 17.3 mm/yr; absolute -26.1 +/- 19.1 mm/yr) (Table 9).

The rock jetties (Figure 30) on the eastern side of Southwest Pass have a lower rate of vertical motion (relative -3.9 +/- 1.1 mm/yr and absolute -5.6 +/- 2.2 mm/yr) compared to west side jetties (Figure 31) (relative -7.2 +/- 3.3 mm/yr and absolute -8.1 +/- 2.2 mm/yr). The structures built along the Southwest Pass reach of the navigation channel have lower rates than the jetties (relative -1.2 +/- 0.8 mm/yr and absolute -3.4 +/- 1.1 mm/yr.): these rates (both relative and absolute) increase toward the mouth of the pass (e.g., offshore). Ground surface points along Southwest Pass, likely from recent dredge spoiling with low vegetation cover, have a much higher rate of vertical motion than the other types (relative -30.1+/- 17.3 mm/yr; absolute -26.1 +/- 19.1 mm/yr) (Table 9).

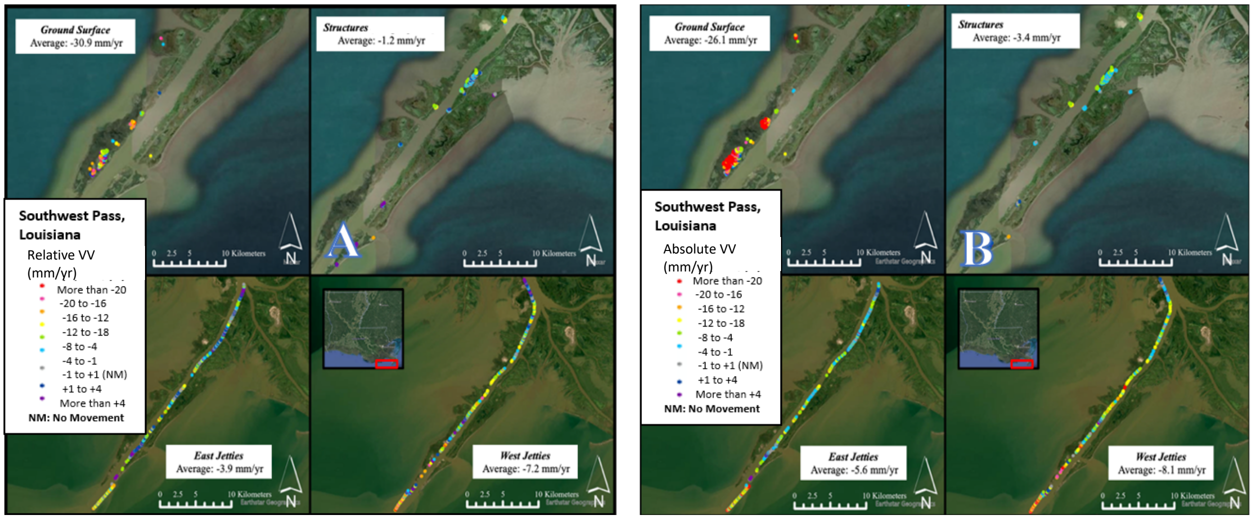

***Figure 30**: Southwest Pass InSAR relative (a) and absolute (b) vertical velocity rates measured in mm/yr for three types of substrates (e.g., jetties, ground surface, and constructed facilities.*

The revetments that line both banks of the Mississippi River above Head of Passes (River Mile 0) (Figure 31) have vertical motion rates increase downriver in general although only selected segments were imaged by InSAR. The highest rates were found on the left descending bank near Tropical Bend and Buras (relative -4.0 +/- 0.3 mm/yr; absolute -6.0 +/- 0.8 mm/yr). Averaged over the entire reach along both banks, the relative vertical velocity was -0.1 +/- 3.0 and the absolute vertical velocity was -1.5 +/- 2.3 mm/yr.

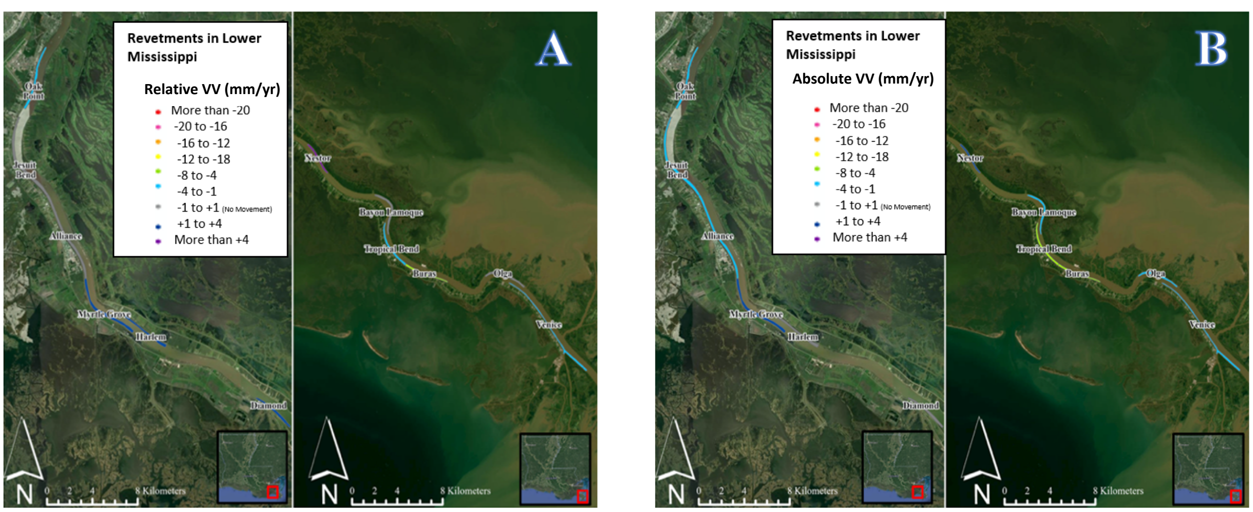

***Figure 31:** Revetments rates of (a) relative and (b) absolute vertical velocities measured in mm/yr using InSAR for the reach from Greater New Orleans to the Head of Passes.*

Table 9. *Defined revetment reaches shown in Figure 10s with rates of vertical motion values along Lower Mississippi River.*

Revetment Name	Relative Vertical Velocity (mm/yr)	Absolute Vertical Velocity (mm/yr)	Data Point Count
Oak Point	-1.6 +/- 0.7	-2.1 +/- 1.1	44
Harlem	1.2 +/- 0.9	-0.3 +/- 0.8	44
Nestor	6.5 +/- 4.4	3.5 +/- 4.1	3
Bayou Lamoque	0.1 +/- 2.2	-1.6 +/- 0.8	26
Olga	-0.9 +/- 0.9	-2.4 +/- 0.7	9
Myrtle Grove	3.1 +/- 1.1	1.1 +/- 1.2	10
Tropical Bend	-3.9 +/- 1.8	-4.8 +/- 1.9	15
Jesuit Bend	-0.6 +/- 0.4	-1.5 +/- 0.8	2
Buras	-4.7 +/- 2.2	-5.3 +/- 2.1	12
Alliance	-0.8 +/- 2.9	-1.8 +/-3.1	384
Diamond	1.2 +/- 0.1	-0.5 +/- 1.1	4
Venice	-1 +/- 0.8	-1.4 +/- 2.2	4

6. DISCUSSION

6.1 Spatial Trends in InSAR Rates of Vertical Ground Motion in the MRD

The subdivision of InSAR absolute rates of vertical motion into ground target types can be amalgamated to determine whether there are spatial trends that can be directly related to subsidence across the MRD (Table 10). Much of the imaged study area can be classified as relatively stable (rates between ~ -3 and ~ +3 mm/yr) in terms of absolute vertical motion. These include all the major roads and community infrastructure (buildings and minor roads) examined except Grand Isle (absolute = 3.0 mm/yr). Areas of high negative vertical motion (>-3 mm/yr) include infrastructure in Southwest Pass (jetties, structures pass revetments) that reaches -13 mm/yr, barrier islands (and the structures and minor roads on Grand Isle), submerged platforms (pre- and post-2000), and sections of the Morganza to the Gulf (MTG) protection system that has been constructed recently (Table 8).

Table 10. *InSAR averages absolute vertical motion of general study areas of focus in decreasing magnitude from largest negative to largest positive rates.*

Section	Location Name	Absolute Vertical Velocity (mm/yr)
MR Revetments and Jetties	SW Pass	-12.9 +/- 8.1
Barrier Islands	Eastern Barrier Islands	-9.0 +/- 6.3
Morganza to the Gulf	Morganza to the Gulf	-7.4 +/- 2.4
Barrier Islands	Western Barrier Islands	-3.7 +/- 1.1
Platforms	Post-2000	-3.5 +/- 2.3
Platforms	Pre-2000	-3.2 +/- 0.8
Communities	Grand Isle	-3.0 +/- 2.7
Roads	Highway 56	-2.7 +/- 1.1
Communities	Houma	-2.3 +/- 0.8
Communities	Towns on MR West Bank	-2.1 +/- 3.3
Roads	Highway 90	-2.0 +/- 1.2
Communities	Towns outside HPW	-2.0 +/- 4.4
Roads	Highway 1	-1.9 +/- 2.8
MR Revetments and Jetties	Revetments south of GNO	-1.8 +/- 0.9
Roads	All Roads	-1.7 +/- 0.4
Roads	Highway 300	-1.5 +/- 3.3
Roads	Highway 23	-1.4 +/- 0.2
Roads	Highway 39	-1.1 +/- 1.1
Roads	Interstate 10	-0.6 +/- 0.1
Communities	Towns on MR East Bank	-0.6 +/- 1.7
Roads	Highway 46	0.1 +/- 0.7

MR Revetments and Jetties
Barrier Islands
Platforms
Communities
Roads
Morganza to the Gulf

Of the features in the MRD in relatively rapid vertical motion, barrier islands and the MTG likely may contain within the InSAR elevation signal changes that are due to soil/sediment removal or addition. In the case of barrier islands, this is likely natural sediment transport by wind and water, except along those islands recently renourished. Sand added on the island through restoration practices is an additional factor on selected islands (see Table 3) and may result in a direct elevation change of the island at the time of sediment placement. Post-placement, this may also result in a non-steady state (declining through time), loading-induced elevation loss on the island due to the weight of new material compacting the underlying Holocene sediments (CPRA, 2021). Those islands that have been recently renourished (after 2016) have slightly higher rates of absolute vertical velocity rates (-6.9 +/- 8.1 mm/yr) compared to the absolute rates that were not replenished of (-6.6 +/- 6.0mm/yr). MTG shows rapid absolute vertical motion (average -18.2 +/- 8.8 mm/yr) in those sections where construction was during or immediately before (post-2000) the InSAR imaging period (Table 10). This construction activity varies from reach to reach and takes the form of bridge construction, the importation of non-native sediment for levee construction, and the excavation of extant (USACE, 2021). Areas of the MTG that have not had any construction activity during our time frame have an average absolute vertical motion of only -6.9 +/- 8.1 mm/yr. Similar to barrier islands, when these construction methods result in the addition of new material, this may be expected to secondarily compound elevation.

Table 11. *History of MTG construction for each reach with time-averaged absolute vertical velocities over the InSAR monitoring period.)*

Reach Name	Data Point Count	Absolute Vertical Velocity (mm/yr)	Comments
Reach J2a	8	-27.6 +/- 17.1	Construction between 2012 to 2015, during this time a gate was built in 2015. Replenished in 2020.
Reach K	70	-5.2 +/ 9.1	Construction from 2012 to 2016,during this time a gate was built in 2016. Replenished in 2020.
Reach E	79	-25.2 +/ 11.2	Construction between 2015-2018, during this time 2 bridges/gates were bult under the road.
Reach J3	80	-14.7 +/10.5	Construction between 2012-2016.
Reach I	584	-0.9 +/ 2.5	Constructed during 2010, with a gate being built this time.
Reach J2	135	-17.0 +/ 14.1	Construction between 2007-2010, and a gate was built from 2011 to 2012.
Reach F	171	-2 +/ 2.1	Construction between 2012-2015, during this time a gate was built in 2012.
Reach B	8	-2.3 +/- 3.9	Reach was built in 2007 with most construction ongoing till sometime between 2012 - 2015. Renourished from 2010-2011, and spring of 2021.
Reach H2	641	-2.3 +/ 3.1	Constructed between 2012-2015, during this time a gate was built in 2012.
Reach G2	136	-26.9 +/ 15.1	Construction between 2012-2015, during this time a gate was built in 2012.
Reach G1	43	-6.2 +/-5.1	Construction between 2012-2015, during this time a gate was built in 2012.
Reach H3	646	-8.1 +/ 6.4	Constructed between 2007-2010, and a gate was built from 2011 - 2012.
Reach F1	384	-8.2 +/ 8.1	Construction between 2012-2015, with a gate being built in 2012.
Reach H1	111	-8.6 +/ 9.1	Canal was built between Reach H1 and G2 during 2012 to 2015.
Levee Barrier Plan	N/A	N/A	No work conducted
Reach A	N/A	N/A	No work conducted
Reach J1	N/A	N/A	No work conducted
Reach L	N/A	N/A	No work conducted
		Average AVV (mm/yr)	
		-18.2	Construction/replenishment during time frame (January 2016-January 2021)
		-9.2	Construction/replenishment outside of time frame
			Not constructed

Large man-made structures (e.g., submerged platforms and infrastructure in SW Pass) have absolute rate areas where the signal is not complicated by soil addition/subtraction (e.g., Morganza to the Gulf and barrier islands), and hence, may be among the best indicators of where ground motion may equate with natural subsidence of the Holocene and deeper substrate. Platforms were divided between pre- and post-2000 emplacement in Table 5 and there is no difference between pre-and post-2000 absolute elevation loss rate (pre-2000 platforms absolute average -3.2 +/- 0.1 mm/yr and post-2000 platforms absolute of -3.5 +/- 0.1 mm/yr). This suggests limited movement by foundation piling settling immediately post-construction, likely because foundation pilings were driven to refusal. The relatively low apparent subsidence of platforms also extends low rates of absolute vertical elevation loss seen in upland areas on roads and communities into the adjacent submerged bays. This is the first available quantitative information about subsidence rates in coastal water bodies in the MRD.

InSAR imaging of infrastructure in Southwest Pass (e.g., rock jetties, buildings, groin pilings, and concrete revetments) show the highest rates of negative vertical motion in the entire study, increasing toward the Gulf. The jetties at SW Pass have an average rate of absolute vertical motion of -12.2 +/- 7.6 mm/yr. Moving upriver, the revetments and buildings along the SW Pass channel to the Head of Passes are moving at a reduced absolute rate of -4.5 +/- 4.2 mm/yr. Upriver of Head of Passes to Venice, LA (river mile 12) absolute rates are -1.2 +/- 2.6 mm/yr, and from Venice to Greater New Orleans upper limit of the Present study rates are only -2.0 +/- 2.3 mm/yr. Along this trend of the Modern (Plaquemine/Balize) delta lobe, rates of land sinking increase approaching the Gulf, following a trend of increasing absolute and Holocene sediment thickness (Kulp et al., 2002; Heinrich et al., 2015) and model results (Meckel et al., 2006) that suggest compaction can contribute at least 5 mm/yr to subsidence in the region. In the region from Head of Passes to the tip of the SW Pass jetties (e.g., the Birdsfoot Delta), the observed InSAR absolute elevation loss ranged between 4 to 6 mm per year and Holocene sediment thicknesses are >90 m (Heinrich et al., 2015). Further inland along the MR channel course, thicknesses decrease to ~30 m at the HSDRRS limit of the study area. Observed InSAR absolute rates of motion from various focus areas in Barataria and Breton Sound Basin of the central MRD, where the Holocene stratigraphy is less thick, fall within the range of approximately 3 to 4 mm/yr. Byrnes et al. (2019) and ACRE (2019) also cited self-compaction of this thickening, very young and high porosity Holocene section to explain increased subsidence toward the Gulf. The data presented here support this explanation for increasing rates of subsidence in the Birdsfoot Delta region due to (a) compaction of the young, thick Holocene section and (b) loading on the deeper stratigraphic section and on the underlying crust (Meckel et al., 2006; Törnqvist et al., 2008).

The Coastal Protection and Restoration Authority has generated shallow, deep and total subsidence rates for the MRD that encompasses the InSAR study area (CPRA, 2023). These map data represent an amalgamation of subsidence measurements by multiple methods and were subsequently utilized in the 2023 Louisiana Coastal Master Plan (LCMP). CPRA calculated shallow subsidence rates across the MRD by aggregating median rate point data from 203 CRMS sites across coastal Louisiana, organized by ecoregion (see Figure 32). These rates were determined using RSET-MG data updated in time from Jankowski et al. (2017). For the 2023 LCMP, CPRA grouped these rates into 25 ecoregions (CPRA, 2023). Deep subsidence rates were derived from geodetic survey data spanning coastal Louisiana sourced from Brynes et al. (2019) and ACRE (2019) and involved analysis of the primary GPS (CORS) benchmarks and secondary geodetic benchmarks from CPRA data from Barataria Basin and Brenton/Pontchartrain Basin. The resulting data was utilized by CPRA (2023) to create an interpolated surface for deep subsidence via the natural neighbor method (Figure 32 and 33).

Figure 32 compares the CPRA Master Plan RSET-derived shallow subsidence in the MRD at an ecoregion level to the relative vertical velocities averaged for each ecoregion from the InSAR results. The results from CPRA are binned for each ecoregion into statistical quartiles of the data range due to the wide scatter observed in the RSET data. Hence, three plots of the CPRA shallow subsidence are shown in Figure 32 representing the lower part of the range (25th percentile), mid (50th percentile), and high (75th percentile), effectively presenting scenarios of low, middle, and high relative subsidence from the range. Areas of higher shallow subsidence in the Birdsfoot delta are apparent in both the RSET and InSAR datasets and overall, the InSAR data matches best with the lower quartile (25th) of RSET results. However, it can be expected that the InSAR results will underestimate the shallow component of subsidence, as all CRMS stations are associated with coastal wetlands and the presence of a highly compressible wetland surface layer (Jankowski et al., 2017; Keogh et al., 2021). InSAR results are largely in upland areas and in submerged bays (platforms), both locations where the wetland layer is absent.

Regarding deep subsidence patterns, when comparing the InSAR deep-based vertical motion by subtracting the relative from the absolute vertical motion, with direct measurements of deep subsidence in Barataria Basin (Byrnes et al., 2019; Figure 32) and Breton-Pontchartrain Basin (ACRE, 2019; Figure 34), magnitudes of negative vertical motion (InSAR) and subsidence (GPS/benchmark) are similar (~2 – 7 mm/y) but the spatial pattern is distinctly different. High elevation loss in the southernmost area of the InSAR results in Barataria Basin is restricted to the area of the Birdsfoot delta, where Holocene thicknesses are greatest. In contrast, the GPS/benchmark results in Barataria suggest increasing subsidence rates toward the coast (Figure 33). In other parts of Barataria Basin, the InSAR results show higher levels of elevation loss (>5 mm/yr) further inland/upriver where the GPS/benchmark studies tend to be lowest (<3 mm/yr).

In Breton-Pontchartrain (Figure 34), the results by the two methods are in better agreement with higher rates in the St. Bernard lobe marshes and along the Orleans Land bridge that separates Lake Borgne and Lake Pontchartrain (Figure 34). InSAR results show moderate deep-based vertical motion (elevation loss of 3-5 mm/yr) along the left-descending (east) bank of the MR in agreement with ACRE (2019) results. It should be noted that left and right-descending bank results from the GPS/benchmark studies (left panels in Figures 33 & 34) are not in agreement with one another while InSAR results are consistent on both side of the river channel.

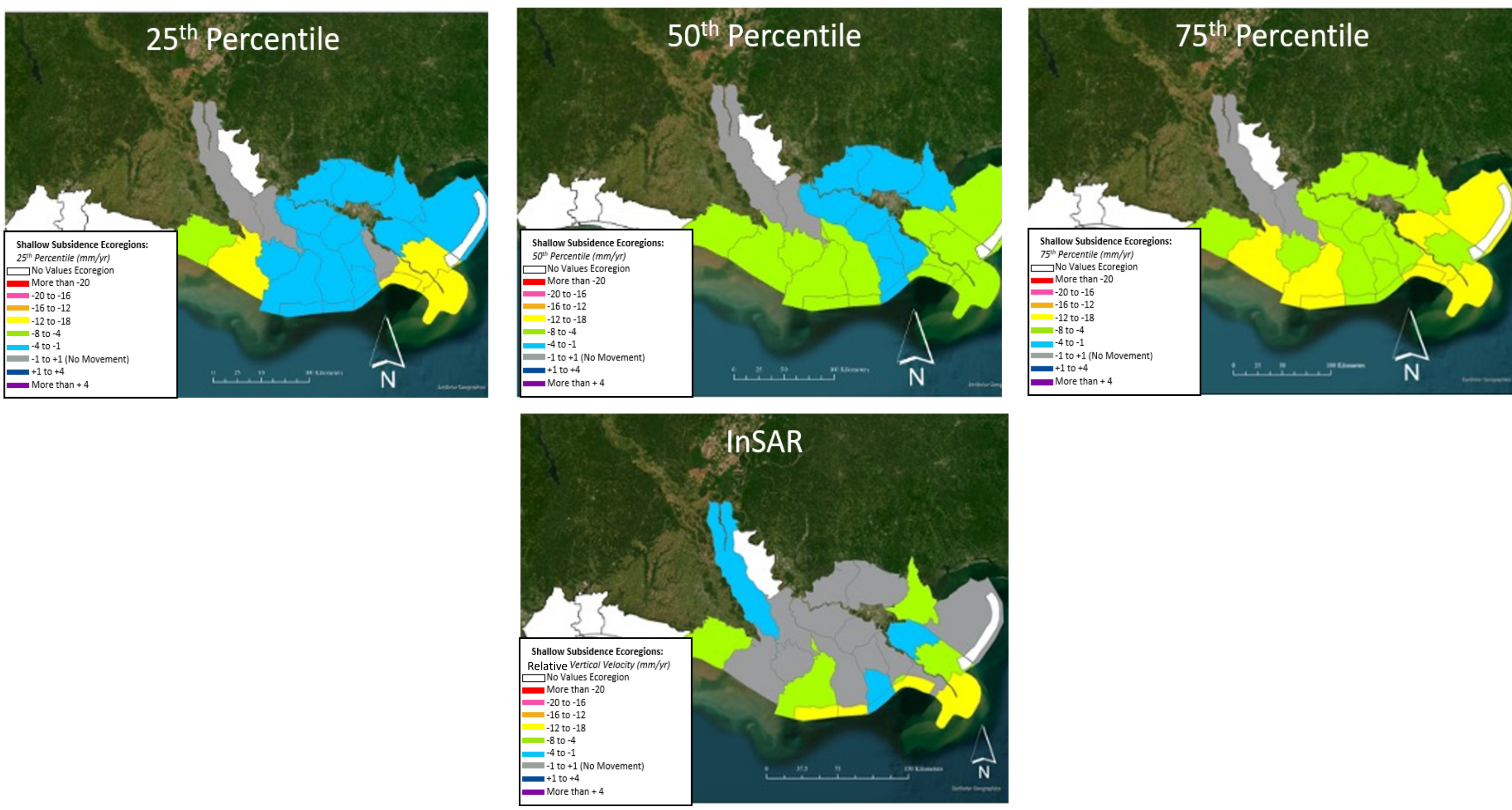

Figure 32: *Relative vertical velocity rates (mm/yr) from InSAR (lower panel) compared to CPRA shallow subsidence rates (3 upper panels) divided into ecoregions. Ecoregion shallow results from CPRA are presented in terms of 25th quartile rates (upper left), 50th quartile (middle left), and 75th quartile rates of the data range from R-SET results for individual ecoregions (in mm/yr).*

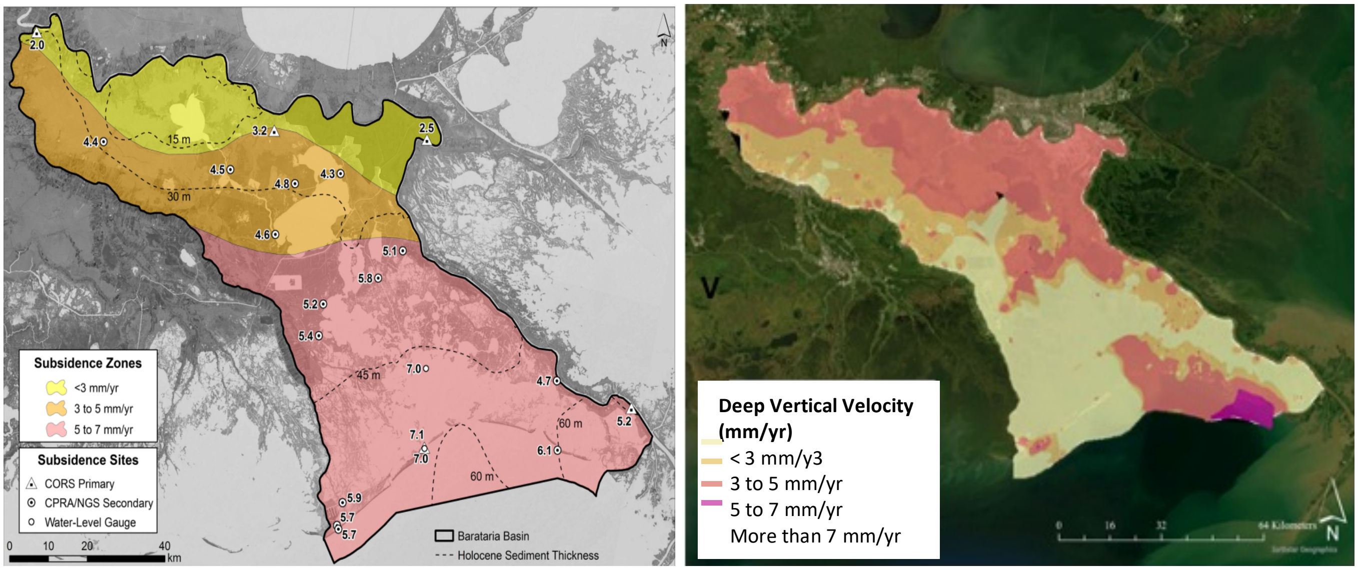

Figure 33: *Deep vertical velocity rates in Barataria Basin from Brynes et al. (2019) compared to deep rates derived from the InSAR "deep" results derived by subtracting the absolute – relative vertical motions for each point and then interpolating a surface.*

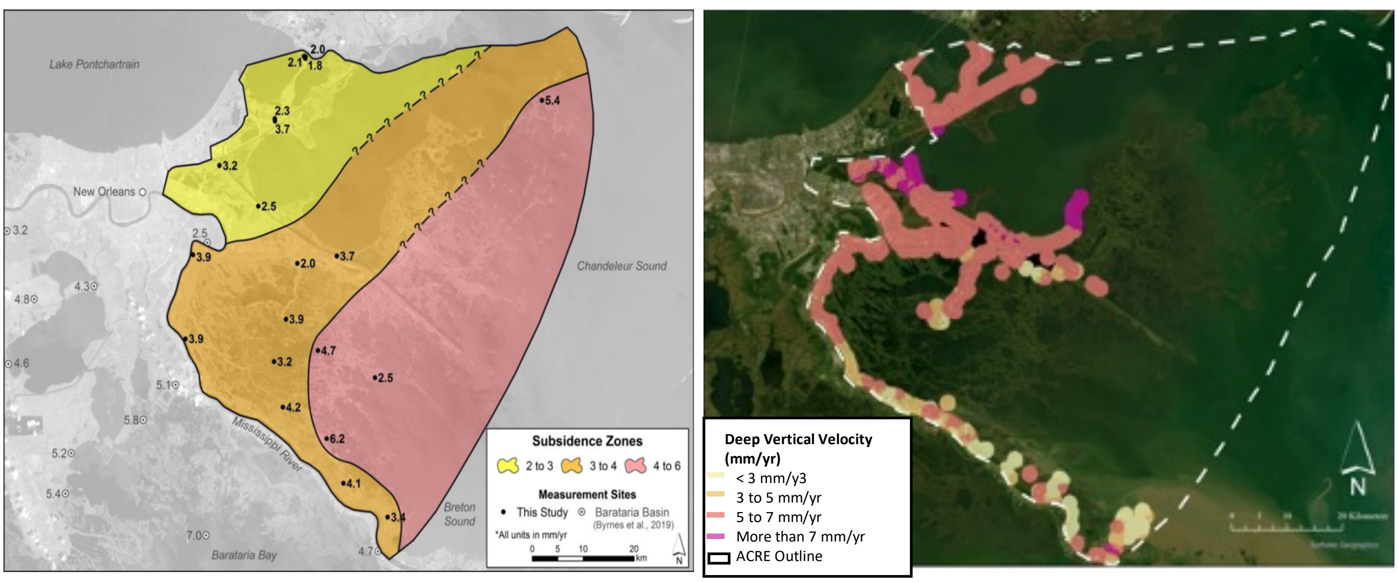

Figure 34: *Deep vertical velocity rates in Breton-Pontchartrain Basin from ACRE (2019) compared to "deep" rates derived from the InSAR results derived by subtracting the absolute – relative vertical motions for each point and then interpolating a surface.*

Several caveats should be considered when making this comparison. First, the Byrnes and ACRE studies are based on a few widely spaced stations whereas the InSAR is based on thousands of points. Second, while both are ground elevation change methods and both are mainly derived from continuous GPS records, the stations, time intervals, and processing methods of the GPS data are distinct. Similar to relative rates, determining deeper rates of subsidence and the subsequent impact on ground motion accurately also requires making broad assumptions about the driving processes across different geological histories (CPRA, 2023).

The InSAR results, in addition to being comparable to previous measurements in the MRD for shallow (R-SET) and deep (GPS) subsidence, can also be compared to previous attempts to measure vertical elevation change using InSAR (Dixon et al., 2006; Jones et al., 2016; Fiaschi et al., in prep.). All these previous efforts (a) utilized different platforms and processing methods, (b) were measured over different time intervals than the present study, and (c) focused only on high-coherence targets in the Greater New Orleans area. Specific areas of higher vertical motion that are pointed out in all three other studies are areas near Louis Armstrong International Airport and along the Mississippi River Gulf Outlet (MRGO) canal/levee in the eastern area.

The Dixon and Jones interpretations focus on general trends across the city. Jones et al. (2016) state that subsidence rates in New Orleans and nearby communities can be rapid, yet these areas are spatially localized. The data in the Jones study is presented from InSAR applied to Uninhabited Aerial Vehicle Synthetic Aperture Radar (UAVSAR) data acquired on 16 June 2009 and 2 July 2012. Examples that are noted include high subsidence centered around industrial facilities that can extend several kilometers distant. This type of subsidence is linked by this study to groundwater pumping, so in principle, the elevation loss can be recovered when the aquifer recharges (Jones et al., 2016). Both the Jones study and the Present study results (Figure 34) note a possible groundwater-induced high subsidence rate near the Entergy power plant at Michoux. Dixon et al. (2006) observe that regions with increased upward movement during 2002–2005 are undergoing moderate sinking rates, exceeding 7 mm/yr locally. These areas of high subsidence are predominantly located along Lake Pontchartrain, notably in Lakeshore and the eastern portion of the East New Orleans district. Additionally, they are situated near the Upper 9th Ward, Chalmette, and western areas along the Mississippi River. The Jones et al. (2016) and Dixon et al. (2006) agree with the Present study results of the present study with similar rates and areas of localized high motion including along the industrial canal connecting to the Mississippi.

Fiaschi et al. (*in prep*) uses the SBAS processing methodology over a shorter time interval (2016-2020) to examine GNO using Sentinel-1 data (Figure 6). This study differs from the present study results (Figure 35) in that this method was able to capture some wetland areas and were able to utilize the InSAR to define vertical motion rates for levees and floodwalls around greater New Orleans including the Hurricane Storm Damage Risk Reduction System (HSDRRS) build after Hurricane Katrina (2005). The results of the SBAS (Figure 35) analysis consist of an average velocity map calculated along LOS and show broad areas of relatively high rates of negative vertical motion (> -4 mm/yr) in the west at the construction site of the new terminal at Armstrong airport and in nearby Kenner, and in selected portions of the West bank of the MR (Figure 6). The highest rates observed (up to -30 mm/yr) were in New Orleans East and in St. Bernard Parish near the Violet Canal. Both of these areas were in wetlands and extend to both sides of the HSDRRS. Similar magnitude high rates of vertical motion were measured on the HSDRRS floodwall in these areas and on selected reaches on the Westbank of the MR as well (Figure 6) on the West bank. The rates shown in the present study are slightly lower overall (Fiaschi et al, = -2.8 mm/yr and Present Study = -1.02 mm/yr). Like the Fiaschi et al. results, the present study results show that the stable area includes eastern Jefferson Parish on the east bank of the river, west bank Jefferson in areas proximal to the river, and St. Bernard Parish near the river in the Chalmette-Arabi corridor. Both studies show high subsidence rates along western Jefferson Parish on the west bank of the Mississippi River near River Birch gas plant complex. This also follows the same pattern as older InSAR studies by Dixon et al. (2006) and Jones et al. (2016). The very high rates in areas such as NO East and Venetian Isles and near the Violet Canal (Figure 35) were in wetland areas and are not resolved in the SqueeSAR methodology. The SqueeSAR was able to resolve portions of the Hurricane and Storm Damage Risk Reduction System (HSDRRS) that are mainly concrete floodwall (not earthen levee) and confirm the e Fiaschi et al. (in prep.) results of high rates of negative vertical motion (10-35 mm/yr, along the Mississippi River-Gulf Outlet (MR-GO) and the GIWW in New Orleans East, and along the western portion of the system on the south shore of Lake Pontchartrain (Figure 34).

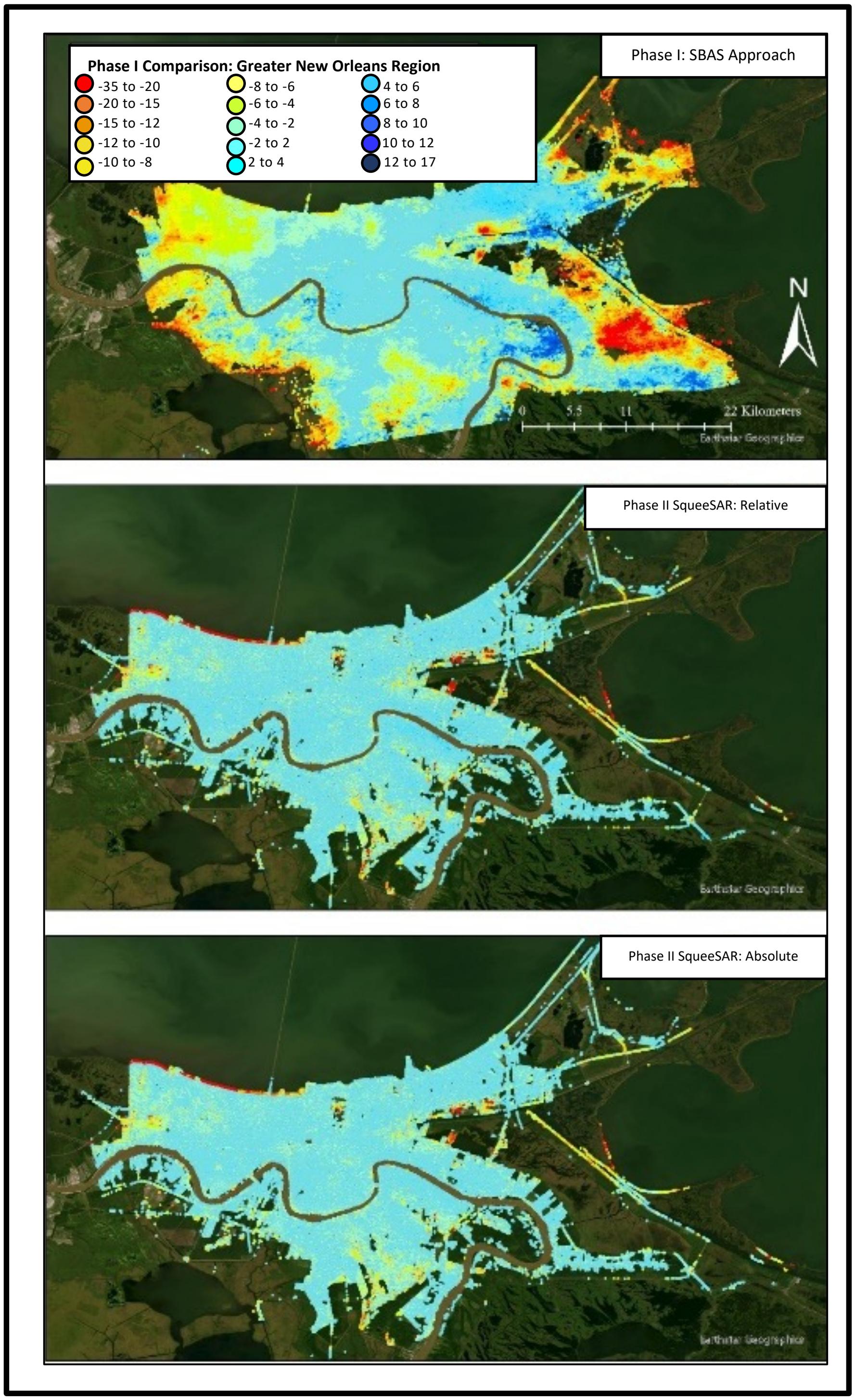

Figure 35: *Comparison of the InSAR results from Fiaschi et al. (in prep.) using SBAS (upper panel) with SqueeSAR results from the present study presented as relative (middle panel) and absolute (lower panel) vertical motion. The Fiaschi et al. study results are relative, and hence, most comparable to the relative results from the present study.*

6.2 Assessing InSAR's Value in Mapping Ground Elevation for Change Coastal Protection and Restoration

Developed for the 2017 Louisiana Coastal Master Plan (LCMP), and utilized in the 2017 and 2023 LCMP, the Integrated Compartment Model (ICM) plays a crucial role in planning for responding to relative sea level rise and other mechanisms of land loss and ecosystem change in the MRD. Numerical simulations are conducted to enhance project design and selection, utilizing the ICM to simulate landscape changes. The MRD (Mississippi River Delta) and the rest of the Louisiana coastal zone are divided into spatial compartments (polygons), each encompassing subareas of upland, wetland, and permanent water (CPRA, 2023). These polygon boundaries are established based on coastal hydrology, wetland morphology, vegetation dynamics, and habitat suitability to support various fish and wildlife. They serve as a means to monitor the performance of proposed projects concerning land change, flooding, and ecosystem response. Rates of total subsidence are assigned in the model on a polygon-specific basis (Figure 36) and then combined with projections of global sea level rise to derive a relative sea level rise (land elevation loss) rate at a polygon level across the MRD. Vertical accretion of wetland areas of each polygon is also derived from a spatial dataset compiled from sediment deposition, organic matter, and bulk density measurements (CPRA, 2023).

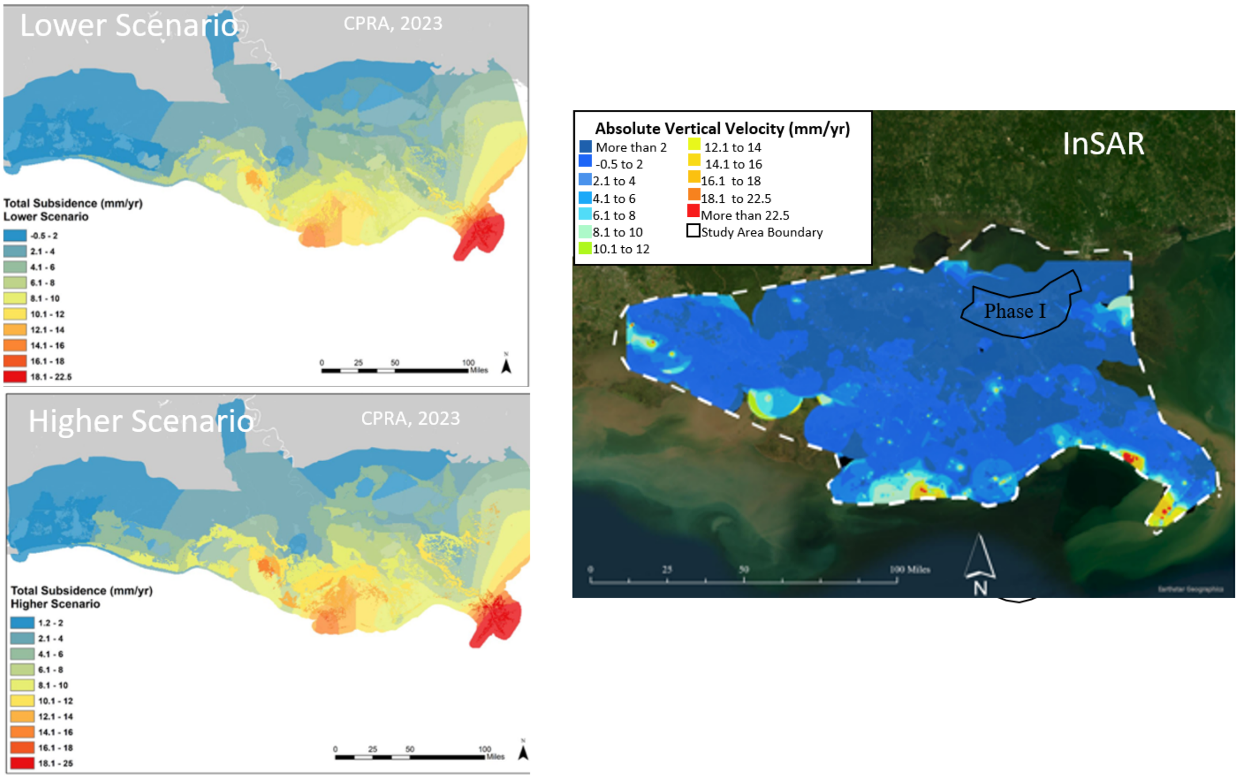

Figure 36: *Total subsidence rate in low and high scenarios (left panels) for the MRD based on CPRA's amalgamation of relative and deep measurement techniques compared against absolute vertical velocities derived from the InSAR results (right panel). The dotted white line represents the limits of the InSAR processing, and the black polygon represents the boundaries of the Phase I (Fiaschi et al., in prep.) study (see Figure 35).*

Figure 36 is the map comparison of the total subsidence rates in the MRD utilized in the Master Plan by CPRA using low and high subsidence scenarios, and absolute vertical velocities from the InSAR results. The center region is extrapolated from the results from "uplands" to wetlands showing an overall rate of the InSAR vertical elevation loss are significantly lower than those utilized by CPRA except in the immediate coastal region (e.g., barrier islands and the Birdsfoot delta) where the youngest Holocene sediment thicknesses are at a maximum (Heinrich et al., 2015). Figure 37 then compares the total subsidence rates in the MRD utilized in the Nienhuis et al, 2017 (upper panel) where upland areas are removed, and no interpolation was conducted over open water. In contrast, the InSAR results in Figure 37 (lower panel) have rates and an interpolation for upland areas and open water, but wetland areas are removed.. Some similarities are present in the comparison, specifically, the presence of higher rates of vertical motion/subsidence near the Gulf coastline and over the Birdsfoot Delta Region. Both maps in Figure 37 also show higher rates of vertical elevation loss near the barrier islands fronting Terrebonne Bay and the Terrebonne headland.

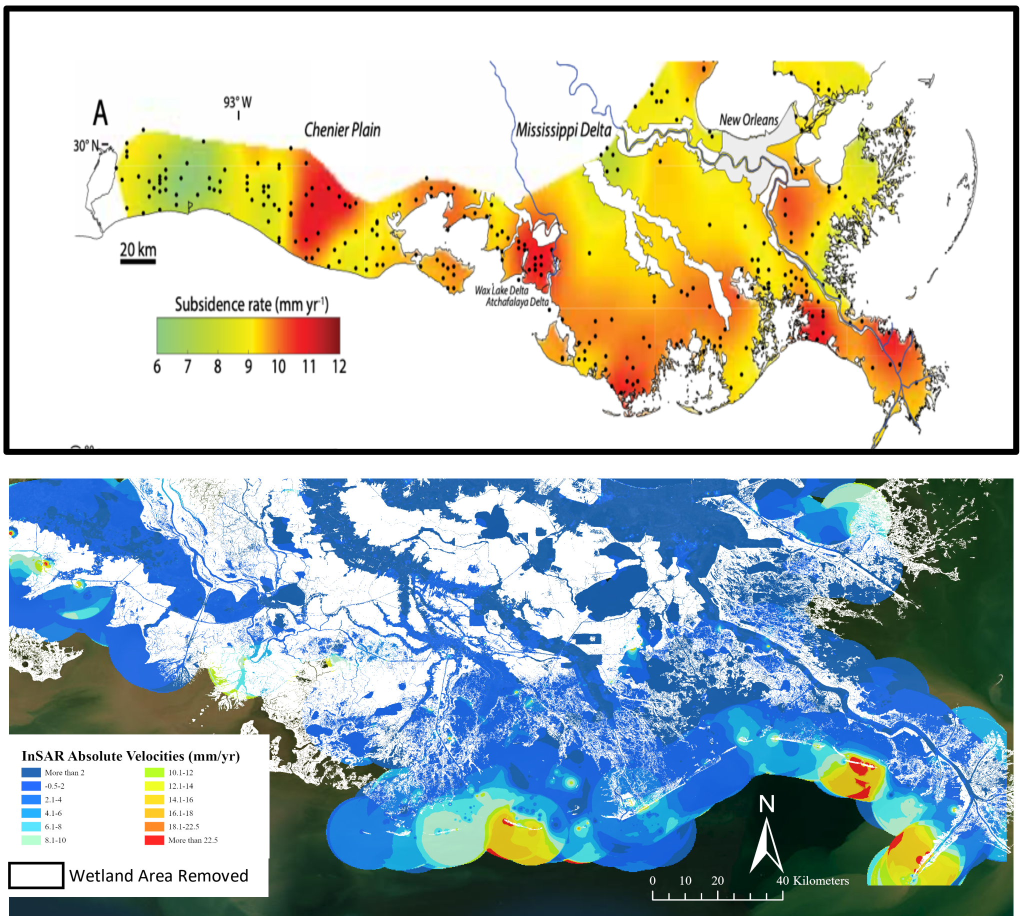

.

Figure 37: *Comparison of Nienhuis et al., 2017 (total subsidence rates (upper panel) derived from point measurements to the absolute vertical velocity rates (lower panel) derived from InSAR results in the present study.. The white outlines on the InSAR map mark the locations vegetated wetlands, unvegetated wetland/Bareground, and flotant marsh determined by landscape composition derived from satellite imagery taken in 2018 by CPRA. These wetland areas are not measured in the InSAR results. In contrast, white areas in the Nienhuis map define some upland areas where their wetland rates were assumed to not hold true.*

Figure 38 shows the range of the absolute vertical velocities measured for the ICM polygons (shown in map form in Figure 39). The latter figure again demonstrates the larger values in the polygon summations using CPRA results than for the InSAR absolute vertical velocities. As outlined in earlier sections, the interpretation for this difference is that the InSAR is an absolute ground elevation change and not a direct measure of subsidence. Hence, it can include ground motions (accretion/erosion/human origin) not due to subsidence. The other key point is that the amalgamation of methods used by CPRA to derive the maps in Figure 38 includes relative wetland subsidence, which is generally not present in the InSAR dataset. The difference that the addition of this relative (wetland) component makes in the absolute rate is clearly shown in Figure 32 as well. It is clear from this comparison that the relative compaction of the organic-rich surficial wetland layer is a major component in the overall subsidence in the MRD (an area dominantly composed of wetlands and open water).

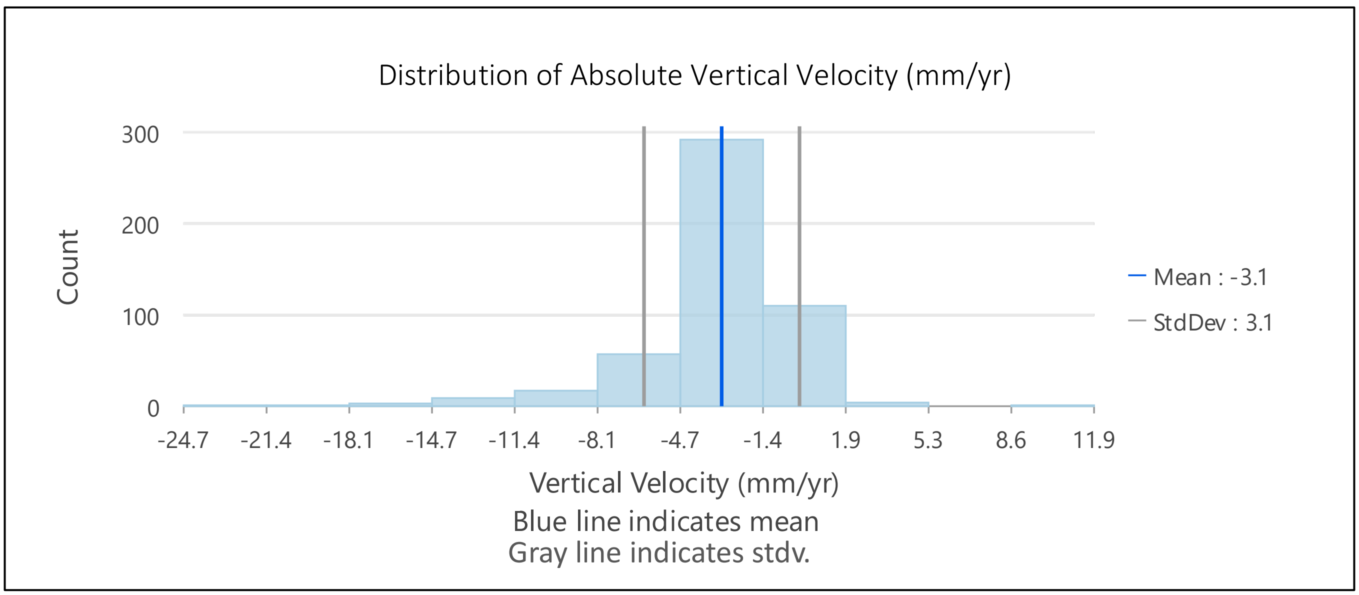

Figure 38: *Distribution of absolute vertical velocity summing the ICM polygon boundaries that lie within the InSAR study area.*

The CPRA-derived total rates of subsidence presented in Figure 36 result from combining information about deep and shallow subsidence rates and are utilized in predictive modeling for coastal restoration and protection project design testing. These rates are amalgamated with additional data (such as sea level rise rates) within environmental scenarios, facilitating the projection of future conditions for model simulations. The key points about their utilization are that (1) the wide scatter in shallow subsidence (R-SET) measurements led to the development of “low” and “high” subsidence scenarios (Figure 36), (2) deep subsidence is represented as a mapped surface rather than values for each ICM polygon, and (3) a single value is applied for each land-water type (e.g., water, wetland, upland).

These boundaries facilitate spatial assessment of InSAR (Interferometric Synthetic Aperture Radar) vertical velocity change across the entire MRD study area in the present study and allow comparison with rates derived by InSAR versus the ICM-assigned values. As the InSAR map in Figure 39 provides more comprehensive data (and is in point-specific form), it is possible to assign averages to each polygon.

Figure 38 (left panels) is a compilation of the CPRA rates utilized in the 2023 Master Plan (CPRA, 2023), expressed as total subsidence (high and low scenarios), and projected as a mapped surface with the ICM polygons overlain since it was provided for the present study in raster form and could not be quantified for individual polygons. If the InSAR vertical velocities shown in Figure 36 are inferred to be equivalent to subsidence (e.g., other sources of land motion are discounted), then these results can be averaged for each polygon and shown as an absolute rate of subsidence/vertical motion (Figure 39 right panels). There was a cutoff applied of less than 10 InSAR points falling in the polygon boundaries then the results of these polygons were not shown. The results show a similar broad pattern of higher rates closer to the Gulf but with much lower magnitude than the CPRA results. As the interpretation outlined above is that these differences mainly stem from the absence of a relative subsidence (wetland) component in the

InSAR results (mainly upland and platforms over water), it is not possible to judge the accuracy of utilizing the lower or higher CPRA scenario. The value of the InSAR results is to provide quantitative results on a polygon-specific basis for the upland and open water components of each polygon. It is this simple tripartite designation of land: water type that is utilized in the ICM modeling. A major utility of the results of the present study is that a more accurate model could be derived for use in future CPRA modeling generations that applies the InSAR vertical velocities (as absolute subsidence) for the upland and open water components and utilizes the existing "lower" and "higher" scenario values for the wetland portion of each polygon.

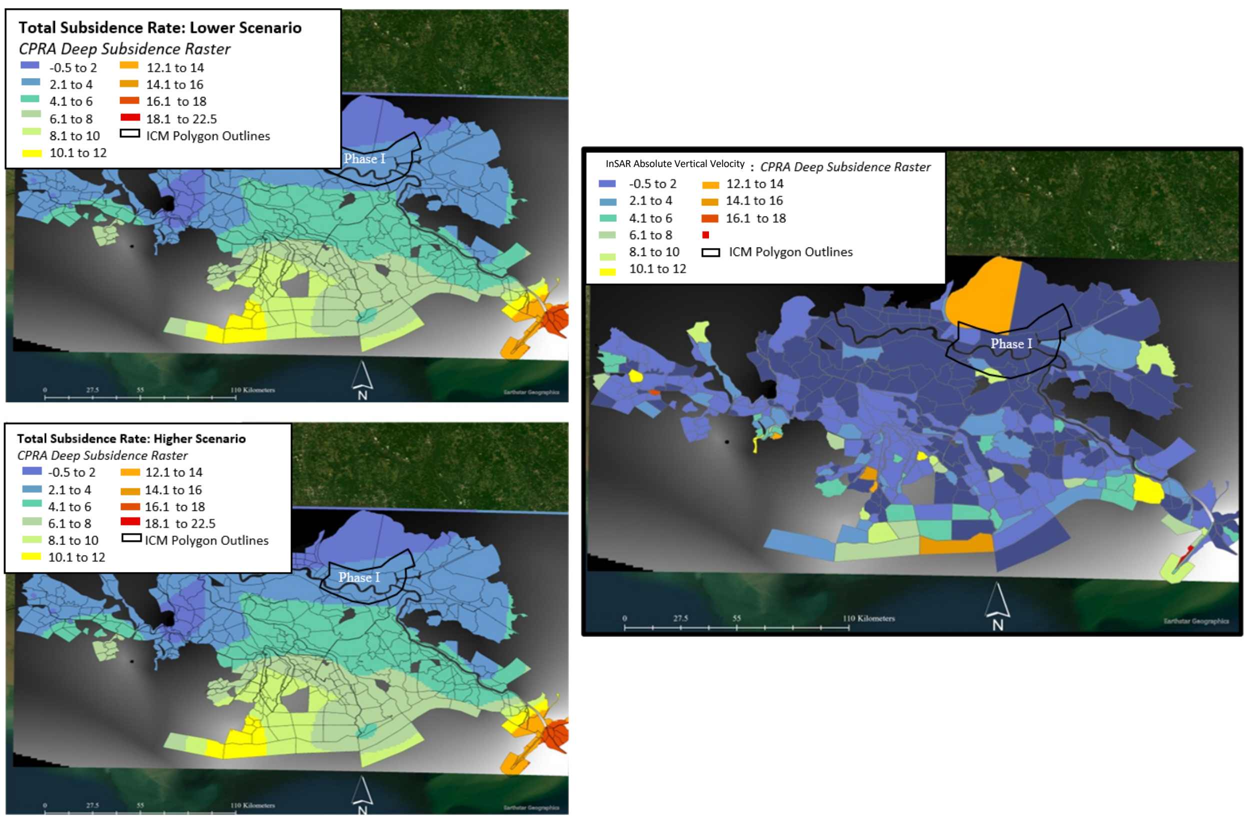

Figure 39: *ICM map of total subsidence rates over the ICM polygon grid as utilized in the 2023 Master Plan (left panels) using lower (upper left) and higher (lower left) scenarios for the shallow contribution. Right panels are absolute vertical velocity rates of motion (elevation loss expressed as a positive to match the CPRA method of expressing subsidence) within each polygon in the InSAR study area. All plots are in units of mm/yr.*

What are the implications if such a strategy is followed? Comparison on a polygon-specific basis indicates that the total subsidence rates are ~2-10X higher than the absolute vertical velocities measured by InSAR (Figure 38). Stated another way, it can be inferred that wetland subsidence rates in the MRD are 2-10 times greater than that of upland areas and areas of open water (landward of the Gulf shoreline). Thus, CPRA modeling projections of future land loss are overestimated for upland areas. If the rate of upland areas in the MRD, and the coastal communities and infrastructure upon them, are subsiding at much lower rates, that is encouraging news for their sustainability in the 21st century. A second, equally important implication, is that open water areas are also subsiding at rates lower than that previously predicted for coastal restoration projects. In the case of river diversions such as Mid-Breton or Mid-Barataria (CPRA, 2023a), a single subsidence value is utilized throughout the growth of the receiving basin splay. The InSAR results suggest a more complicated aggradation/progradation history over the evolutionary life of the diversions, where in the initial phases prior to emergence and vegetation colonization, subsidence is a combination of the low open-water rate for that polygon area (InSAR value) plus loading-induced subsidence of the underlying substrate. With emergence and vegetation colonization, subsidence increases to the wetland subsidence rates (plus continued loading minus organo-mineralic accretion in the wetland). In both phases, the aggradation and progradation rates of the splay are also balanced against sediment accretion (unvegetated splay and wetland surface) and oceanic sea level rise. Marsh creation projects (CPRA, 2023a) that utilize long-distance pipelined material could also be envisioned as subsiding in a multi-phase way (before and after colonization by vegetation and initiation of marsh compactional subsidence) that would impact their lifespan and post-emplacement degradation rate.

7. CONCLUSIONS

Having a map that displays vertical motion across the Mississippi River Delta using InSAR is crucial for various purposes, including environmental management, infrastructure planning, resource utilization, and disaster preparedness. However, the present study results used in this study have limited coverage of wetland areas due to low radar imagery coherence. A previous study (Fiaschi et al., in prep.) conducted more intensive processing in the Greater New Orleans area, which showed promise in recording wetland substrates in some regions. The widespread application of satellite InSAR for measuring absolute ground elevation change in wetlands awaits the launch of future satellite platforms and/or new processing methodologies. Previous efforts primarily focused on measuring subsidence below the substrate surface, but utilizing InSAR provides a more comprehensive view of elevation changes at the substrate surface.

While subsidence measurements, such as those obtained using the R-SET method, differentiate subsidence by subtracting marsh aggradation rates from absolute elevation change, this approach introduces two sources of variability: measuring aggradation rates and measuring absolute elevation change. Additionally, the absolute elevation change is limited to the upper "shallow" section above the foundation depth of the R-SET rod. In the present study, results using SqueeSAR processing yielded 4.2 million ground elevation change points for the Mississippi River delta between 2016 and 2021. These results primarily pertain to upland (non-wetland) areas but extend to submerged shallow coastal bays with oil/gas infrastructure platforms.

These results can be further subdivided to distinguish absolute vertical velocities of ground motion for various features, including major roads, communities, barrier islands, platforms, jetties, revetments, and areas of coastal project construction like Morganza-to-the-

Gulf. InSAR is appealing in principle because it directly measures elevation changes of the ground surface, potentially accounting for sediment erosion/accretion and subsidence. It also measures elevation changes from the substrate surface to the center of the Earth. However, the utility of InSAR in wetland-dominated systems, such as the MRD, is strongly influenced by the sensor/platform and post-processing methodology.

The main conclusions of this study are as follows:

1. Upland rates differ significantly (are generally lower) from wetland rates when using InSAR to map ground elevation change in the Mississippi River delta. For future planning purposes, numerical models used to test restoration and protection projects on the landscape in coastal Louisiana could use distinct rates to define rates for upland sections of polygons compared to wetland sections. This would provide a more accurate picture of the effects of subsidence on the future coastal landscape. This finding has two significant implications for the future sustainability of southern Louisiana. First, the present study suggests that communities, roads, and infrastructure may not be inundated as quickly as anticipated by projected rates of global sea level rise (Blum and Roberts, 2009). Instead, it presents a scenario where the more rapidly subsiding wetland fringe adjacent to these areas may experience rapid degradation. Secondly, lower subsidence rates in open water areas than previously anticipated could be beneficial. Major coastal wetland restoration projects, such as long-distance pipelines and marsh creation or river diversions, require a specific volume of sediment to convert open water areas into areas above mean sea level. If subsidence is lower in open water areas, these projects would have a longer lifespan before subsiding below sea level post-construction, and river diversion projects would require less sediment volume to become emergent. This would enable more rapid land building in the early stages of diversion operations and likely result in a larger ultimate splay footprint.

2. Rates of vertical motion (vertical velocities in mm/yr) obtained using the SqueeSAR InSAR methodology indicate that the Birdsfoot Delta region in Southwest Pass are losing elevation at a faster rate than the rest of the coast. This confirms earlier studies that have suggested that this region is more subject to subsidence because of the thick, young sedimentary section, but previously has been difficult to measure. This finding highlights the existential threat to this portion of the Mississippi River Delta in the 21st century of rising global sea levels.
3. InSAR will not be a widely useful tool for measuring subsidence in coastal wetlands. Likely this is a function of seasonally variable canopy heights of vegetation and periodic tidal inundation by water. However, the present study has shown that it is an effective tool for measuring subsidence in delta regions where vegetation cover is low.

8. References Cited

Allison, M.A., Yuill, B.T., Tornqvist, T., Amelung, F., Dixon, T., Erkens, G., Stuurman, R., Jones, C., Milne, G., Steckler, M., Syvitski, J., and Teatini, P., 2016. Coastal subsidence: global risks and mitigation. 2016. EOS—Transactions of the American Geophysical Union. 97: 22-27.

Applied Coastal Research and Engineering (ACRE), 2019. Determining Recent Subsidence Rates for Breton Sound and Eastern Pontchartrain Basins, Louisiana: Implications for Engineering and Design of Coastal Restoration Projects. Final Report prepared for Louisiana Coastal Protection and Restoration Authority. Contract 4400009020, Task 8, 58 p.

Berardino, P., Fornaro, G., Lanari, R., Sansosti, E. 2002. A new algorithm for surface deformation monitoring is based on small baseline differential SAR interferograms. IEEE Transactions on Geoscience and Remote Sensing, 40, 11, 2375-2383, Nov. 2002, doi: 10.1109/TGRS.2002.803792.

Blum, M. D., and Roberts, H.H., 2009. Drowning of the Mississippi Delta due to insufficient sediment supply and global sea-level rise. Nature Geoscience 2: 488–91, https://doi.org/10.1038/ngeo553.

Byrnes, M. R., Britsch, L. D., Berlinghoff, J. L., Johnson, R., & Khalil, S., 2019. Recent subsidence rates for Barataria Basin, Louisiana. Geo-Marine Letters, 39(4), 265–278. https://doi.org/10.1007/s00367-019-00573-3

Cahoon, D. R., Lynch, J. C., Perez, B. C., Segura, B., Holland, R. D., Stelly, C., ... Hensel, P., 2002. High-precision measurements of wetland sediment elevation: II. the rod surface elevation table. Journal of Sedimentary Research, 72: 734-739. doi:10.1306/020702720734.

Cahoon, D.R., 2015. Estimating relative sea-level rise and submergence potential at a coastal wetland. Estuaries and Coasts, 38: 1077–1084. https://doi.org/10.1007/s12237-014-9872-8

Couvillion, B.R., Beck, H., Schoolmaster, D., and Fischer, M. M., 2017. Land area change in coastal Louisiana (1932 to 2016), U.S. Geological Survey Scientific Investigations Map 3381, U.S. Geological Survey, Reston, VA, 16 p.

CPRA (Coastal Protection and Restoration Authority). 2023a. Louisiana's Comprehensive Master Plan for a Sustainable Coast, Barrier Island Status Report Baton Rouge, LA.

Coastal Protection and Restoration Authority (CPRA), 2023b. Barrier Island Status Report: Draft Fiscal Year 2023 Annual Plan. Coastal Protection and Restoration Authority of Louisiana (CPRA), Baton Rouge, LA, 53p.

CPRA (Coastal Protection and Restoration Authority). 2017. Louisiana's Comprehensive Master Plan for a Sustainable Coast, Barrier Island Status Report Baton Rouge, LA.

CPRA (Coastal Protection and Restoration Authority). 2021. Louisiana's Comprehensive Master Plan for a Sustainable Coast, Barrier Island Status Report Baton Rouge, LA.

Dangendorf, Sönke, et al. 2014 "Evidence for Long-Term Memory in Sea Level." *Geophysical Research Letters*, vol. 41, no. 15, 2014, pp. 5530–5537, https://doi.org/10.1002/2014gl060538.

DeLaune, R. D., et al. 2013. Freshwater diversions as an ecosystem management tool for maintaining soil organic matter accretion in coastal marshes. Catena (Giessen) 107: 139–44, https://doi.org/10.1016/j.catena.2013.02.012.

Devanthery, Nuria et al., 2014. An approach to persistent scatterer interferometry. Remote Sensing (Basel, Switzerland) 6.7:6662–6679. Web.

Dixon, T. H., F. Amelung, A. Ferretti, F. Novali, F. Rocca, R. Dokka, G. Sella, S. W. Kim, S. Wdowinski, and D. Whitman, 2006. Space geodesy: subsidence and flooding in New Orleans, Nature 441(7093): 587–588, doi:10.1038/441587a.

Edmonds, Douglas A., et al., 2023. Land loss due to human-altered sediment budget in the Mississippi River Delta. Nature Sustainability 6: 644–651, https://doi.org/10.1038/s41893-023-01081-0.

EGMS (European Ground Motion Service), 2021, End-to-end implementation and operation of the (EGMS) Algorithm Theoretical Basis Document, EGMS-SC1.

Fiaschi, S., Kooi, H., Allison, M.A., Jones, C., Melman, R., and Stuurman, R. in prep. InSAR-derived rates of land subsidence in Greater New Orleans: insights into underlying causes and mechanisms and future storm surge risk. Journal of Remote Sensing.

Frazier, D.E., 1967. Recent deltaic deposits of the Mississippi River: their development and chronology. Gulf Coast Association of Geology Soc. Transcripts 27: 287-315.

Fruergaard, M., et al., 2015. Stratigraphy, evolution, and controls of a Holocene transgressive-regressive barrier island under changing sea level; Danish North Sea Coast. Journal of Sedimentary Research, 85: 820–44, https://doi.org/10.2110/jsr.2015.53.

Gagliano, S. M., Meyer-Arendt, K. J., and Wicker, K. M., 1981. Land loss in the Mississippi River deltaic plain. Transactions of the Gulf Coast Association of Geological Societies, 31: 295-300.

Hammond, William C., et al., 2018. Uplift of the Western Transverse Ranges and Ventura Area of Southern California; a four-technique geodetic study combining GPS, InSAR, leveling, and tide gauges. Journal of Geophysical Research. Solid Earth, 123:836–858, https://doi.org/10.1002/2017JB014499.

Heinrich, Paul, Robert Paulsell, Riley Milner, John Snead, and Hampton Peele, 2015, Investigation and GIS development of the buried Holocene-Pleistocene surface in the Louisiana coastal plain: Baton Rouge, LA, Louisiana Geological Survey-Louisiana State University for Coastal Protection and Restoration Authority of Louisiana, 140 p., 3 pls.

Hijma, M.P., et al. (2017), Late Holocene Evolution of a Coupled, Mud-Dominated Delta Plain-Chenier Plain System, Coastal Louisiana, USA, Earth Surface Dynamics, 5(4), 689-710, https://doi.org/10.5194/esurf-5-689-2017.

"Home." *New Orleans District, U.S. Army Corps of Engineers*, www.mvn.usace.army.mil/About/Projects/Morganza-to-the-Gulf/. Accessed 12 July 2023

IPCC, 2022: Climate Change 2022: Impacts, Adaptation, and Vulnerability. Contribution of Working Group II to the Sixth Assessment Report of the Intergovernmental Panel on Climate Change [H.-O. Pörtner, D.C. Roberts, M. Tignor, E.S. Poloczanska, K. Mintenbeck, A. Alegría, M. Craig, S. Langsdorf, S. Löschke, V. Möller, A. Okem, B. Rama (eds.)]. Cambridge University Press. Cambridge University Press, Cambridge, UK and New York, NY, USA, 3056 pp., doi:10.1017/9781009325844.

Jankowski, K. L., Törnqvist, T. E., & Fernandes, A. M., 2017. Vulnerability of Louisiana's coastal wetlands to present-day rates of relative sea-level rise. Nature Communications, 8. https://doi.org/10.1038/ncomms14792

Jones, C. E., An, K., Blom, R. G., Kent, J. D., Ivins, E. R., & Bekaert, D., 2016. Anthropogenic and geologic influences on subsidence in the vicinity of New Orleans, Louisiana. Journal of Geophysical Research: Solid Earth, 121(5):3867–3887. https://doi.org/10.1002/2015JB012636

Jones, Cathleen. Meeting. Conducted by Rory Escobedo. Between November 2021-August 2023

Karegar, M.A., et al. (2015), A Three-Dimensional Surface Velocity Field for the Mississippi Delta; Implications for Coastal Restoration and Flood Potential, Geology (Boulder), 43(6), 519-522, https://doi.org/10.1130/G36598.1.

Keogh, M. E., Törnqvist, T. E., Kolker, A. S., Erkens, G., & Bridgeman, J. G., 2021. Organic matter accretion, shallow subsidence, and river delta sustainability. Journal of Geophysical Research: Earth Surface, 126, e2021JF006231. https://doi.org/10.1029/2021JF006231.

Kolker, A.S., Allison, M.A., and Hameed, S., 2011. An evaluation of subsidence rates and sea-level variability in the Northern Gulf of Mexico. Geophysical Research Letters 38: L21404, doi:10.1029/2011GL049458

Kulp, Mark A., et al., 2002. Latest Quaternary stratigraphic framework of the Mississippi River Delta region. Transactions - Gulf Coast Association of Geological Societies, 52: 573–82.

Meckel, ten Brink, U. S., & Williams, S. J., 2006. Current subsidence rates due to compaction of Holocene sediments in southern Louisiana. Geophysical Research Letters, 33(11), L11403–n/a. https://doi.org/10.1029/2006GL026300

Meckel, T. A, U. S Ten Brink, and S. J Williams, 2007. Sediment compaction rates and subsidence in deltaic plains: numerical constraints and stratigraphic influences Basin Research 19: 19–31.

Minderhoud, Philip S. J. et al. 2020"Towards Unraveling Total Subsidence of a Mega-Delta – the Potential of New PS InSAR Data for the Mekong Delta." Proceedings of the International Association of Hydrological Sciences 382 (2020): 327–332. Web.

Morales, J.A., 2022.. Wave-Dominated Systems I: Barriers and Barrier Islands. In: Coastal Geology. Springer Textbooks in Earth Sciences, Geography and Environment. Springer, Cham. https://doi.org/10.1007/978-3-030-96121-3_16

Nienhuis, J.H. et al., 2017. A new subsidence map for coastal Louisiana. GSA Today, https://doi.org/10.1130/GSATG337GW.

O'Leary, & Gottardi, R., 2020. Relationship between growth faults, subsidence, and land loss: an example from Cameron Parish, Southwestern Louisiana, USA. Journal of Coastal Research, 36(4): 812–827. https://doi.org/10.2112/JCOASTRES-D-19-00108.1

Schmidt, Charles W., 2015 "Delta Subsidence: An Imminent Threat to Coastal Populations." Environmental health perspectives 123.8 (2015): A204–A209. Web.

Sherwood, Christopher R. et al. 2023"Sound-Side Inundation and Seaward Erosion of a Barrier Island During Hurricane Landfall." Journal of geophysical research. Earth surface 128.1n. pag. Web.

Stanley, Daniel J., and Andrew G. Warne. "Nile Delta; Recent Geological Evolution and Human Impact." Science (American Association for the Advancement of Science) 260.5108 (1993): 628–634. Web.

"Topographic Boundaries." Louisiana Department of Transportation and Development, OpenData, Accessed on 19 July 2023, https://maps.dotd.la.gov/topo/rest/services/OpenData/Boundaries/FeatureServer/5.

Törnqvist, T. E., Wallace, D. J., Storms, J. E. A., Wallinga, J., Van Dam, R. L., Blaauw, M., et al., 2008. Mississippi Delta subsidence primarily caused by compaction of Holocene strata. Nature Geoscience, 1, 173–176.

United States Census Bureau. "Population and Housing Data 2020." 2020 Census. United States Census Bureau, 2021, www.census.gov/2020census/data.

Wang, H., Xu, W., & Bianchi, T. S., 2019. Factors contributing to sediment compaction and subsidence in a deltaic coastal wetland. Estuaries and Coasts, 42(2): 552–565. https://doi.org/10.1007/s12237-018-04536.

Zhang, Y., et al. 2019. Small baseline InSAR time series analysis; unwrapping error correction and noise reduction. Computers & Geosciences, 133, https://doi.org/10.1016/j.cageo.2019.104331.

8. APPENDICES

Appendix A

Individual rates of relative and absolute motion for platforms measured in the present InSAR study divided into those constructed pre- and post-2000.

Pre-2000 Platforms

Relative Vertical Velocity (mm/yr)	Absolute Vertical Velocity (mm/yr)	Established Date	Description
-1.2	-4.0	< 1985	Boat Yard
1.7	-1.6	1985-1990	Platform
-2.3	-4.8	1985-1990	Platform
-2.9	-5.2	1985-1990	Platform
-2	-4.6	< 1985	Platform
-12.3	-13.0	<1985	Platform
-2.4	-4.8	<1985	Platform
0.1	-2.6	< 1985	Platform
-3.2	-5.3	< 1985	Platform
-5.2	-7.1	< 1985	Platform
-1.1	-3.6	< 1985	Platform (Had a long boardwalk, but fell off between 1985-1999)
-1.1	-3.6	< 1985	Platform
-1	-3.5	<1985	Platform
0.5	-2.3	<1985	Platform
-6.6	-8.1	<1985	Platform
-6.8	-8.3	< 1985	Platform (Had a long boardwalk, but fell off between 1985-1999)
-0.9	-3.4	<1985	Platform
6.3	2.7	<1985	Platform
-1.6	-4.0	<1985	Platform (massive platform at first building)
3.9	0.6	< 1985	Platform
-1.3	-3.6	< 1985	Platform
0.4	-2.2	<1985	Platform
2	-0.9	< 1985	Platform
-4.1	-6.2	< 1985	Platform
2.2	-0.7	< 1985	Platform
-2.9	-5.1	< 1985	Platform
4	0.8	< 1985	Platform
-12.7	-13.1	< 1985	Platform
-1.7	-4.1	< 1985	Platform
-0.7	-3.1	< 1985	Platform
0.5	-2.1	< 1985	Platform
7.8	3.9	<1985	Platform

1.1	-1.9	< 1985	Platform
-0.5	-2.9	< 1985	Platform
-5.7	-7.2	< 1985	Platform
0.7	-1.8	< 1985	Platform
-3.3	-5.3	< 1985	Platform
-7.1	-8.3	< 1985	Platform
-8.8	-9.7	< 1985	Platform
-11.5	-11.8	< 1985	Platform
-1.2	-3.3	< 1985	Platform
4.1	0.9	< 1985	Platform
8.9	4.5	< 1985	Platform
1.2	-1.3	< 1985	Platform
3.7	0.7	< 1985	Platform
-6.4	-7.1	< 1985	Platform
0.1	-1.9	< 1985	Platform
2.3	-0.4	< 1985	Platform
-8.5	-8.5	< 1985	Platform
-0.9	-2.8	< 1985	Platform
4.6	1.4	< 1985	Platform
1.3	-1.0	< 1985	Platform (Interesting time series)
0.9	-1.4	< 1986	Platform
-7	-7.9	< 1985	Platform
-12.9	-11.7	<1985	Platform
1	-1.8	< 1985	Platform
-3.6	-4.8	< 1985	Platform
-7.3	-7.5	< 1985	Platform (home) interesting homes along HWY 1)
0.8	-1.5	< 1985	Homes?
4.5	1.0	< 1985	Home (completely not there anymore)
-2.5	-4.0	< 1985	Platform (completely destroyed)
-7.3	-7.6	< 1985	Platform (Gone as of 2022)
-8.1	-8.1	< 1985	Platform
1.3	-1.0	< 1985	Platform
0.8	-1.7	< 1985	Platform
0.5	-1.7	< 1985	Platform
1.8	-0.7	< 1985	Platform
8.9	5.0	< 1985	Platform
8	4.4	< 1985	Platform
0.5	-1.7	< 1985	Platform
1.1	-1.2	< 1985	Platform
1.6	-0.3	< 1985	Platform
4.8	2.1	<1985	Platform
1.3	-0.9	1985-1998	Platform
0.1	-1.4	< 1985	Platform
1	-0.7	1985-1998	Platform
0.9	-1.4	< 1985	Platform

1.8	-0.6	< 1985	Platform
-0.5	-2.4	<1985	Platform
1.5	-0.8	< 1985	Platform
2.5	0.0	< 1985	Platform (was large then smaller in size)
0.3	-1.7	< 1985	Platform (was large then smaller over time)
-4.1	-4.8	< 1985	Platform
7.5	4.1	< 1985	Platform
1.9	-0.3	< 1985	Platform
9.3	5.2	< 1985	Platform (practically gone as of 2022)
5	2.2	< 1985	Platform
0.1	-1.9	< 1985	Platform
5.1	2.0	< 1985	Platform
2.1	-0.2	< 1985	Massive island connected at one time
-3.2	-4.3	< 1985	Platform
-3.3	-4.3	< 1985	Platform
6.8	3.6	< 1985	Platform
-1.7	-2.9	< 1985	Platform
-0.3	-2.1	< 1985	Platform
3.2	0.7	< 1985	Platform
-0.1	-2.0	< 1985	Platform
-15.3	-13.7	< 1985	Platform
-1.9	-3.3	< 1985	Platform
-3.9	-4.8	< 1985	Platform
0.9	-1.2	< 1985	Platform
-1.2	-2.7	< 1985	Platform
-1	-2.6	< 1985	Platform (weird curve)
-6.3	-6.7	< 1985	Platform
0.4	-1.5	< 1985	Platform
-3.6	-4.7	< 1985	Platform
-1.4	-3.0	< 1985	Platform
1.9	-0.3	< 1985	Platform
-4	-5.0	< 1985	Platform
-4	-3.8	< 1985	Platform
-2.5	-5.8	< 1985	Platform
-5	N/a	<1985	Platform
3.4	0.6	1985-1998	Platform
-0.3	-2.2	< 1985	Platform
1.4	-0.9	< 1985	Platform
-2.1	-3.5	< 1985	Platform
-2	-3.6	< 1985	Platform
-6.4	-6.9	< 1985	Platform
-0.3	-2.1	< 1985	Platform
0.9	-1.3	< 1985	Platform
-5.6	-6.3	< 1985	Platform
-1.3	-3.0	< 1985	Platform

-1	-2.7	1985-1999	Platform
3.6	0.8	1985-1999	Platform (chart is sporadic)
1.1	-1.1	1985-1999	Platform
-4.5	-5.3	1985-1999	Platform
0.8	-1.3	1985-1999	Platform
1.8	-0.6	1985-1999	Platform
0.3	-1.8	1985-1999	Platform
0.9	-1.2	1985-1999	Platform
0.1	-1.9	1985-1999	Platform
-6.9	-7.1	<1985	Platform
-6.9	N/a	<1985	Platform
-7.1	-7.3	<1985	Platform (sporadic chart)
2.1	1.6	<1985	Platform
-0.1	-1.8	<1985	Platform
-1.2	-2.6	< 1985	Platform (Interesting curve on graph)
-1.1	-2.5	< 1985	Platform (gone as 2016)
-3.8	-4.6	<1985	Platform
-7.9	-7.7	< 1985	Platform
0.1	-1.5	< 1985	Platform
-3.8	-4.6	< 1985	Platform
0	-1.7	< 1985	Platform
-0.8	-2.2	< 1985	Platform
-2.4	-3.5	< 1985	Platform
-3.2	-4.1	< 1985	Platform (Interesting curve on graph)
-1.3	-2.6	< 1985	Platform
2.2	0.0	< 1985	Platform
2.4	0.1	< 1985	Platform
0.9	-1.0	< 1985	Platform
0.5	-1.2	< 1985	Platform
0.4	-1.4	< 1985	Platform
-0.3	-1.8	< 1985	Platform
0.9	-0.9	< 1985	Platform
1.1	-0.8	< 1985	Platform (interesting curve)
-0.1	-1.8	< 1985	Platform
-1.6	-2.8	< 1985	Platform (interesting curve)
1.9	-0.2	< 1985	Platform

Post-2000 Platforms

Relative Vertical Velocity (mm/yr)	Absolute Vertical Velocity (mm/yr)	Established Date	Description
2.5	-0.4	2005-2007	Platform
-4.8	-5.8	2004	Platform
-7.6	-7.8	2012-2015	Platform

-6.6	-7.1	2004-2006	Platform
-0.4	-2.3	1998-2004	Platform
0.5	-1.8	1998-2204	Platform
-0.8	-2.7	1998-2004	Platform
3.4	0.5	2004-2005	Platform
-8.5	-8.2	2004-2006	Platform
1.2	-1.1	2006-2006	Platform
2.3	-0.2	2012-2015	Platform
3.6	0.8	2021	Platform
-3.9	-4.9	2006	Platform
-5.3	-5.9	2012-2015	Platform
-11	-10.4	2012-2015	Platform
-2.3	-3.7	2011-2012	Platform
-3.8	-4.8	2015-2018	Platform
-5.3	-5.9	1998-2004	Platform (Sporadic)
-1.4	-2.9	2005-2007	Platform
-1.8	-3.2	2004-2007	Platform (massive at first then became smaller, and gone by 2022)
-2.3	-3.6	2004-2005	Platform
-4.9	-5.6	1998-2004	Platform
-1.8	-3.2	1998-2004	Platform
3	0.5	1998-2004	Platform
-0.6	-2.3	1998-2004	Platform
-0.8	-2.4	1998-2004	Platform
-1.4	-2.9	1998-2004	Platform
-0.4	-2.1	1998-2004	Platform
-2.6	-3.9	1998-2004	Platform
-8.3	-8.4	1998-2004	Platform
2.8	0.5	1998-2004	Platform

0.5	-1.1	1998-2004	Platform
4.6	1.0	1998-2004	Platform
-3.4	-5.6	1998-2004	Platform
2.2	-1.0	1998-2004	Platform
-0.5	-3.1	1998-2004	Platform
-4.8	-6.9	1998-2004	Platform
-2.5	-5.0	1998-2004	Platform
-0.5	-3.2	1998-2004	Platform
-3	-5.2	1998-2004	Platform
0.1	-2.9	2015	Platform
-4.1	-6.2	2019	Platform (Gone as 2022)
1.2	-1.8	2012	Platform
-2.8	-5.1	2010-2012	Platform
-0.4	-2.7	1998-2004	Platform
1.6	-1.1	1998-2004	Platform (vegetated)
-0.5	-2.7	2007-2010	Platform
-0.4	-2.5	2007-2011	Platform

Appendix B

Maps and rates of relative and absolute vertical motion of individual roads analyzed in the present InSAR study.

I. Highway 1

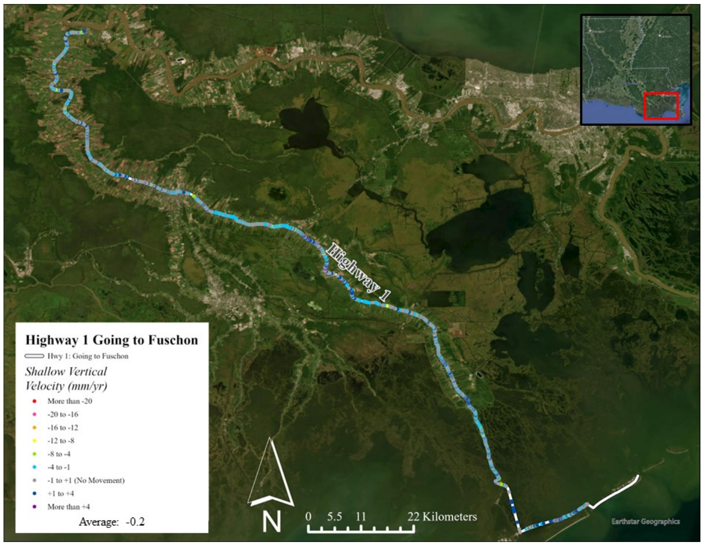

II. Highway 23

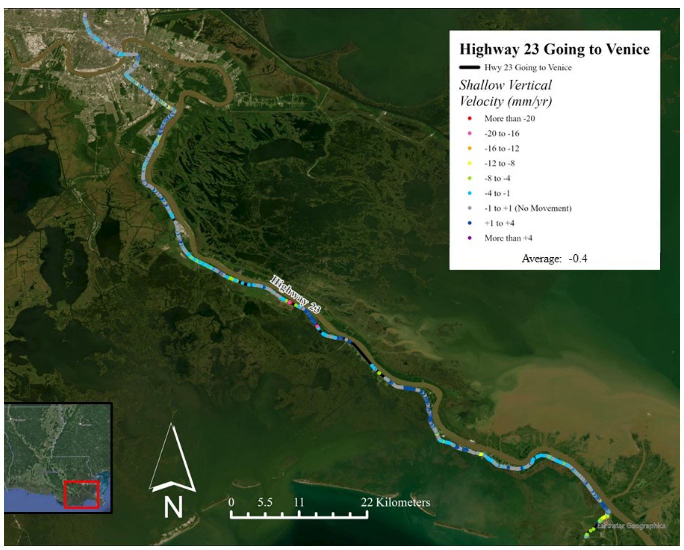

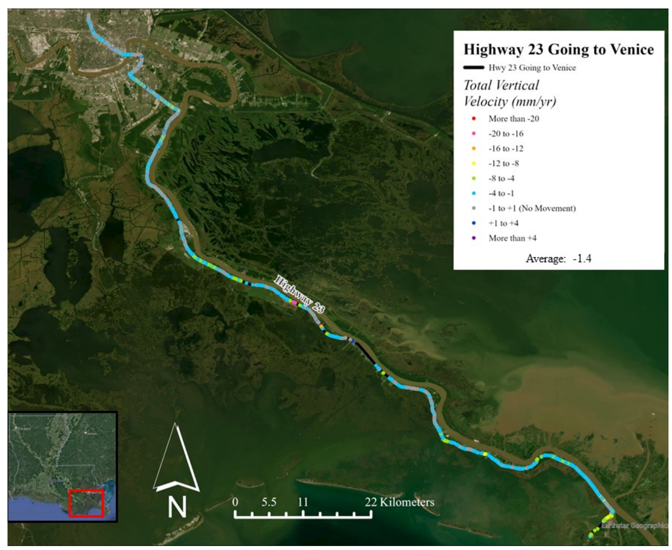

III. Highway 39

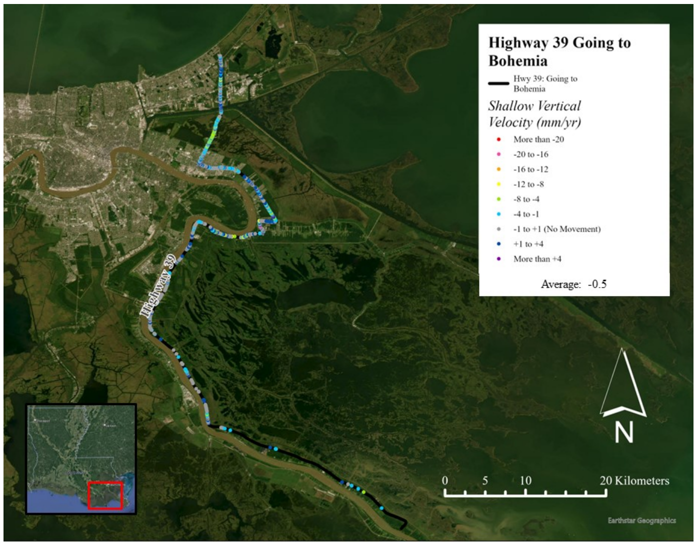

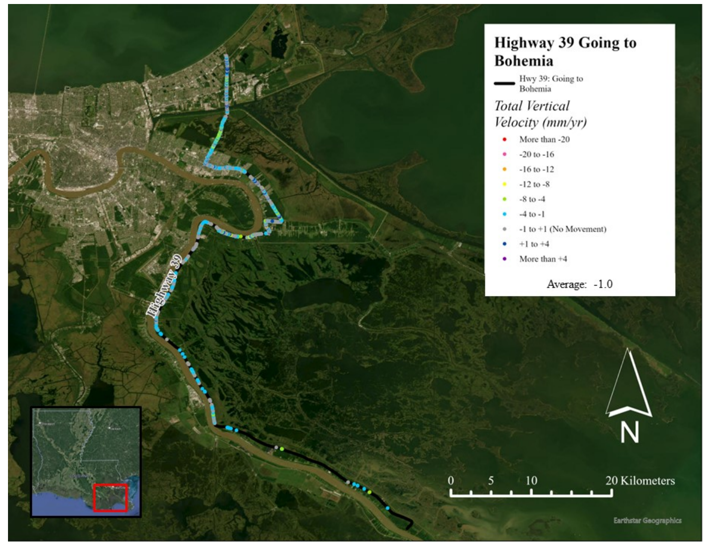

IV. Highway 56

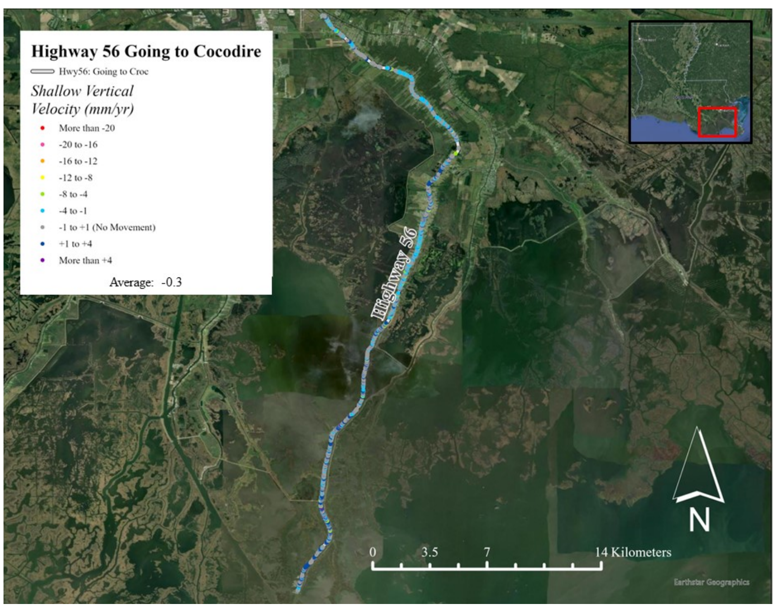

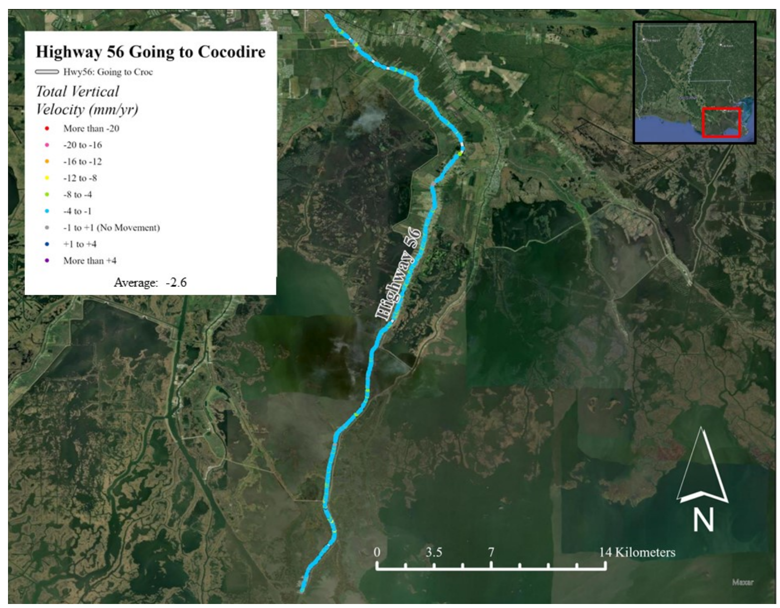

V. Highway 90

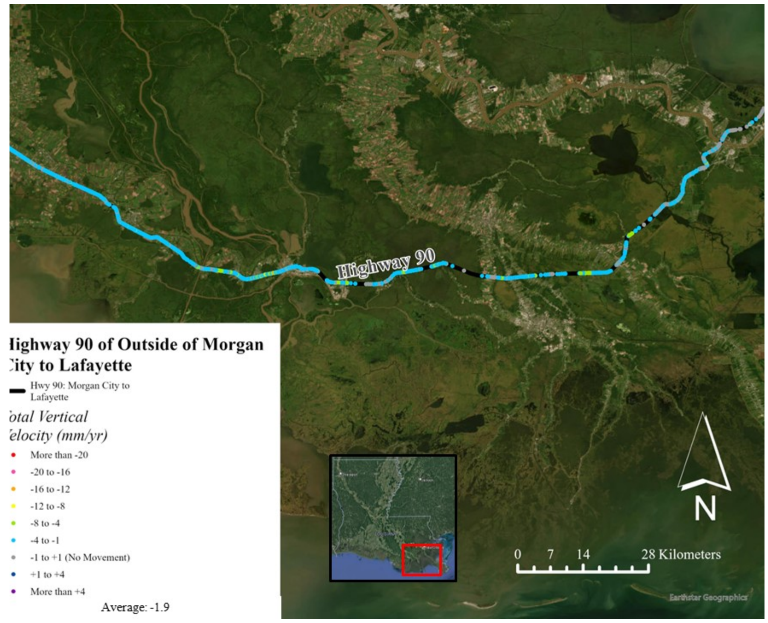

VI. Highway 300

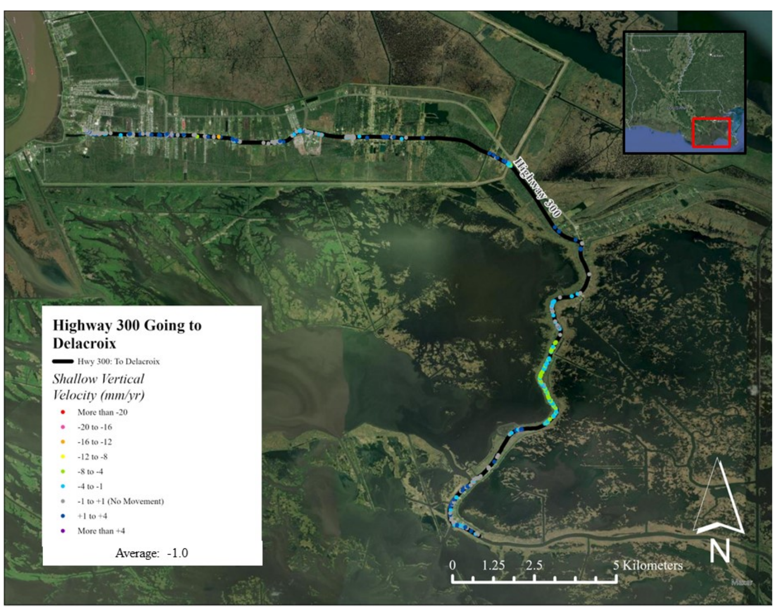

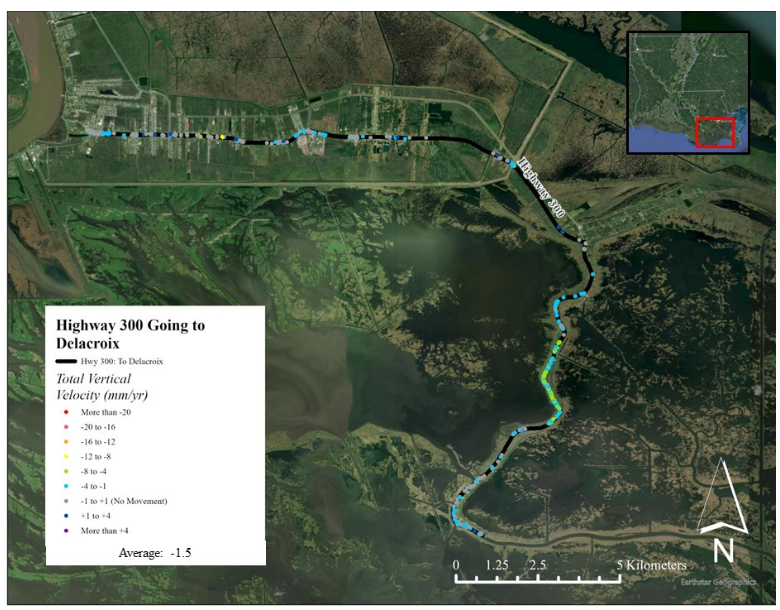

VII. Interstate 10

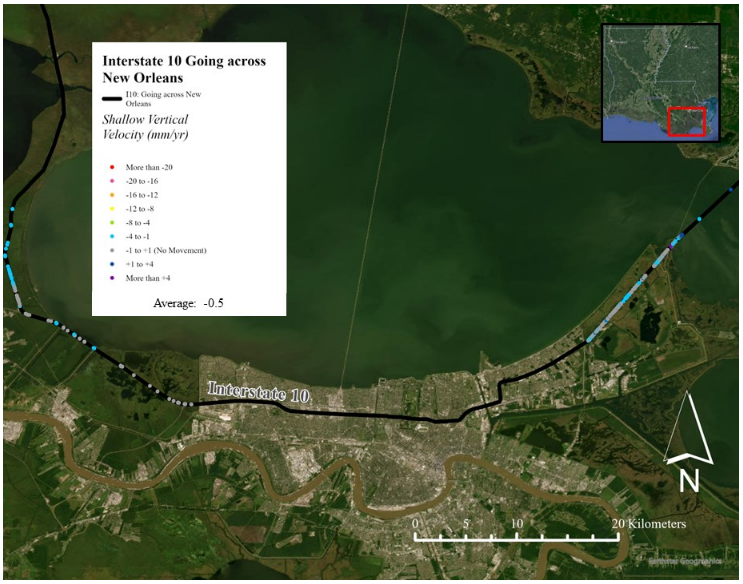

Tabular Results for each road analyzed and presented in the map results.

I. Highway 1

ID	LAT	LONG	Absolute VV (MM/YR)	Number of Points	STDV
1	30.099712	-90.994695	-0.31	79	0.97
2	30.089906	-91.029544	-0.13	77	0.78
3	30.052478	-91.039246	-0.05	146	0.81
4	30.005312	-91.048427	-0.16	271	0.85
5	29.979224	-91.019189	0.05	357	0.83
6	29.900049	-90.989469	-0.09	332	0.86
7	29.841313	-90.956079	-0.03	306	0.88
8	29.816959	-90.886401	0.18	312	0.84
9	29.795813	-90.823824	0.14	782	0.92
10	29.696107	-90.555241	-0.03	446	1.47
11	29.630272	-90.506162	-0.22	166	1.2
12	29.574879	-90.394594	0.07	212	0.78
13	29.531289	-90.336654	-0.26	256	0.93
14	29.490311	-90.327246	0.29	1129	1.05
15	29.386969	-90.262298	0.17	981	0.98
16	29.355098	-90.250459	-1.05	233	2.84

17	29.339117	-90.245417	0.19	137	0.88
18	29.301346	-90.235007	-0.69	284	2.07
19	29.276813	-90.226844	-0.11	73	-0.71
20	29.248199	-90.211157	0.09	234	1.54
21	29.157896	-90.177726	0.23	754	1.59
22	29.120606	-90.049256	-0.28	171	2.27
23	29.204597	-90.037508	-1.77	532	1.52
24	29.240855	-89.9801	-0.3	110	1.44

II. Highway 23

ID	LAT	LONG	Absolute VV (MM/YR)	Number of Points	STDV
1	29.855404	-89.985255	0.52	129	0.68
2	29.844939	-89.994403	0.62	133	0.84
3	29.829535	-90.00415	-0.51	121	0.98
4	29.814044	-90.009836	0.21	133	0.73
5	29.80445	-90.015986	-0.33	145	0.62
6	29.800104	-90.017168	-0.03	450	0.91
7	29.755346	-90.030069	0.29	385	0.63
8	29.726766	-90.001907	-0.53	524	0.77
9	29.697394	-89.985828	0.17	802	0.76
10	29.649197	-89.967407	-3.15	247	1.49
11	29.635217	-89.947758	-1	476	1.73
12	29.585429	-89.833172	-7.37	69	7.12
13	29.573882	-89.811068	1.38	350	0.85
14	29.544893	-89.779801	-14.76	41	8.05
15	29.541279	-89.776993	-9.48	576	1.59
16	29.447184	-89.626345	-1.32	230	0.89
17	29.387336	-89.60426	-1.24	436	1.61
18	29.356644	-89.541147	-1.17	623	1.93
19	29.353424	-89.443289	-0.05	428	1.35

III. Highway 39

ID	LAT	LONG	Absolute VV (MM/YR)	Number of Points	STDV
1	30.055194	-89.939104	0.3	85	2.26
2	30.046415	-89.938832	0	0	0
3	30.040856	-89.939592	0	0	0
4	30.035247	-89.939643	0.13	74	2.36
5	30.029384	-89.939584	0	0	0
6	30.023069	-89.939598	0	0	0
7	30.013925	-89.939633	0.27	63	2.21
8	30.00504	-89.939111	0.9	155	0.33
9	29.981199	-89.945635	-2.41	254	2.09
10	29.94998	-89.960166	-0.52	362	2.14
11	29.938809	-89.937655	0.1	137	0.37
12	29.937195	-89.92602	0.17	78	0.87
13	29.933174	-89.918722	0	0	0
14	29.926499	-89.911117	0	0	0
15	29.923364	-89.907764	0.79	31	0.85
16	29.920281	-89.904544	0	0	0
17	29.915791	-89.900228	0	0	0
18	29.906856	-89.894676	36	0.1	0.79
19	29.903925	-89.892992	0	0	0
20	29.898776	-89.889794	0	0	0
21	29.890669	-89.884647	-0.98	213	2.61
22	29.878466	-89.885889	0.27	272	1.16
23	29.872746	-89.895245	0.25	45	1.23
24	29.866271	-89.891746	0.39	20	2.35
25	29.865022	-89.894147	0	0	0
26	29.864558	-89.900323	0	0	0
27	29.863893	-89.907489	-1.08	71	3.38
28	29.861235	-89.912016	0	0	0
29	29.861216	-89.92779	0	0	0
30	29.866538	-89.944152	-3.39	121	3.46
31	29.872556	-89.951533	0	0	0
32	29.862804	-89.970997	0	0	0
33	29.861113	-89.971171	0.07	13	0.77
34	29.860401	-89.971242	0	0	0
35	29.853513	-89.972867	0	0	0
36	29.850581	-89.97396	0.64	26	0.91

37	29.847676	-89.976542	0	0	0
38	29.81438	-89.997348	0	0	0
39	29.798684	-90.003275	-0.03	35	0.47
40	29.791695	-90.007379	0	0	0
41	29.775365	-90.016899	0	0	0
42	29.762854	-90.018016	-0.01	66	0.6
43	29.75177	-90.01223	0	0	0
44	29.720488	-89.982635	0	0	0
45	29.681729	-89.95936	-0.15	198	1.38
46	29.648132	-89.937951	-0.36	5	0.48
47	29.647579	-89.936114	0	0	0
48	29.585098	-89.797281	0	0	0
49	29.55762	-89.758974	-0.67	11	1.17
2	30.046415	-89.938832	0	0	0
3	30.040856	-89.939592	0	0	0
5	30.029384	-89.939584	0	0	0
6	30.023069	-89.939598	0	0	0
13	29.933174	-89.918722	0	0	0
14	29.926499	-89.911117	0	0	0
16	29.920281	-89.904544	0	0	0
17	29.915791	-89.900228	0	0	0
19	29.903925	-89.892992	0	0	0
20	29.898776	-89.889794	0	0	0
25	29.865022	-89.894147	0	0	0
26	29.864558	-89.900323	0	0	0
28	29.861235	-89.912016	0	0	0
29	29.861216	-89.92779	0	0	0
31	29.872556	-89.951533	0	0	0
32	29.862804	-89.970997	0	0	0
34	29.860401	-89.971242	0	0	0
35	29.853513	-89.972867	0	0	0
37	29.847676	-89.976542	0	0	0
38	29.81438	-89.997348	0	0	0
40	29.791695	-90.007379	0	0	0
41	29.775365	-90.016899	0	0	0
43	29.75177	-90.01223	0	0	0
44	29.720488	-89.982635	0	0	0
47	29.647579	-89.936114	0	0	0
48	29.585098	-89.797281	0	0	0

IV. Highway 56

ID	LAT	LONG	Absolute VV (MM/YR)	Number of Points	STDV
1	29.557767	-90.643768	-0.34	175	1.01
2	29.551712	-90.636712	0	0	0
3	29.548436	-90.633191	0	0	0
4	29.543847	-90.62979	-0.18	74	0.72
5	29.533637	-90.610301	-0.35	155	0.77
6	29.517801	-90.594362	-0.57	142	0.58
7	29.511528	-90.588436	0	0	0
8	29.507381	-90.585494	0	0	0
9	29.501358	-90.578614	-0.63	118	1.81
10	29.494537	-90.574408	0	0	0
11	29.486427	-90.57654	0	0	0
12	29.463808	-90.589328	0.07	325	0.81
13	29.424325	-90.601835	-0.58	458	0.8
14	29.380918	-90.621896	0.07	342	0.91
15	29.354298	-90.626345	0.22	46	0.93
16	29.346866	-90.628466	0	0	0
17	29.342642	-90.633517	0	0	0
18	29.32726	-90.644194	0.25	426	0.74
19	29.271506	-90.647605	0.23	420	0.97
2	29.551712	-90.636712	0	0	0
3	29.548436	-90.633191	0	0	0
7	29.511528	-90.588436	0	0	0
8	29.507381	-90.585494	0	0	0
10	29.494537	-90.574408	0	0	0
11	29.486427	-90.57654	0	0	0
16	29.346866	-90.628466	0	0	0
17	29.342642	-90.633517	0	0	0

V. Highway 90

ID	LAT	LONG	Absolute VV (MM/YR)	Number of Points	STDV	Notes
2	29.911744	-91.716432	-0.05	871	1.41	
3	29.856688	-91.610615	-0.19	566	0.74	
4	29.823393	-91.554554	0.11	431	0.69	
5	29.771868	-91.501228	-0.76	782	0.82	
6	29.743248	-91.435949	-0.66	407	0.85	
7	29.698976	-91.37293	-0.79	981	1.45	
8	29.677857	-91.289617	0.25	631	0.87	
9	29.687415	-91.245773	-1.42	462	1.71	
10	29.697166	-91.210459	0.29	864	0.73	
11	29.697219	-91.163493	0.28	316	1.01	
14	29.668303	-91.060613	0.23	578	1.11	
15	29.691851	-90.980037	-1.04	145	1.36	
16	29.705695	-90.918816	394	-0.37	1.1	
19	29.680428	-90.776772	-0.01	811	1.05	
20	29.688447	-90.664797	-0.74	192	1.04	
21	29.691405	-90.58994	-0.03	538	1.75	
22	29.745732	-90.556499	-0.07	357	1.11	
23	29.798588	-90.504816	-0.73	372	1.8	
24	29.84792	-90.447988	-0.66	484	1.5	
25	29.887793	-90.4182	-0.15	514	1.8	
1	29.950473	-91.79576	0	0	0	START
12	29.691291	-91.4749	0	0	0	
13	29.675656	-91.132824	0	0	0	
17	29.70249	-90.89013	0	0	0	
18	29.683867	-90.830914	0	0	0	
26	29.893464	-90.402712	0	0	0	END

VI. Highway 300

ID	LAT	LONG	Absolute VV (MM/YR)	Number of Points	STDV
1	29.86839	-89.8909	0.23	13	1.53
2	29.868	-89.8862	0	0	0
3	29.86768	-89.8699	0	0	0
4	29.86755	-89.8625	0.65	14	1.08
5	29.86708	-89.8564	0	0	0
6	29.86647	-89.8515	0	0	0
7	29.86604	-89.8504	0.87	3	0.25
8	29.86565	-89.8492	0	0	0
9	29.8657	-89.8397	0	0	0
10	29.86627	-89.8363	0.1	7	0.73
11	29.86795	-89.8345	0	0	0
12	29.86712	-89.8204	0	0	0
13	29.86709	-89.8193	0.5	6	0.6
14	29.86706	-89.8179	0	0	0
15	29.86706	-89.8093	0	0	0
16	29.86702	-89.8083	0.35	2	0.75
17	29.86699	-89.8075	0	0	0
18	29.86153	-89.7791	0	0	0
19	29.86027	-89.7769	-1.42	16	1.23
20	29.85901	-89.775	0	0	0
21	29.83675	-89.7559	0	0	0
22	29.83647	-89.756	1.36	5	0.14
23	29.83628	-89.756	0	0	0
24	29.8223	-89.763	0	0	0
25	29.81849	-89.7634	-0.36	27	0.93
26	29.80641	-89.7647	-2.82	97	1.33
27	29.79376	-89.7633	-3.09	109	0.99
28	29.77968	-89.7793	0.85	38	1.71
29	29.76371	-89.7918	0.2	26	1.41

VII. Interstate 10

ID	LAT	LONG	Absolute VV (MM/YR)	Number of Points	STD V	Notes
3	30.125339	-90.447468	-0.89	329	0.64	
4	30.080808	-90.414305	-1.27	39	1.56	
5	30.052015	-90.36612	-0.26	62	0.53	
6	30.014411	-90.310608	0.12	77	0.36	
7	30.006371	-90.285189	0.58	165	0.46	
8	30.141147	-89.866489	-0.37	453	0.77	
9	30.151385	-89.858162	-0.94	523	0.9	
10	30.188392	-89.817711	0.3	384	0.85	
1	30.006775	-90.279619	0	0	0	NOLA (Phase I)
2	30.132905	-89.872928	0	0	0	NOLA (Phase I)